OIL-FOAM INTERACTIONS IN A MICROMODEL

SUPRI TR 110 Report

By

Neeraj S. Sagar

Louis M. Castanier

November 1997

Work Performed Under Contract No. DE-FG22-96BC14994

Prepared for
U.S. Department of Energy
Assistant Secretary for Fossil Energy

Thomas Reid, Project Manager
National Petroleum Technology Office
P.O. Box 3628
Tulsa, OK 74101

TABLE OF CONTENTS

	Page
List of Figures	v
List of Tables	x
Acknowledgments	x
Abstract	xi
1. Introduction	1
2. Literature Review	4
2.1 What is Foam?	5
2.2 Early Work on Mobility and Propagation of Foam	6
2.3 Recent Work on the Mobility and Propagation of Foam	6
2.4 Work on Effect of Wettability of the Rock on Oil-Foam Interactions	11
3. Experimental Apparatus	13
3.1 Equipment: General Description	13
3.2 Pressure Transducer and Demodulator	16
3.3 Surface Tensiometer	17
3.4 Interfacial Tension Measurement Using Spinning Drop	19

4. The Silicon Micromodel 27

4.1 Design of the Micromodels 27

4.2 Micromodel Characteristics 30

5. Experimental Procedure and Experiments Performed 34

5.1 Procedure 34

5.2 Experiments Performed 35

6. Results 37

6.1 Experiment 1 37

6.1.1 Observations 38

6.2 Experiment 2 39

6.2.1 Observations 39

6.3 Experiment 3 41

6.3.1 Observations 41

6.4 Interfacial Tension Measurements 42

6.5 Scanning Electron Microscopy 43

Experiment 1 44

Experiment 2 57

Experiment 3 78

References 96

Appendix A 100

Appendix B 101

LIST OF FIGURES

		Page
1.	Line diagram of the Experimental Apparatus	14
2	Schematic of spinning-drop apparatus	20
3.	The video camera mounted on the microscope	21
4.	The micromodel in the specially designed holder with the plastic connector in between	21
5.	Photograph of the experimental set-up in the lab	22
6.	The high pressure CO_2 cylinder used in the experiments	22
7.	The micromodel holder. Refer Figs. 11(a) and (b) for the design	23
8.	Photograph of the acid resistant plastic (Teflon) connector which is mounted between the micromodel holder shown in Fig. 7	23
9.	Surface Tensiometer	24
10.	Spinning drop apparatus used for interfacial tension measurement	24
11(a)	Design of the micromodel holder	25
11(b)	Design of the micromodel holder	26
12.	Flow channels in the two silicon micromodels	31
13.	SEM of model A (old)	32
14.	Photograph of the repeat etch pattern on the silicon wafer	32

15. SEM of model A (old) 33

16. SEM of model B (new) showing the melted glass on the etched pattern due to bonding of the wafer with Pyrex at extreme conditions 33

17. CO_2 bubbles flowing in the outlet channel during CO_2 flood. Flow is top to bottom diagonally 45

18. CO_2 bubbles have just emerged from the porous network into the outlet channel 45

19. Crude oil emulsions seen in the large pores in the model after 0.01% surfactant flood 46

20. Water films in the outlet port during waterflooding. The water contains dissolved CO_2 gas 46

21. The CO_2 bubbles are generated near the corner. Flow is from top to bottom diagonally. The bubbles coalesce to form bigger bubbles almost instantaneously 47

22. Crude oil invading the inlet channel. It can be seen that the oil does not fill the model uniformly 47

23(a) 48

23(b) 48

23(c) 49

23(d) 49

23(e) 50

23(f) An emulsion forming sequence 50

24(a) 51

24(b) 51

24(c) 52

24(d) 52

24(e) A bubble coalescence sequence 53

25(a) 54

25(b) 54

25(c) Emulsion breakdown sequence 55

26. A crude oil emulsion still 56

27. An oil film can be seen surrounding the gas 56

28. Emulsions as seen after 1% surfactant flood 58

29. Very stable emulsions seen at the end of the experiment (after 1% Surfactant flood) 58

30(a) 59

30(b) Water snapping off into a kersosene bubble. No emulsions are formed here as there is no surfactant present 59

31(a) 60

31(b) 60

31(c) 61

31(d) Emulsions seen after 0.001% flood. At this time there is only kerosene and no gas is present 61

32. CO_2 is discontinuous and does not flood the entire model. This is done after 0.001% Nansa surfactant flood 62

33(a) 63

33(b) 63

33(c) 64

33(d) 64

33(e) 65

33(f) A sequence of moving emulsions seen during CO_2 flooding (after 0.001% Nansa surfactant flood). Ther eis however not much CO_2 present in this part Of the model 65

34(a) 66

34(b) 66

34(c) 67

34(d) An emulsion moving sequence observed with the 40X magnification lens. As can be seen there is no CO_2 present in this part of the micromodel (after 0.001% surfactant flood) 67

35(a) 68

35(b) 68

35(c) An emulsion moving sequence observed after 0.01% Nansa surfactant flood, just before starting CO_2 flood 69

36. Both emulsions and gas at this time are flowing. This is observed after 0.1% Nansa surfactant flood 70

37. Emulsions observed near the outlet channel after 0.1% surfactant flood 70

38. Different sizes of emulsions seen in different pore/throat sizes. Indicates that Emulsions depend on pore/throat size 71

39. A very fine oil film seen in the pore (after 0.1% surfactant flood and CO_2 Flood) 71

40(a) 72

40(b) 72

40(c) 73

40(d) 73

40(e) An emulsion forming and breaking sequence observed after 0.1% surfactant flood and during CO_2 flood (just before beginning 1% surfactant flood) 74

41(a) 75

41(b) 75

41(c) 76

41(d) 76

41(e) Another emulsion forming and breaking sequence observed after 0.1% surfactant flood and during CO_2 flood (just before beginning 1% surfactant flood) 77

42. Water can be seen residing in the narrow throats 79

43. A lot of small CO_2 bubbles with surfactant film seen. The CO_2 phase is not continuous any more. Seen after 0.1% FC740 surfactant flood 79

44(a) 80

44(b) 80

44(c) 81

44(d) A CO_2 bubble snap-off sequence 81

45(a) 82

45(b) 82

45(c) 83

45(d) 83

45(e) A lamella forming and breaking sequence observed after 0.1% FC740 surfactant flood 84

46. A drop of water in a lamella. It doesn't seem to affect the lamella stability 85

47. A stable lens 85

48. A tripod like lamellae construction 86

49. Four unstable lamellae seen after 0.1% FC740 surfactant flood. 86

50. Stable lamella seen in the big pore after 0.1% surfactant flood 87

51. The foam lamella seen here seems to be thinner than usually seen in this Pore geometry and is still stable 87

52. Another stable foam lens 88

53. A similar pore geometry to some earlier figures with stable lamellae in a Different configuration 88

54(a) 89

54(b) 89

54(c) 90

54(d) 90

54(e) Some different lamellae configurations seen throughout the micromodel after 1% surfactant (FC740 in kerosene) flood 91

LIST OF TABLES

Page

1. Properties of Objective Lenses 15

2. Experiments Conducted 36

3. Composition of Brine (Wetting Phase in Experiments 2 and 3) 36

4. Interfacial Tension Measurement 43

ACKNOWLEDGEMENTS

Financial aid for this work was provided by the Department of Energy under Contract DE-FG22-96BC14994 and the SUPRI-A Industrial affiliates. This support is gratefully acknowledged.

Abstract

This report presents results of a pore-level visualization study of foam stability in the presence of oil. Many laboratory investigations have been carried out in the absence of oil, but comparatively few have been carried out in the presence of oil. For a field application, where the residual oil saturation may vary from as low as 0 to as high as 40% depending on the recovery method applied, any effect of the oil on foam stability becomes a crucial matter.

Sandstone patterns were used in this study. The micromodels used are two-dimensional replicas of the flow path of Berea sandstone etched on to a silicon wafer to a prescribed depth, adapting fabrication techniques from the computer chip industry. After flooding the models up to connate water and residual oil saturations, surfactant flood followed by gas injection to generate foam was done. Starting with lower concentrations of surfactant and gas injection the procedure was followed up to higher concentrations of surfactant. Visual observations were made using a high resolution microscope and pictures were recorded on videotape before being processed as they appear in this report.

The single most important reason for this study on silicon micromodels compared to previous micromodel work is pore dimensions. With glass micromodels, for example, the reaction kinetics of acid etching makes it necessary to enlarge the pores by a factor of 5 to 50 thus providing a serious limitation for their use in studying processes that depend critically on capillary forces or involve thin films as compared to real rock pores.

Two different surfactants were used, a fluoro-surfactant (for generating an oil foam) and an Alpha-Olefin Sulfonate. Oseberg crude was the non-wetting phase in the first set of experiments, and Kerosene in the next two sets. While the fluoro-surfactant created a strong static gas-blocking foam in the presence of oil, the Alpha-olefin Sulfonate (AOS) foamer did not.

The fluoro-surfactant foam gave the oil-tolerant behavior expected from its non-entering, non-spreading characteristics. The AOS on the other hand, did not behave in accordance with its bulk observations and its behavior was seen to be controlled by formation of oil/foam emulsions. Generation sites for both foam and the emulsions were seen to be controlled by pore geometry and local saturation. For the foam, no obvious link could be found with the number of films observed and the strength of gas blockage. A lot of other interesting observations included snap-off, emulsion formation and breakdown sequences, foam lamella formation and breakdown sequences, and static emulsion and foam in different configurations within the model usually at higher concentrations of surfactant.

Section 1

Introduction

Oil production from a petroleum reservoir involves primary and secondary production modes, which may recover less than half of the original oil in place. To recover additional oil, it is necessary to apply Enhanced Oil Recovery (EOR) techniques such as miscible or immiscible gas displacement (CO_2, hydrocarbon gases, etc.). However, major problems occur in these EOR methods because the displacing agent has high mobility and low density compared with that of reservoir fluids. Fingering (channeling) and gravity override reduce the sweep efficiency, contribute to early breakthrough of injected fluid, and thus reduce the amount of oil recovered.

The use of surfactant stabilized foams to counteract these kinds of problems was suggested decades ago. The use of foam is advantageous compared with the use of a simple fluid of the same nominal mobility because the foam, which has an apparent viscosity greater than the displaced fluids, lowers the gas mobility in the swept or higher permeability parts of the formation. This diverts at least some of the displacing gas into other parts of the formation that were previously unswept or underswept. From these underswept areas, the additional oil is recovered. Because foam mobility is reduced more

in higher permeability zones than in lower permeability zones, improvement in both vertical and horizontal sweep efficiency can be achieved.

This report will focus on the stability of foams flowing in porous media in presence of oil. Many laboratory investigations have been carried out in the absence of oil, but comparatively few have been carried out in the presence of oil. For a field application, where the residual oil saturation may vary from as low as 0 to as high as 40% depending on the recovery method applied, any effect of the oil on foam stability becomes a crucial matter.

Two different approaches have been used in an attempt to scale up foam properties to the reservoir scale. They represent different levels of ambition in describing the physics of confined foam. One approach is purely empirical and relies on calibrating a flexible simulator by selected laboratory data, which are measured on conventional core-sample scale and believed to represent those foam effects which are most critical. The empirical foam model implemented in STARS™, a pseudo-compositional reservoir simulator is probably the best example of this approach (Coombe, 1992; Surguchev, 1995). It has the advantage of relative simplicity, but depends heavily on obtaining "correct" values of the lab parameters and on the assumption that these parameters can be measured in a manner that is not too strongly dependent on the mode and conditions of the experiment. Recent work by Hanssen and Dalland (1993, 1994) have shown that this critical assumption may not hold.

The other approach to scaling up foam properties attempts to extract information about the physical flow mechanisms as actually observed on the pore-level, and construct mathematical relationships between experimental parameters that, if correct, can be used to translate foam properties to different scales. The best known such foam simulator is the one developed at the University of California at Berkeley. The physical mechanisms in the Berkeley model rely on observations of foam flow in etched-glass micromodels, especially a comprehensive study by Chambers and Radke (1991).

Micromodels, designed to represent the geometric structure of a rock pore network, while allowing direct visual observation of the flow phenomena, have proven useful for viewing pore-level events in several reservoir processes. Currently accepted theories on foam flow are largely built on the basis of pore model observations by Mast (1972), Owete et al. (1984), Huh et al. (1989), Schramm (1990) etc. Most micromodels have been made by etching a flow pattern into a glass plate using. e.g., hydrofluoric acid (HF) and are two-dimensional representations of the pore structure. With glass micromodels, the reaction kinetics of acid etching makes it necessary to enlarge the pore sizes of typical sandstone pores, usually by a factor of 5 to 50 compared to their natural size. Obviously, this could be a serious limitation for their use in studying processes that depend critically on capillary forces and involve thin films.

The silicon micromodel on the other hand, replicates a pore structure of any design on a silicon wafer rather than a glass plate, adapting fabrication techniques from the computer chip industry. The pore cavities are created photochemically, a process which is not rate-limited such as acid etching. The micromodels used in this study offer 1:1 scaling of typical sandstone pores and were made to represent Berea sandstone. This is a major step forward for visual studies of pore-level events.

This section of the report is followed by a section on Literature survey, after which the experimental apparatus is defined. A brief description of the fabrication techniques used for the silicon micromodel comes next followed by the experimental procedure and the experiments performed. To the end of the report we have a section on results and discussion closely followed by the conclusions.

Section 2

Literature Survey

There has been a considerable amount of work published regarding foam research. The literature provides valuable insight into the occurrence, properties, importance and propagation mechanisms of foams based on colloid science. Many laboratory investigations of foam flooding have been carried out in the absence of oil, and comparatively few have been carried out with oil present. An argument for not including oil was simply, that a need to understand the basic propagation mechanisms of foam dictated such a move. Any additional components would only serve to complicate matters. As research on foam and its propagation in porous media progressed, foam was seen as a fascinating fluid, both because of its unique microstructure, and because of its dramatic influence on the flow of gas and liquid.

When research began to include oil, it was seen that the effect of oil on foam stability was indeed complicated. Oil saturation could alter foam stability and its propagation mechanisms to a great extent. From a practical viewpoint for example, a field application where the residual oil saturation may vary from as low as 0% to as high as 40%, depending on the recovery method applied, any effect of oil on foam stability becomes a crucial matter. Also the nature of the foam, foam injection procedures, reservoir

wettabilities and pore geometry were beginning to be seen as affecting the oil-foam interactions making it even more complicated.

Clearly, more work is required in this area. This need provides a basis for our study.

2.1 What is Foam?

A foam is a dispersion of gas in liquid, usually with a surface-active agent present. Foams are not thermo-dynamically stable and ultimately decay into their constituent phases, but can be mechanically stable.

When a foam exists inside a confining medium, dimensions of this confining medium relative to the average bubble size determine the texture and properties of the foam. When the confining diameter is large relative to typical bubble size, such as in a pipe, the foam is similar to bulk foam. Its flow can then be treated as that of a non-Newtonian, compressible pseudofluid. Where the diameter of the confining body is comparable to, or smaller than the minimum bubble size, the foam exists as a network of lamellae rather than bubbles. Such a lamellar-structure foam can not be treated as a single fluid, because liquid and gas flows by different mechanisms. Holm (1968) found liquid to flow as a continuous phase, but gas flow to occur by a sometimes very slow process of continually breaking and re-forming the liquid films. This explains why gas flow may be essentially blocked by foam in pores, while the permeability to liquid is merely reduced in proportion to the liquid saturation.

The ability of foam to reduce gas mobility has led to its application in a number of processes, including gas flooding, steam flooding, and well treatment techniques. It has been somewhat uncertain whether foam in these cases actually works by gas blockage and flow diversion, or whether it is better described as a “viscosifying agent” for the gas.

2.2 Early Work on Mobility and Propagation of Foam

The use of surfactant stabilized foams to counteract problems such as Fingering and gravity override were suggested several decades ago. Fried (1961) demonstrated that aqueous surfactant stabilized foam could dramatically reduce the mobility of gases in porous media. At that time foam was studied mainly from a phenomenological perspective. In the intervening 35 years, foam has been recognized as a fluid with unique rheological properties within porous media, and the scope of research has expanded to include local pore scale phenomena and local microstructure. Considerable work was published by Raza, Marsden, Bernard et al, Mast, Khan, Nahid in the 1960's and 70's regarding the behaviour of foam. Details of these are not covered in this literature survey as they have been exhaustively covered earlier by Marsden (1986).

However none of these proposed early mechanisms adequately accounted for all the observed properties of foam in porous media. The only general agreement was that foam generally hindered the flow of gas in porous media.

2.3 Recent Work on the Mobility and Propagation of Foam

Marsden (1986) reviewed previous findings, surmising that apparent gas viscosity was indeed a function of the gas flow rate, flow history and surfactant concentration, and that 'breaking and reforming' processes are a dominant mode of foam propagation in micromodels. Sanchez and Schechter (1986) suggested that gas permeability was a function of wetting phase film thickness.

Owete et al (1984) suggested that air was propagated by displacement of lamellae in long bubbles flowing and extending across several pore lengths while the liquid flowed through the network of films. They also observed snap-off occurring at pore constrictions and the resultant bubble 'break and reform' process. Radke and Ransohoff (1986) categorized the various mechanisms of foam generation within glass bead packs

as ‘snap-off’, ‘lamella leave behind’, and ‘lamella division’, with snap-off being the primary mechanism for strong foam propagation.

Roof (1970) and Mohanty *et al*. (1980) each studied and reported specific pore geometry necessary for snap-off mechanisms. Roof noted that the front is always at least seven pore radii from the throat of the constriction before snap-off can occur. Mohanty *et al.* calculated that snap-off occurs when the ratio of pore body radius to adjacent throat exceeds three. Falls *et al* (1988) and Kovscek *et al*. (1994) proposed that the rate of generation of lamella must be equal to their collapse at steady state conditions.

Castanier and Hanssen (1995) noticed the sliding of lamellae (bubble train flow) over liquid films covering the grains in silicon micromodels. Using atomic force microscopy between the liquid/solid interface, a thick layer of surfactant was found. This layer they state could explain the apparent bubble train effect observed.

Spreading and Entering Coefficient Theory for Oil-Foam Interactions :

The spreading coefficient, S, for an oil-foam system is given by:

$$S = \gamma^{\circ}{}_{f} - \gamma_{of} - \gamma^{\circ}{}_{o}$$

where : $\gamma^{\circ}{}_{f}$ = Foaming solution surface tension

γ_{of} = Initial foaming solution/oil interfacial tension

$\gamma^{\circ}{}_{o}$ = Surface Tension of the oil

When oil spreads over the gas-aqueous interface, a certain amount of both gas-oil and aqueous-oil interface is created, and some gas-aqueous interface is eliminated. For a unit

surface area, the Gibbs free energy change (ΔG) is given by '-S'. The spreading is predicted to be favored when ΔG is negative and S is positive. Rapid spreading of a drop of oil that has a low surface tension over the lamella can cause rupture by providing a weak spot. The spreading oil lowers the surface tension, increases the radius of curvature of the bubbles, alters the original surface elasticity, and also changes the surface viscosity. Thus the interfacial film loses its foam stabilizing capability. If S is negative, then the oil should not spread at the interface.

Another mechanism of rupture involves the drawing up of a droplet of defoamer into the lamella region between two adjacent bubbles so that it can bridge the two bubbles. The breaching of the aqueous-gas interface by the oil from within the lamellar liquid is termed 'entering'. The process is thermodynamically favorable if the 'Entering Coefficient' is positive (originally defined by Robins and Woods (1948) as a rupture coefficient, R). For a oil-foam system, the entering coefficient is given as :

$$E = \gamma^{\circ}{}_{f} + \gamma_{of} - \gamma^{\circ}{}_{o}$$

For unit surface area, the Gibbs free energy change is given by '-E'. The entering is predicted to be favored and spontaneous when ΔG is negative and E is positive.

Work on "Effect of Oil on Foam Stability and Propagation":

Oils such as Castor oil, are among the earliest chemicals to be used for foam inhibition and foam breaking. Literature by Harkins (1941), Robinson et al (1948), Ross (1944) etc. deals with it. Some theories for the mechanisms of anti-foaming action have emerged from this work. In general matters are not simple. Apparently foams can be destabilized by oils by several mechanisms, and more than one mechanism may be operating in a given case.

Some possibilities for the mechanisms of foam destabilization by a given oil phase include:

* Foam-forming surfactant may partition in the oil, especially if there is emulsification , causing depletion in the aqueous phase and hence from the gas-liquid interface.
* Surfactants from the oil may be adsorbed by the foam lamellae, from either a mixed or replaced adsorption layer, and produce a less favorable state of foaming.
* Components from the oil may be adsorbed by the porous medium altering the wettability of the solid phase, and this alteration makes it more difficult for foam to be generated and regenerated.
* The oil may spread spontaneously on foam lamellae and displace the foam stabilizing interface.
* The oil may emulsify spontaneously and allow the drops to break and rupture the stabilizing interface.

Nikolov *et al* (1986), when studying bulk oil-foam interactions, reported the possible occurrence of three distinct films during the process of three phase foam thinning. They are 'foam films', which are water films between air bubbles; 'emulsion films', which represent water films between oil droplets; and 'pseudo-emulsion films' where water film resides between air and oil droplets. Their findings said that pseudo-emulsion films, droplet size and droplet numbers may all contribute to foam destabilization.

Rendall *et al*. (1990) investigated the behavior of several commercial surfactant destabilized foams, in the presence of crude oil. On the basis of dynamic bulk foaming tests, gas mobility reduction factors measured in reservoir cores, and observations in a microvisual apparatus, it was found that all but one of the foams studied were destroyed when brought into contact with oil.

Similarly Kuhlman (1988) and Manlowe and Radke (1990) observed in micromodel studies that oils were capable of destroying foams. Work done by Novosad *et al*. (1989), Jensen and Friedmann (1987) and Holt (1991) suggested that foam sensitivity to oil is

also manifested as an increased difficulty of forming and in propagating foams through porous media containing oil. Novosad and Ionescu (1987) found lower mobility reduction factors in foam floods conducted in cores containing residual oil compared to the same floods conducted in cores that were completely free of oil. The lower mobility reduction factors were interpreted to be due to some kind of foam destruction by the oil.

Lau and O'Brien (1988) provided further insight into the effects of oil saturation on foam propagation. Their work relies upon an understanding of oil spreading ability in which spreading is determined from 'spreading coefficients' or free surface energies. Through the use of sandpacks and both spreading and non-spreading oils, they were able to show an increase in foam generation time, a reduction in foam propagation rate, and an increased foam destruction rate with spreading oils. This finding is contrary to Manlowe and Radke's who argue that there is no correlation between oil spreading and foam stability. Instead, they state that pseudo-emulsion film collapse is the general destabilization mechanism.

Hanssen *et al* (1990), in a model system (glass bead pack) of a gas blocking foam in an oil reservoir, observed clear trends in the mobility reduction as measured in a gas-blockage test, with varying concentrations of oil and surfactant. They concluded that the change in interfacial tension between gas and the aqueous phase, upon equilibration with oil, appeared to be a good predictor of gas-blockage efficiency for the systems studied.

Oil interactions with foam have been studied by Dalland *et al.* (1993). On conducting experiments with flowing and gas blocking foams in porous media, using a set of conventional and fluorinated surfactants and various oils, they found varying oil tolerance and sensitivities. In all cases it was found that the combination of non-spreading and non-entering oil created a strong gas-blocking foam or a low mobility flowing foam. The 'Lamella number', L, calculated from interfacial tensions was found to be of no predictive power. The results indicated that the mechanisms of oil-foam interactions are the same for gas blocking and for flowing foams in porous media.

From unpublished work by Castanier on oil-foam interactions using a fluorosurfactant foam and an AOS foam, the fluorosurfactant foam seems to give the oil tolerant behavior expected from its non-entering, non-tolerant characteristics. AOS foam by contrast, is seen to be controlled by formation of oil-water emulsions which appear to prevent the formation of strong foam until a large excess of foaming agent is present.

2.4 Work on Effect of Wettability of the Rock on Oil-Foam Interactions

Most of the research on foam sensitivity to oils in porous media, whether in microvisual apparatus or core-fluid tests, has been concerned with water wetted pore and throat surfaces. Because petroleum reservoirs are of intermediate, mixed or oil wettability, some researchers have spread their work to include reservoir wettabilities.

Huh et al. (1988) found that micromodel wettability was altered to intermediate or oil-wet as a result of crude oil saturation. The effects of various phase affinities to grain surfaces was studied by Sanchez and Hazlett (1989) as well. An indication of surface reaction, from hydrophobic to hydrophilic, was detected after the addition of surfactant. This fact, along with a shift in liquid phase relative permeability of the oil-wet medium, suggested wettability alteration.

Kuhlman (1990) commented on similar results of his own, remarking that the deleterious effect of oil on foam was due, in part at least, to the high concentration of light hydrocarbons in the oil, and the oil wetness of the medium itself. Work by Hornbrook et al. (1992) noted that wettability alteration was due to the surfactant injection procedure. They found that with surfactant slug injection, oil appeared to be the wetting phase, and with foam injection, surfactant appeared to wet the medium.

Schramm and Mannhardt (1994) conducted oleophilic microvisual cell experiments with several foams. They found that the foams were significantly less stable in the presence of crude oil and oleophilic solid surfaces, compared with some crude oils and hydrophilic

surfaces. Suffridge *et al*. (1989) reached the same conclusions on the basis of core-flood experiments. They found that the foams were more effective (stable) in water wet cores than in oil wet cores. Holt and Kristiansen (1991) studied foams flowing in cores under North Sea reservoir conditions that were either partially or completely oil wetted. They found that foam effectiveness was favored by water-wet conditions. Any degree of oil-wet character reduced the effectiveness of the flowing foam.

A complication is that the foam forming surfactants may adsorb onto the solid surfaces and may alter the wettability. In the microvisual experiments of Schramm and Mannhardt (1992), some of the foaming systems investigated appeared to change the wettability back to water-wet, in which case the foam sensitivities to oil reverted back to those appropriate to the water-wet cases. The result is consistent with the core-flood tests of Sanchez and Hazlett (1992) in which foaming surfactants apparently caused wettability reversal in oil wet porous media. This reversal, in turn, was postulated to be the reason that stable foams could be generated and propagated in their oil-wetted cases.

Section 3
Experimental Apparatus

All the experiments were done at constant pressure. Fluid injection (Carbon Dioxide, surfactant, oil, water etc.) was facilitated by using pressure bottles (connected by the pressurized lines). A basic line diagram of the apparatus is shown in Figure 1.

A photograph of the experimental set-up along with the pressure cylinders used is shown in Figures 5 and 6. The various equipment used are outlined below. All the tubing used was made of Teflon with a diameter of 1/16". The silicon micromodels used and the fabrication techniques are discussed in Section 4.

3.1 Equipment: General Description

1. **Microscope**: A Nikon Optiphot-M with a photo tube allowing for video imaging was used (Figure 3). The Objective lenses used along with their properties are as outlined in Table 1. Working distance is the distance between the tip of the lens and the focal plane of the objective. Numerical Aperture relates to the light gathering ability and is a dimension less number between 0 and 1. Higher the value, better the light gathering.

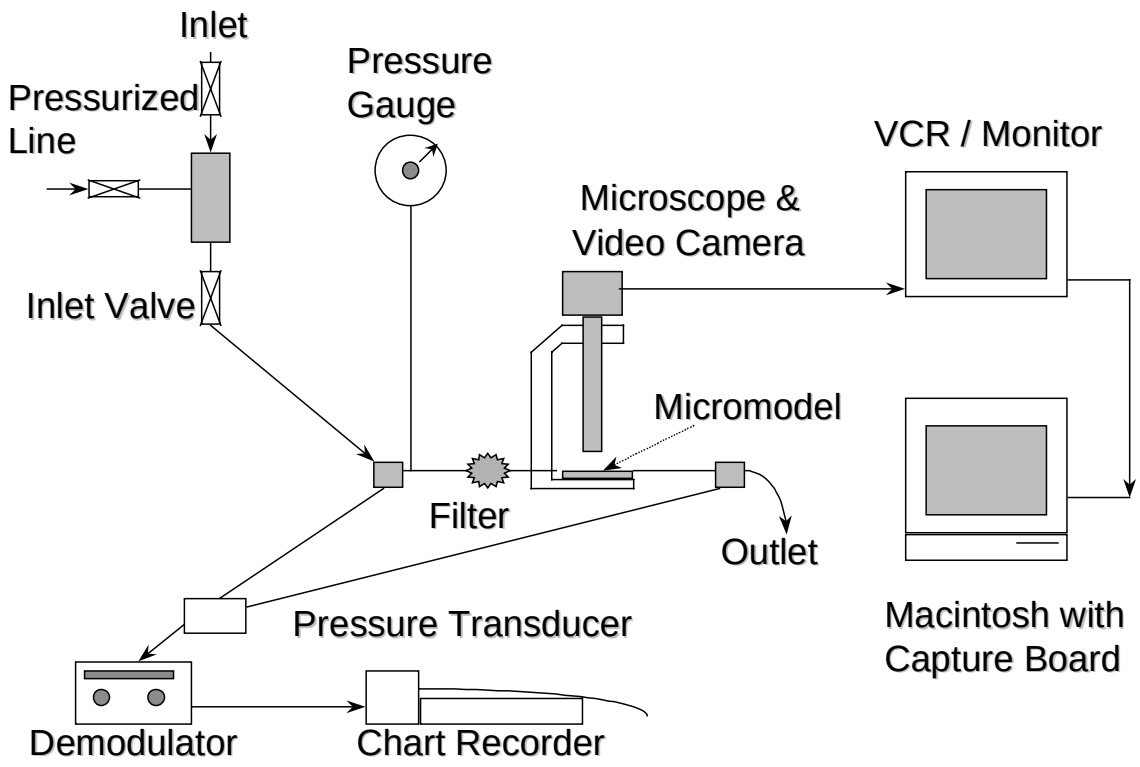

Figure 1. Line diagram of the Experimental Apparatus.

Table 1: Properties of Objective Lenses

Model	Magnification	Working Distance (mm)	Numerical Aperture	Viewable Diameter (μm)
5X	5X	20.0	0.1	3000
0.4LWD	20X	6.0	0.4	800
0.5ELWD	40X	10.1	0.5	375

2. **Video Camera**: A Sanyo closed circuit television camera was used to convert the images through the microscope into electric impulses. An attached photo tube allowed image viewing (Figure 3).

3. **Video Cassette Recorder**: The image from the video camera was recorded on a Mitsubishi NTSC format video cassette recorder. Its NTSC format allowed recording and playback at a speed of thirty frames per second (Figure 5).

4. **Television Monitor**: In order to view the recorded pore-level events, the VCR was connected to a high definition Sony Color Monitor (Figure 5).

5. **Macintosh**: The images from the VCR were captured with the aid of a Spigot II tape video capture board in an Apple Macintosh computer. Image enhancement was done using Adobe Photoshop (Figure 5).

6. **Transducer**: A Celesco differential pressure transducer with a fifty psi pressure plate was used to measure fluid pressure differential across the silicon model. Refer section 3.2 for details.

7. **Demodulator**: A Celesco carrier demodulator was used to convert the electrical signals from the transducer into pressure units. Refer section 3.2 for details.

8. **Chart Recorder**: A Soltec strip chart recorder was used to plot the differential pressure as recorded by the transducer (Figure 5).

9. **Micromodel Holder**: A holder was specially designed (Figures 11(a) and 11(b)) to mount the micromodel for unobstructed viewing under the microscope (Figures 4,8).

10. **Micromodel Connector**: An acid-resistant plastic (teflon) holder was used to mount the micromodel on the holder and was provided with an inlet and outlet port (Figure 4,8).

3.2 Pressure Transducer and Demodulator

A series CD 10D Celesco Carrier Demodulator was used with a variable reluctance type transducer (for measuring the pressure drop across the micromodel) to produce a DC signal output proportional to both steady-state and dynamic parameters sensed by the transducer. The series CD10 D Carrier Demodulator operates on 95 to 125 VAC, 60 to 400 Hz at %W, and is used with a variable reluctance transducer to provide DC signal output voltages. A 10V pk 4Hz Sine excitation is applied to a bridge circuit which incorporates the two inductance arms of the transducer. Bridge unbalance proportional to transducer actuation produces an AC signal which is amplified and demodulated for final DC signal output. The linear output capability of the Demodulator was +/- 10VDC which corresponds to a nominal +/- 25mV/V transducer output. Zero adjustability can compensate for a transducer unbalance of +/- 15mv/V (+6V at nominal sensitivity).

Calibration and Operation

Although no calibration of the demodulator itself is required, it is necessary to calibrate the system comprised of the demodulator, transducer and the readout printer. With the demodulator connected to a voltmeter, set the zero and span potentiometers to their respective midscales. After the power switch has been turned on, and with no force on the transducer, adjust the zero potentiometer on the demodulator until zero is indicated on the voltmeter.

Next, impose a full-scale calibrating force on the transducer. For a 0-50 psi range transducer, 50 psi should be applied with a deadweight tester or monitored using a precision gauge. Adjust the modulator span potentiometer until the voltmeter indicates the desired full scale value. Exercise the transducer-demodulator system through at least three successive cycles to ensure stable zero and span reading.

3.3 Surface Tensiometer

A FISHER Surface Tensiometer, Model 20 (Figure 9) was used to determine the apparent surface tension and interfacial tension of the liquids used in the experiment. The Tensiometer utilizes the principles of operation originally devised by Dr. Pierre Lecomte du Nouy, a noted biochemist, for studies of blood serum and other biological fluids. Essentially a torsion-type balance, it is a kind of instrument currently specified by the American Society for Testing Materials in Methods D-971 (interfacial tension of oil against water) and D-1331 (surface and interfacial tensions of detergents).

In the du Nuoy method, a platinum-iridium ring of precisely known dimensions is suspended from a counter-balanced lever arm. The arm is held horizontal by torsion applied to a taut stainless steel wire, to which it is clamped. Increasing the torsion in the wire raises the arm and the ring, which carries with it a film of the liquid in which it is

immersed. The force necessary to pull the test ring free from this surface film is measured.

The Surface Tensiometer shows this “apparent” surface or interfacial tension (the latter measured at the interface between two immiscible liquids) on a calibrated dial. The dial readings can be used directly for comparative studies or converted to “true” values by using a correction factor chart.

Operation

The sample should be placed in a glass beaker or cylindrical vessel with a diameter of at least 45 millimeters. For testing oil samples according to ASTM Method D-971, the glassware should be cleaned according to a definite procedure. Any residual oil from the previous sample is removed with petroleum naphtha or benzene followed by several washes with methyl ethyl ketone and water, then the glassware is immersed in a hot cleaning solution of chromic acid. The glassware also should be rinsed thoroughly with tap water, then with distilled water.

The platinum-iridium ring should be cleaned by first dipping it in benzene (to remove hydrocarbons), then squirting it with acetone (to remove the benzene) and allowing the acetone to evaporate. Following this, flash the ring in a Bunsen burner flame to remove residual hydrocarbons.

Measuring Surface Tension

The cleaned platinum-iridium ring should first be attached to the hook at the end of the lever arm. The arrest mechanism should be holding the arm at this time.

The liquid to be measured is transferred to the clean glass vessel and placed on the sample table. The sample table is moved around until it is directly beneath the platinum-iridium ring. Raise the sample table until the ring is immersed in the test liquid. The ring should be in the liquid, beneath the surface so that the entire liquid ring will be wetted. About 1/8 inch immersion is generally considered sufficient.

The torsion arm is now released and the instrument adjusted to a zero reading. Adjust the knob on the right side of the case until the index and its image are exactly in line with the reference mark on the mirror. Be careful to keep the ring in the liquid during this manipulation, raising or lowering the sample table (if necessary) by means of the knob adjustment underneath the table. Now turn the knob beneath the main dial on the front of the case until the vernier reads zero on the outer scale of the dial.

Lower the sample table until the ring is in the surface of the liquid, adjusting the knob on the right side of the case to keep the index lined up with the reference mark on the mirror. The surface of the liquid will become distended, but the index must be kept on the reference. Continue the two simultaneous adjustments until the distended film at the surface of the liquid breaks. The scale reading at the breaking point of the distended film is the apparent surface tension.

3.4 Interfacial Tension Measurement Using Spinning Drop

The spinning drop apparatus used in this experiment was designed at the University of Texas. A schematic of the apparatus used is shown in Figure 2. A hysteresis synchronous motor was used. Its speed was controlled by varying the frequency from a frequency generator. The rotational stability was 1 part in 10^5 as determined by a period averaging counter stable to 1 part in 10^8. The range of speeds used was from 1,200 RPM to 24,000 RPM. A Gaertner traveling microscope with a filar eyepiece was used to

measure the length and width of the drop and to calibrate the glass tubes for their magnification of the drop diameter. This effect was determined to be a constant for the experiment of y-measured/y-true=1.332 for all the aqueous phases studied. The tube housing and assembly had a design precision ground 0.245" O.D. pyrex glass tube rounded on one end and sealed against a rubber septum on the other. A glass cell enclosed the apparatus (Figure 10).

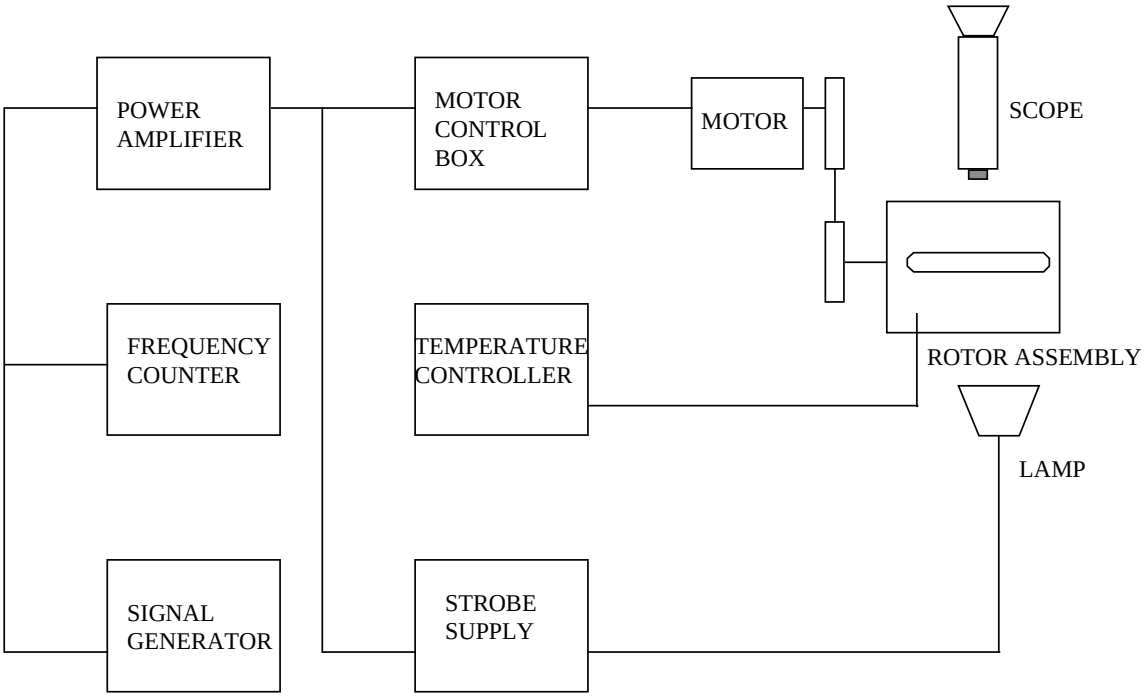

Figure 2: Schematic of spinning-drop apparatus.

The procedure for loading the cell is to fill the glass tube and metal cap completely with the more dense phase. Holding the tube upside down (capillary pressure retains the more dense phase in the tube), the less dense phase is then injected with a microlitre syringe, the tube is then placed in the cap and the whole assembly is placed in the shaft and secured by screwing the cap onto the shaft. A small hypodermic needle is inserted into the cell through the septum to release any pressure build-up caused by screwing the cap on.

A simple Fortran program to do the calculation is attached in Appendix A.

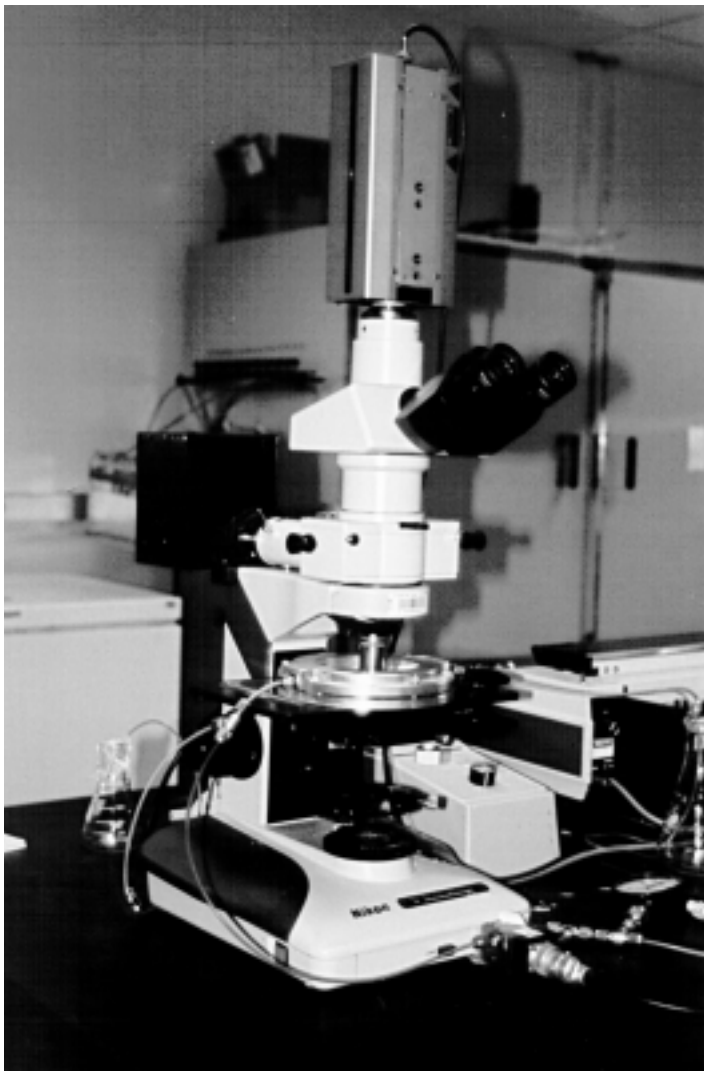

Figure 3: The Video Camera mounted on the microscope

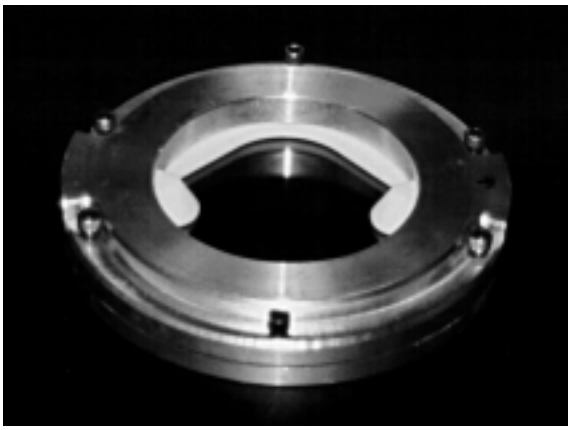

Figure 4: The micromodel in the specially designed holder with the plastic connector in between.

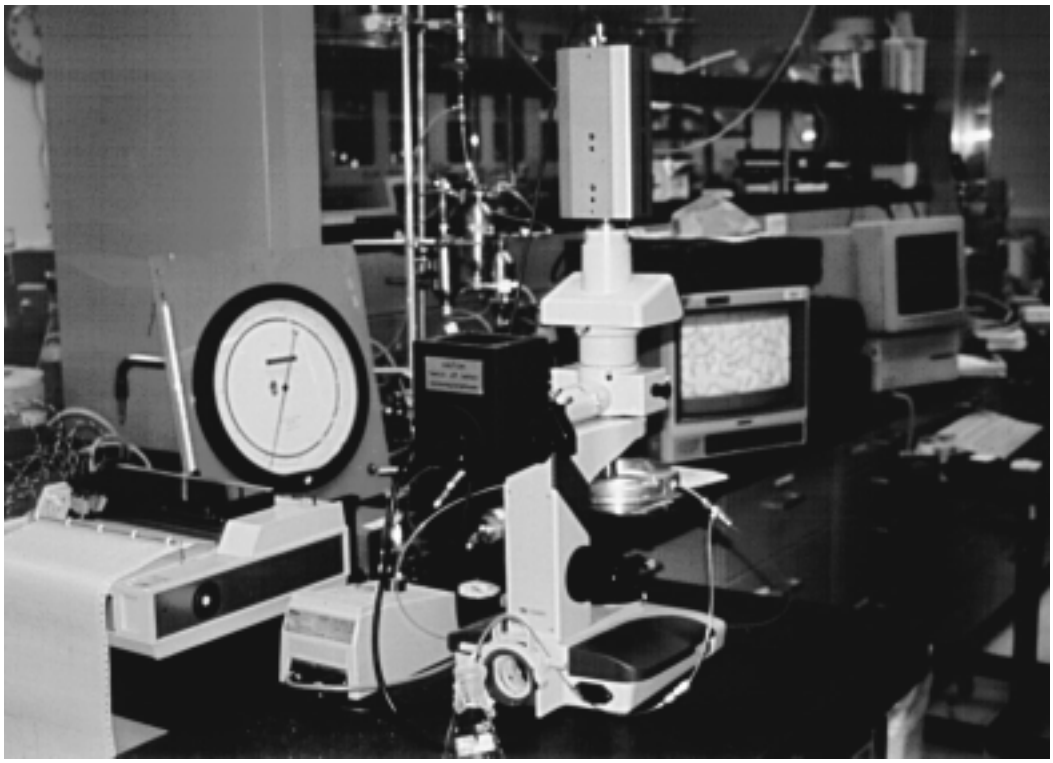

Figure 5: Photograph of the experimental set-up in the lab.

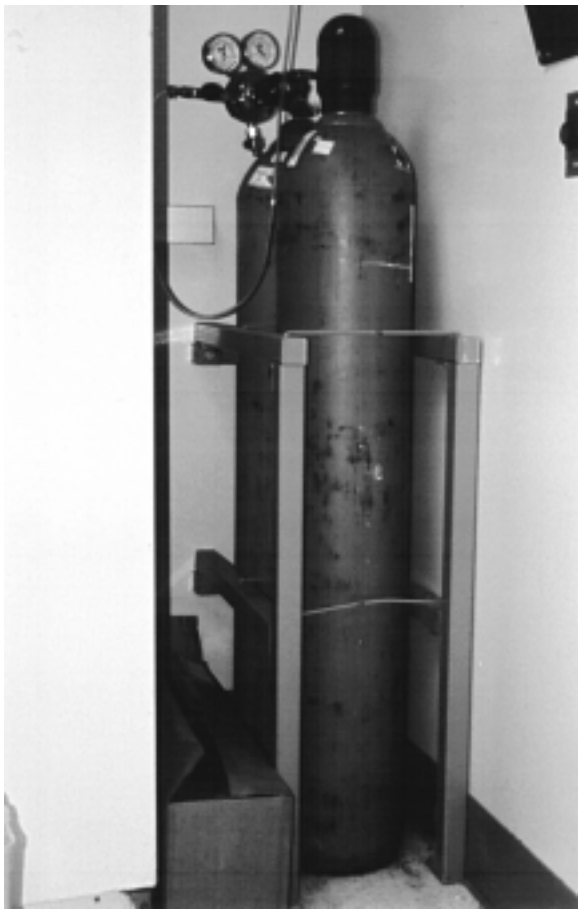

Figure 6: The high pressure CO_2 cylinder used in the experiments.

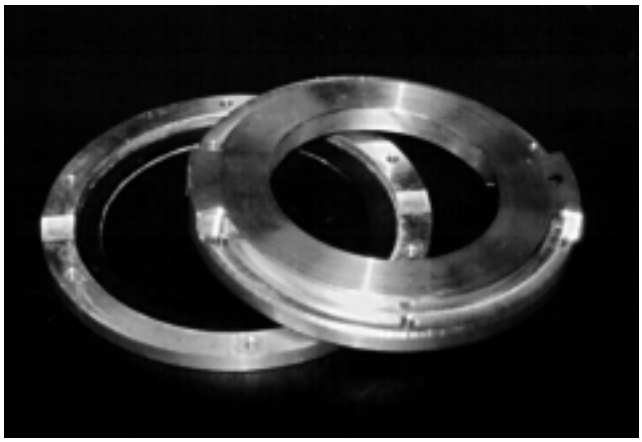

Figure 7: The micromodel holder. Refer figures 11(a) & (b) for the design.

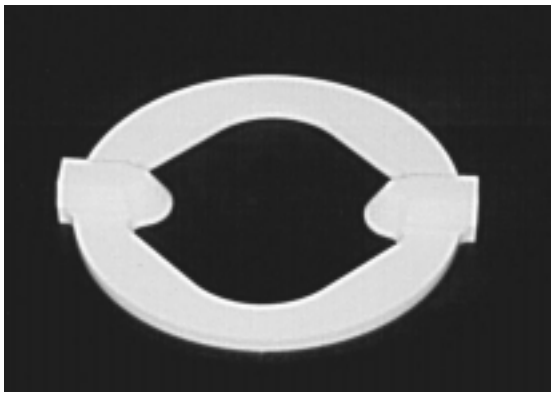

Figure 8: Photograph of the acid resistant plastic (Teflon) connector which is mounted between the micromodel holder shown in Figure 7.

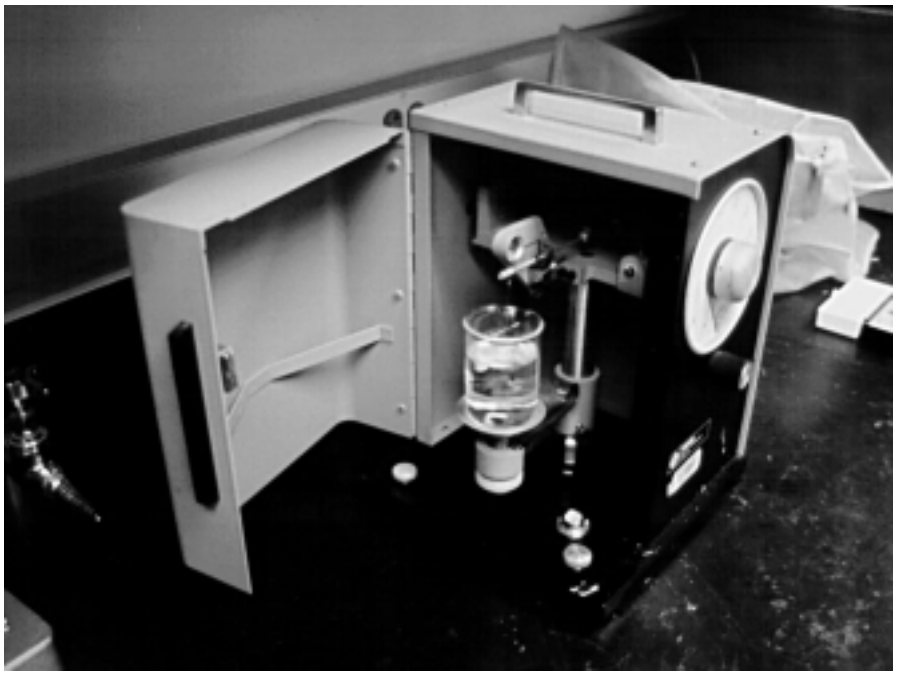

Figure 9: Surface Tensiometer

Figure 10: Spinning drop apparatus used for interfacial tension measurement.

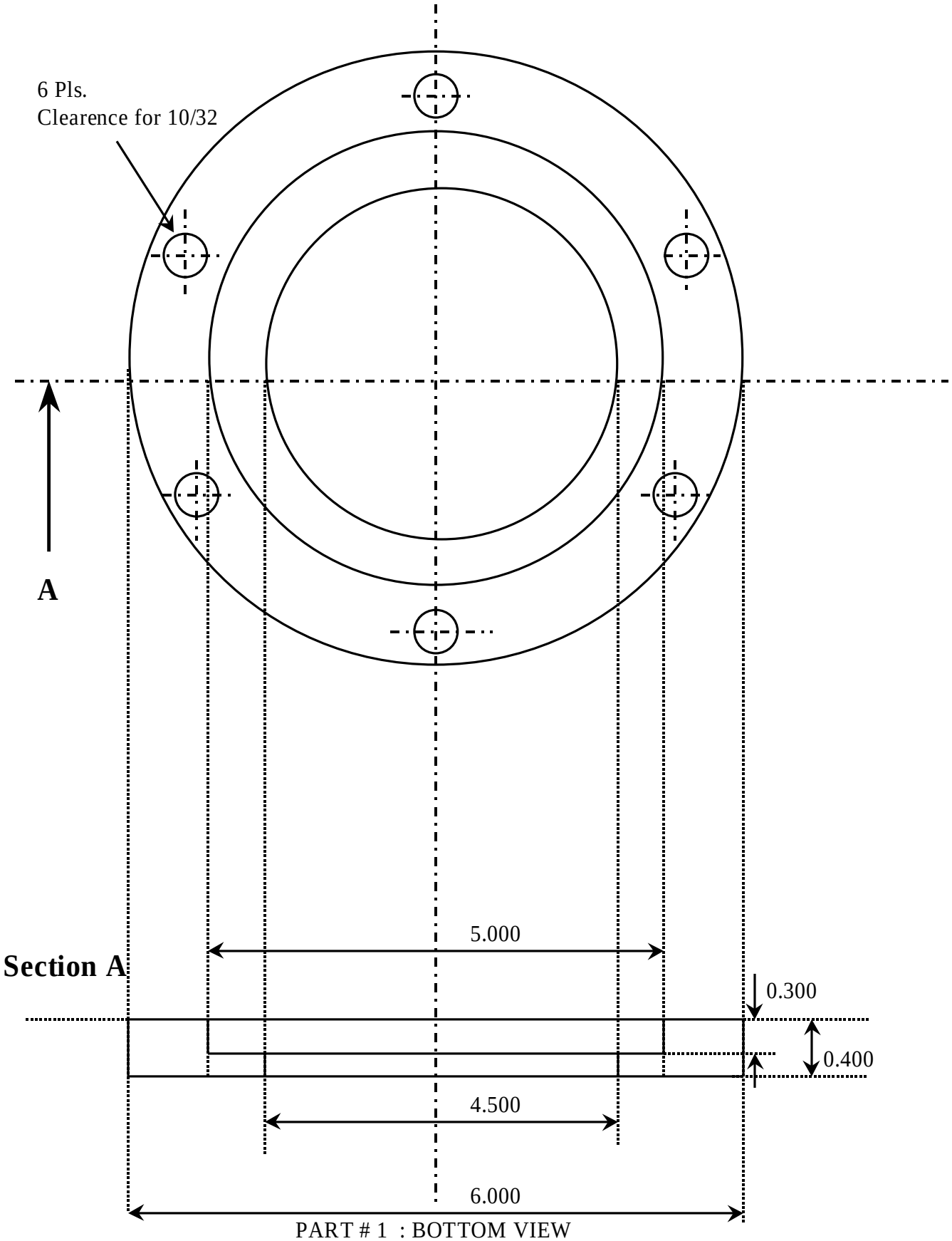

Figure 11(a): Design of the Micromodel Holder

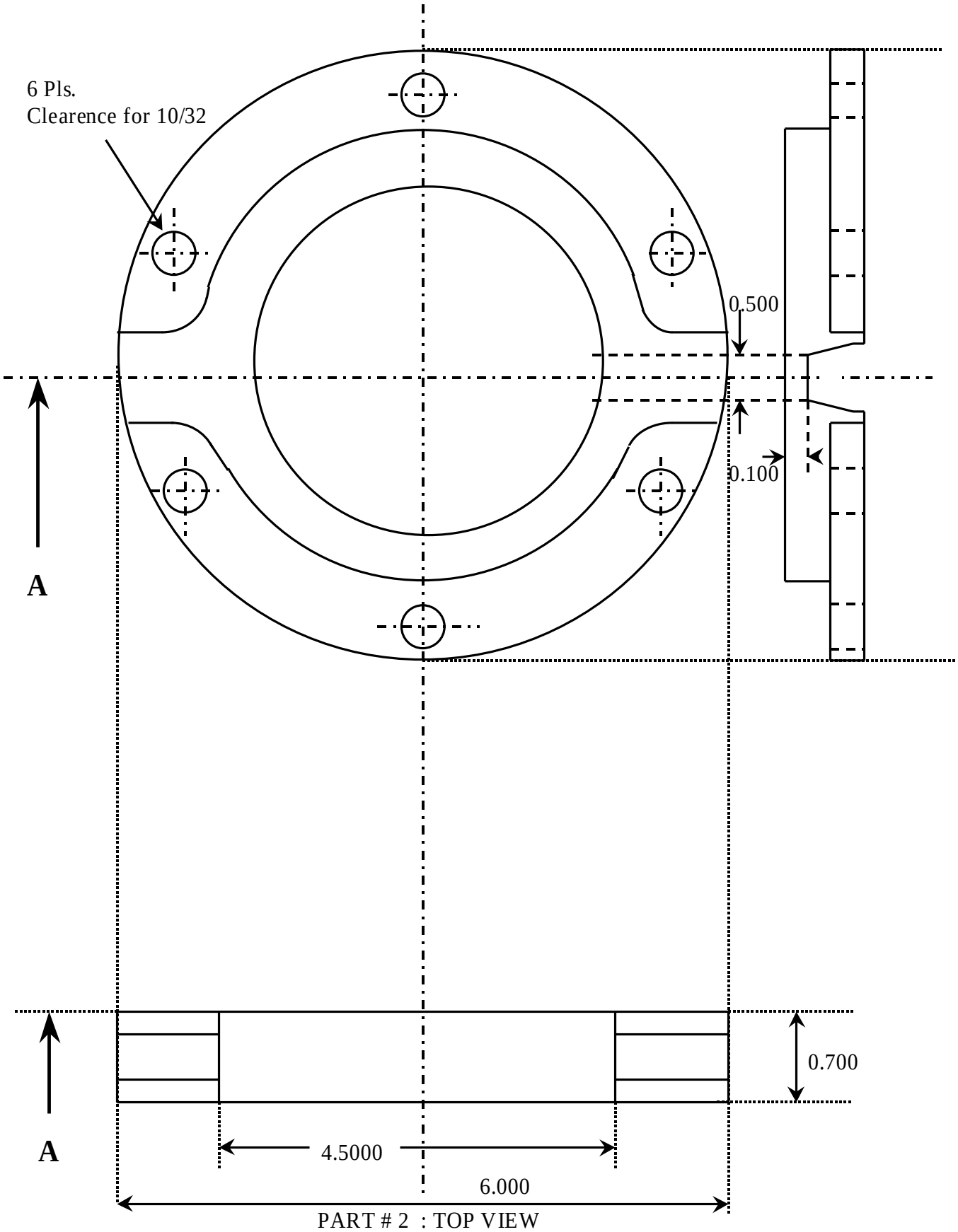

Figure 11(b): Design of the micromodel Holder

Section 4

The Silicon Micromodel

Microvisual apparatus of several kinds have been used to visualize the interaction of constrained foam lamella with oil. This section talks briefly of the design of the silicon micromodels as opposed to the glass micromodels. It then goes on to define the characteristics of the two different types of silicon models which were used for the experiments.

4.1 Design of the Micromodels

Initially micromodels were etched in glass. The first type consisted of regular, straight or constricted channels, made into an interconnected lattice. They are useful in comparing experimental observation with theories of fluid flow in regular systems and provide a useful conceptual link to other media such as capillary tubes. Later the designs were improved upon to include images of actual rock pores. Three dimensional continuity was a natural loss.

For glass micromodels, the reaction kinetics of acid etching makes it necessary to enlarge the pore sizes of typical sandstone by a factor of 5 to 50 compared to the original size.

This turns out to be a limitation in studying processes that depend critically on capillary forces. Acid etching also introduces a degree of surface roughness to the pore walls.

The micromodels used in our experiments comprise the next generation of pore-models. The design replicates the pore structure of Berea sandstone on a silicon wafer. The fabrication technique is a direct adaptation of the etching techniques used by the computer industry. The pore cavities are created photochemically, a process which is not rate-limited such as acid etching. These high resolution silicon micromodels offer 1:1 scaling of the Berea sandstone pores and throats. A detailed description of the fabrication and construction process of the models used can be found in Hornbrook *et al*. (1992), Woody *et al*. (1995) and Lolomari *et al*. (1996).

The construction involves four major steps.

1. Imaging
2. Etching
3. Bonding
4. Finishing

Imaging of the model onto the silicon wafer involves the digitization of a rock section into a computer from a high quality photograph. The section, which is approximately 500µm across is replicated to fill an area of 5 cm^2. After assuring two dimensional continuity, the image is reproduced on a chrome or glass mask. The grains being opaque and the pores being transparent. A coating of photoresist is placed on the silicon wafer. An ultravilolet ray is passed through the mask onto the wafer producing the image. After the exposure, the flow path image exists as clean silicon for the pores and photoresist coated silicon for the grains.

Once the pattern has been created using the photoresist, a dry etch technique is used to create the network of pores and grains on the wafer.

Anodic bonding of the silicon wafer requires the placing of a glass plate (pyrex) on top of the silicon wafer. At elevated temperatures (limited by the softening point of the pyrex), the positive sodium ions in the glass become quite mobile. They are attracted to the negative electrode on the glass surface where they are neutralized forming a bond. A description of the anodic bonding process is provided by Terry (1975). Pyrex is ideally suited for the above procedure because its coefficient of linear expansion (3.25×10^{-6} /^{o}C) is very close to that of silicon (2.56×10^{-6} / ^{o}C) and it is inexpensive and readily available. Detailed properties of the pyrex are attached in Appendix B.

Port holes are drilled and aligned to match those on the wafer. Electrodes are attached to the model and the bonding is done. An additional glass plate is epoxied to the bottom of the wafer to provide support. The bond strength of the silicon to the glass due to the anodic bonding is great but the strength of the silicon itself is not. Therefore large pressure drops can cause the wafer to break. To strengthen the micromodel, this additional glass plate is epoxied to the bottom of the silicon wafer.

A description of the pore structure of the model along with permeability calculations can be found in Woody et al. (1995). A photograph of the repeat etch pattern can be seen in Figure 14. Scanning Electron Microscopy (SEM) photographs of the model can be seen in Figures 13, 15 & 16.

Models Currently Being Made

The new models currently under construction are being etched at the 'Center for Integrated Systems' at Stanford. The etching will be done using the STS DRIE etcher. The details of the silicon wafer being used are:

Diameter	: 4”
Type/Dopant	: P/Boron
Orientation	: <100>
Grade	: Prime
Resistivity	: 10-20 ohm-m
Thickness	: 500-550 µm
Flats	: SEMI Standard
Frontside	: Polished
Backside	: Etched
Lot	: # 4514
Manufacturer	: Silicon Valley Microelectrics Inc., San Jose.

A positive photoresist (Type 1813) will be used up to a thickness of 1µm. Photoresist-postbake will be based on the standard program, and the photoresist side wall profile will be vertical.

4.2 Micromodel Characteristics

Two different types of micromodels were used in the study. The characteristics of these models are outlined below:

- 500 micron repeat pattern repeated 10,000 times on a 5 sq. cm silicon wafer
- Etch depth 15 to 35 microns.
- Porosity 35%
- Permeability: 1 millidarcy.
- Pore Sizes : 1-150 µm
- Throats : 0.5-10 µm

Specific Characteristics of 'Model A (old)'

- Bonding at 200-400°C & 600 Volts
- Etch depth of 15 μm
- Flow Channels only near the inlet and outlet ports.

Specific Characteristics of 'Model B (new)'

- Bonding at 450°C & 1500 Volts.
- Etch depths of 15, 25 and 35 μm.
- Flow Channels extended to the length of the sides near the inlet and outlet ports.
- Flow channel depth was up to a maximum possible etch depth of 35 μm (for all models).

Model B (new) was used for experiments one and two. Model A (old) was used for experiment three.

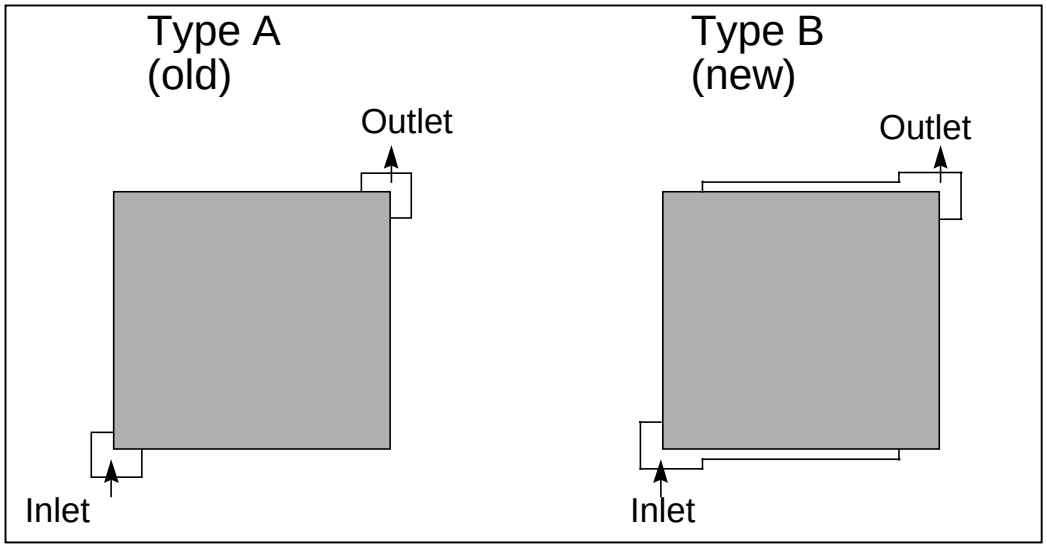

Figure 12: Flow Channels in the two silicon Micromodels

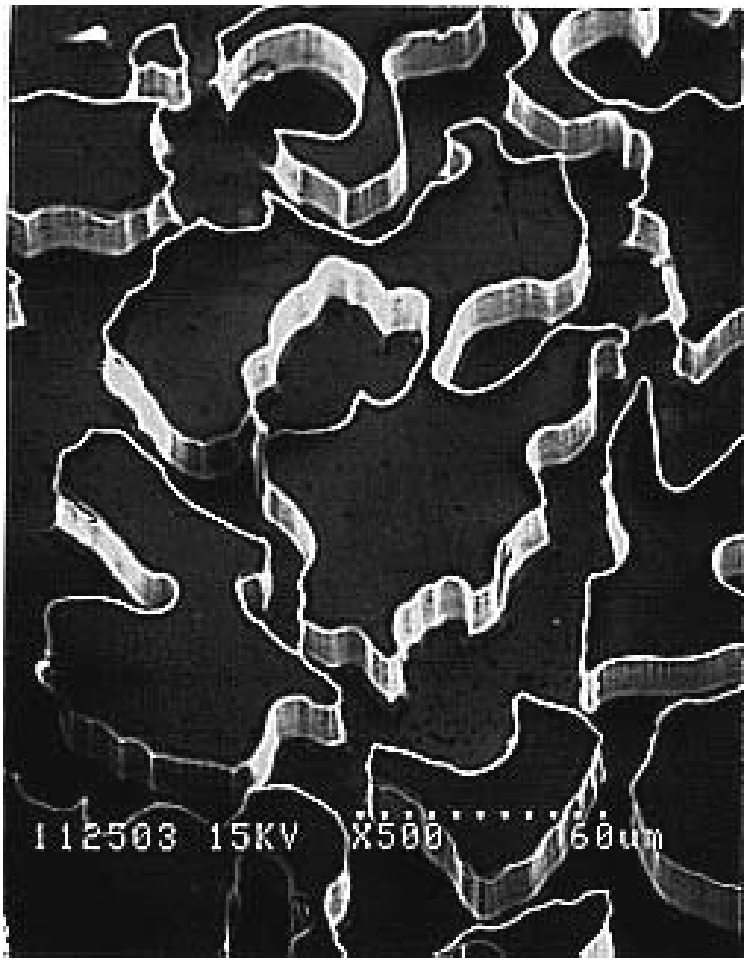

Figure 13: SEM of model A (old)


Figure 14: Photograph of the repeat etch pattern on the silicon wafer.

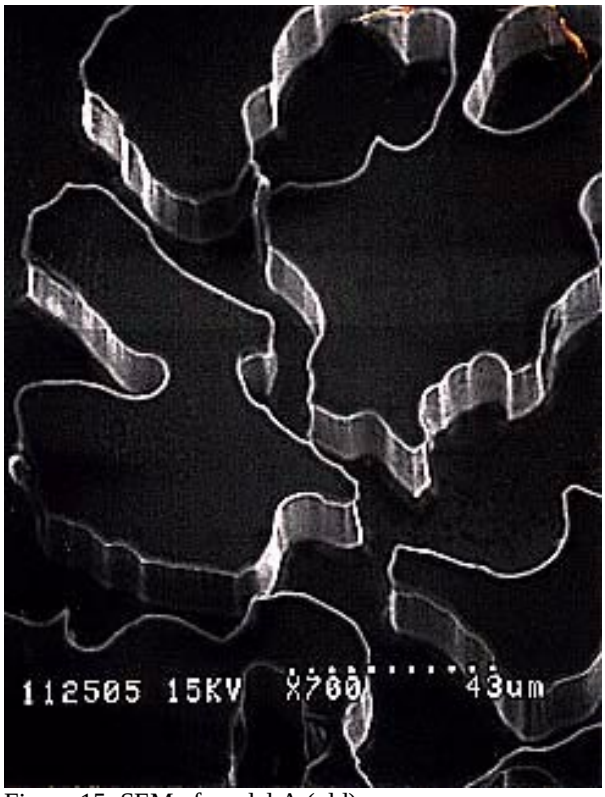

Figure 15: SEM of model A (old)

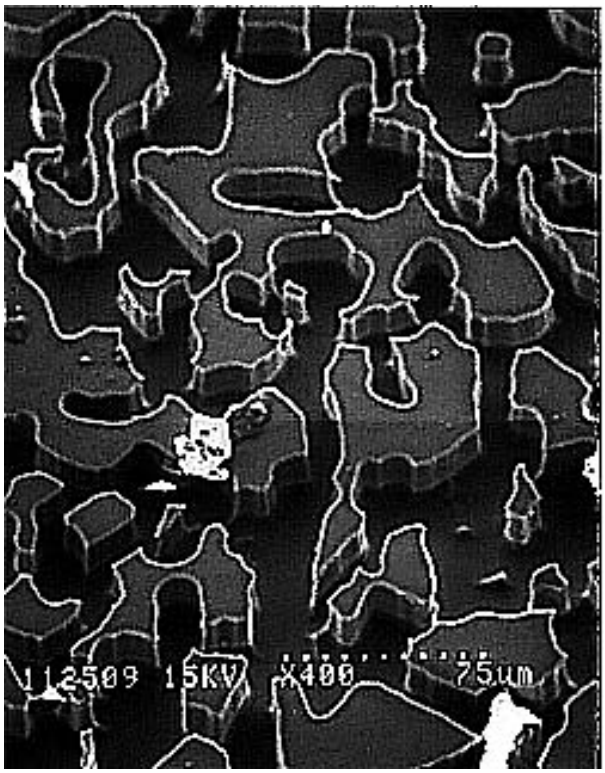

Figure 16: SEM of model B (new) showing the melted glass on the etched pattern due to bonding of the wafer with Pyrex at extreme conditions

Section 5

Experimental Procedure & Experiments Performed

5.1 Procedure

Before beginning the experiments, the model was first cleaned with water followed by methanol to remove traces of foam or solvent. All the experiments were performed at ambient temperatures using the following generic procedure:

1. CO_2 Flood
2. Water / Brine flood to dissolve all CO_2.
3. Oil flood to connate water saturation.
4. Water / Brine flood to residual oil saturation.
5. Surfactant flood.
6. Gas Injection to generate foam
7. Surfactant flood (Higher concentration)
8. Gas Injection to generate foam

Steps 5 and 6 were repeated (as shown in 7 and 8) for higher concentrations of surfactant. Before beginning each experiment, the models were cleaned using water and methanol. The outlet was at atmospheric pressure and the inlet pressure was measured. All fluids

entering the micromodel were filtered to 0.22μm. A soluble dye was used to color the surfactant so that it could be visualized better. The dye used was an ethyl-oil soluble dye: benzene-azo-2-Napthol. Note that interfacial properties were not affected by the dye.

5.2 Experiments Performed

All the experiments were recorded on videotape. The following procedure was adapted to generate the pore level photographs you see in this report.

1. Image capturing on the Macintosh using 'Spigot' capture board from the tapes being played on the Video Cassette Recorder.

2. Using 'Adobe Photoshop, Version 4' for enhancing the quality of the captured image.

3. Converting the image to JPEG format to enable viewing of the images with a web browser and also for importing into Microsoft Applications.

4. Transferring the images in JPEG format from the Macintosh to our mainframe computer from where they were transferred to 'Microsoft Powerpoint' for generating the presentation material and 'Microsoft Word' for use in this report.

The SEM and equipment photographs were all scanned using an Apple Scanner and the quality enhanced using 'Adobe Photoshop'. Steps 3 and 4 were then repeated for the scanned images.

The experiments conducted are tabulated in Table 2.

Table 2: Experiments Conducted.

Experiment	Surfactant	Concentration	Oil	Model Type
1.	AOS 1618	0.001% 0.01%	Oseberg Crude	B
2.	Nansa (AOS)	0.001% 0.01% 0.1% 1%	Kerosene	B
3.	FC 740 (In Kerosene)	0.01% 0.1% 1%	Kerosene	A

For Experiments 2 & 3, brine was used as the aqueous phase instead of water. The following table lists the brine formulation. This formulation is based on actual North Sea water. The brine was filtered with a 0.45 Milli-Pore filter.

Table 3: Composition of Brine (Wetting Phase in Experiments 2 & 3)

Chemical	Grams/ Liter
NaCl	24.79
$MgCl_2.6H_2O$	11.79
KCl	0.80
$CaCl_2.2H_2O$ **	1.60 **
$SrCl_2.6H_2O$	0.021
Na_2SO_4	4.14
$NaHCO_3$	0.206
Formaldehyde (1000ppm)	2.7

** $CaCl_2.2H_2O$ was not added because of possible precipitation problems.

Section 6
Results

The results of the three sets of experiments conducted are described in this section. Each set of experiments is discussed separately, and is accompanied by images captured during the course of the experiment.

6.1 Experiment 1

Experiment 1 was the only experiment in which crude oil (Oseberg) was used as the non-wetting phase. The surfactant used was an Alpha Olefin Sulfonate AOS 1618 and the gas used for foam generation was carbon dioxide. The aqueous (wetting) phase was water and the model used was 'B'.

The pressure difference applied to the micromodel was usually 35psig. During this experiment we did not have the fabricated micromodel holder (Figures 7, 11) and used the holding technique described by Lolomari et al. (1996).

Only two different concentrations of the AOS surfactant were used in this experiment after which the experiment was discontinued due to excessive clogging and asphaltene deposition.

6.1.1 Observations

The flow through the micromodel was extremely slow as compared to the flow mentioned by Hornbrook et al. (1992) and Woody et al. (1995) even though the etch depth for the new models (Type B) was greater then those used by Hornbrook and Woody. The time it took to flood the model with carbon dioxide or water was in the region of a couple of days.

Carbon dioxide was seen to bubble out through the outlet channels rather slowly. The bubbles would originate on the extreme corner of the channel (Figures 17, 18, 21) and would start out as very small bubbles coalescing to form bigger bubbles before flowing towards the outlet port. The water along with dissolved carbon dioxide (during water flood) could be seen flowing in films in the outlet channel (Figure 20).

On injecting crude oil through the inlet channel it could be seen that the crude oil did not fill the model uniformly (Figure 22). After injection of the surfactant stable crude oil emulsions were observed in the model (Figures 19, 26). These emulsions were seen at concentrations of 0.01% and were observed to be stable in certain pore geometries in the micromodel. An oil film could also be seen encapsulating the injected carbon dioxide in the inlet port (Figure 27).

An emulsion forming sequence with the crude oil was observed where crude oil bubbles started forming in a narrow throat and were seen being pushed into a pore where these bubbles conjoined to form an emulsion (Figure 23). This was in the presence of 0.01% surfactant concentration.

A bubble coalescence sequence was also observed where carbon dioxide bubbles coated with crude oil were generated from a very narrow throat and were pushed into a pore where they coalesced to form a bigger carbon dioxide bubble (Figure 24).

An emulsion breakdown sequence was also seen to occur in a pore. A very visible crude oil emulsion broke down in a matter of seconds and was captured in the stills shown (Figure 25).

Emulsion sizes with crude oil varied from 10µm to 60µm in size. The emulsions were usually composed of water surrounded by oil films. The color of the water seemed to be darker (brownish) after contact with the crude oil. This shows some still unexplained mass transfer mechanism between oil and water.

As can be seen from the above observations, the oseberg crude oil clearly formed emulsions in the presence of the AOS surfactant indicating the non tolerant behavior of the oseberg crude oil to the AOS surfactant. No foam lamella were observed during the experiment. The displacements were according to the theory of immiscible displacement: Displacement of water by gas caused viscous fingering and displacement of water by oil was a stable front propagation.

6.2 Experiment 2

In Experiment 2, the surfactant used was also an Alpha Olefin Sulfonate (1618) and the gas for foam generation was carbon dioxide. The wetting phase was brine and the non-wetting phase (oil) was kerosene. The model type used was ‘B’.

6.2.1 Observations

Oil (kerosene) emulsions were observed at as low as 0.001% concentration of surfactant (Figure 31). During carbon dioxide flood the gas phase was discontinuous and did not fill the model completely (Figure 32). The emulsions were very mobile at low

concentrations of surfactant (< 1%) as can be seen in some of the captured stills (Figures 33, 34, 35).

Not more than one gas bubble (Carbon dioxide) was seen to in one pore. In fact in some areas one gas bubble was seen to occupy more than one pore (Figure 36). Before surfactant flood water was seen snapping off into a kerosene bubble. No emulsion was seen to form because of the absence of any surfactant in the system (Figure 30). The diameter of the emulsions were smallest at lower concentrations and were seen to increase with higher concentrations. The stability of the emulsions also increased at higher concentrations (Figures 28, 29, 37). Certain areas in the model which had less oil were seen to have thinner emulsions (Figure 39). Although at increased concentrations the oil present in the model had decreased the emulsions were still widely present and were more stable.

The emulsion size also was seen to depend on the pore geometry (Figure 38). Different sizes of emulsions seem to co-exist but varied in size with the size being the smallest in the throats and the smaller pores.

The emulsions were all composed of water covered by oil films. The size of the emulsions at 0.001% surfactant concentration was as low as 1µm (Figures 33, 34) and up to 20µm. The emulsions at this stage flowed very rapidly through the narrow throats till they clogged the flow path.

Emulsion sizes, as mentioned earlier, also increased with surfactant concentration. Although the pore geometry had also some effect, emulsion sizes after 0.1% surfactant flood varied from a few microns to about 60µm (Figures 38, 39, 40, 41). Emulsion composition after 1% surfactant flood was very similar to that seen at 0.1% except that they were more stable (Figures 28, 29). The emulsion were hardly seen to move, as was observed with lower concentrations because most of the narrow throats had been blocked by the smaller emulsions.

Two emulsion forming and breaking sequences were also observed providing a frame by frame view of the process (Figure 40, 41).

No foam was observed during the experiment. Also, flow through the model was observed to be extremely slow and was comparable to the flow in Experiment 1. This observation prompted us to investigate further into the problem. The results of the investigation are discussed after Experiment 3.

6.3 Experiment 3

In Experiment 3, we formed an oil-foam. The surfactant was a Fluoro-Carbon, FC 740, diluted in kerosene. The wetting phase was brine and the non-wetting phase was kerosene. Carbon dioxide was used to generate the foam in-situ. The model type used was 'A'.

The exploitation of the gas-blocking properties of foam by using it as a gas-coning barrier is an old idea. An attractive means of achieving a favorable barrier geometry is by using low density non-aqueous foams. This is the primary reason for our focus on the oil-foam studied in this experiment.

6.3.1 Observations

Flow through this model was extremely fast as compared to the Experiments 1 and 2. It took only about 20 minutes to flood the model completely with carbon dioxide.

After the water flood and the oil flood, water was seen residing in the narrow throats indicating that the model was water wet (Figure 42). Before foam was generated in the system, the carbon dioxide phase was observed to be very discontinuous (Figure 43). Stable foam lamellae were seen beginning at 0.01% surfactant concentration. A snap off sequence of a carbon dioxide bubble coated with surfactant was seen (Figure 44).

In certain areas at 0.1% concentration of the fluoro-surfactant, a lamella formation and breakdown sequence was captured in a five frame sequence (Figure 45).

Foam was observed as lamella all over the model at the different concentrations of the surfactant. Certain pore geometries were seen to be more conducive to forming stable lamellae then others (Figure 50). Many different lamellae configurations were seen (Figures 48, 49, 53, 54). Stable lenses were also observed to co-exist with the lamellae (Figures 47, 52).

In one configuration, a water droplet in a foam lamella did not seem to affect the lamella stability (Figure 46). Also, in a certain pore geometry a thinner stable lamella was seen as compared to lamella thickness in similar geometries (Figures 50, 51).

No significant increase in the number of foam lamellae were seen from 0.1% to 1.0% surfactant concentration, in spite of a noticeably higher gas blockage as seen from flow rate reduction.

6.4 Interfacial Tension Measurements

Interfacial tension between the surfactant solution and the oil (kerosene) was measured for Experiments 2 and 3 and is listed below. No significant difference in the interfacial tension was observed because of the presence of an ethyl-oil soluble dye: benzene-azo-2-Napthol.

Table 4: Interfacial Tension Measurement.

Surfactant	Concentration	Interfacial Tension (dynes/cm)
Nansa (AOS)	1%	1.4
	0.1%	0.71
	0.01%	1.63
	0.001%	7.9
FC740 (in Kerosene)	1%	14.928
	0.1%	8.868
	0.01%	19.686

6.5 Scanning Electron Microscopy

The flow problems encountered in experiment sets 1 and 2 as opposed to the very good flow observed in the old model (Type A) used in experiment 3 led us to investigate the etching and bonding process for the two models. SEM's were taken of both the types of models (Figures 13, 15, 16). It was observed that although the etching was similar in the two model types, melted glass could be spotted in the SEM for model B (Figure 16). It was also very difficult to separate the etch pattern from the Pyrex glass for usage in the SEM machine.

This led us to conclude that the extreme bonding conditions of the Pyrex glass in the batch of the new micromodels (450°C, 1500 Volts) was the reason for the reduction in flow rates in Experiments 1 and 2. The glass had melted in sections of the silicon micromodel reducing its permeability.

EXPERIMENT 1: FIGURES

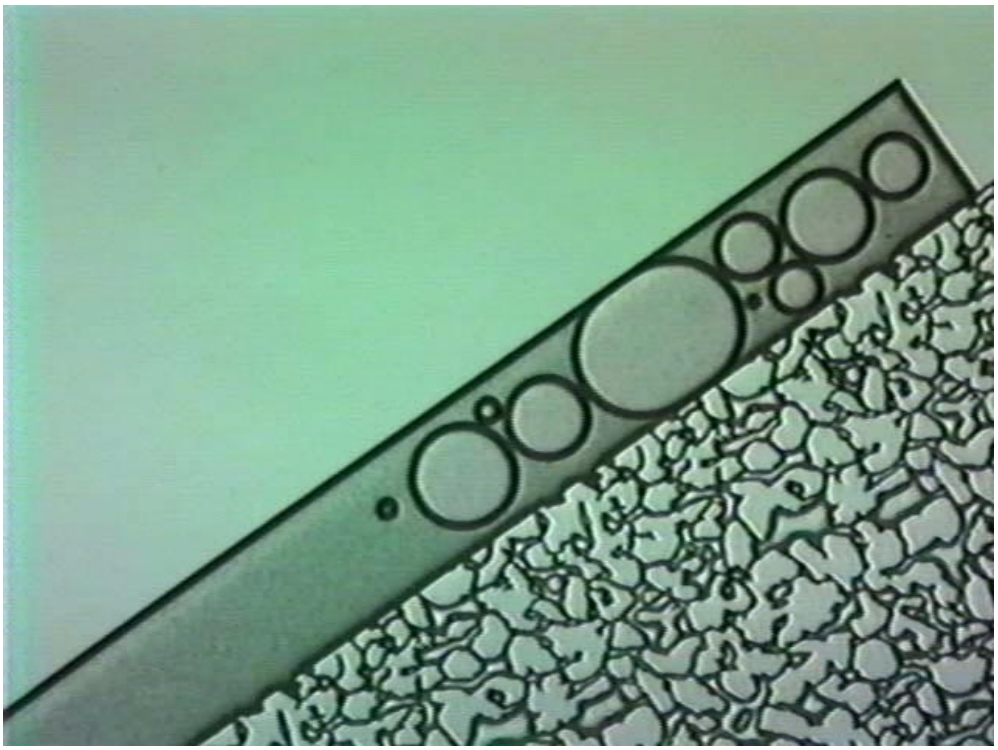

Figure 17: CO_2 bubbles flowing in the outlet channel during CO_2 flood. Flow is top to bottom diagonally.

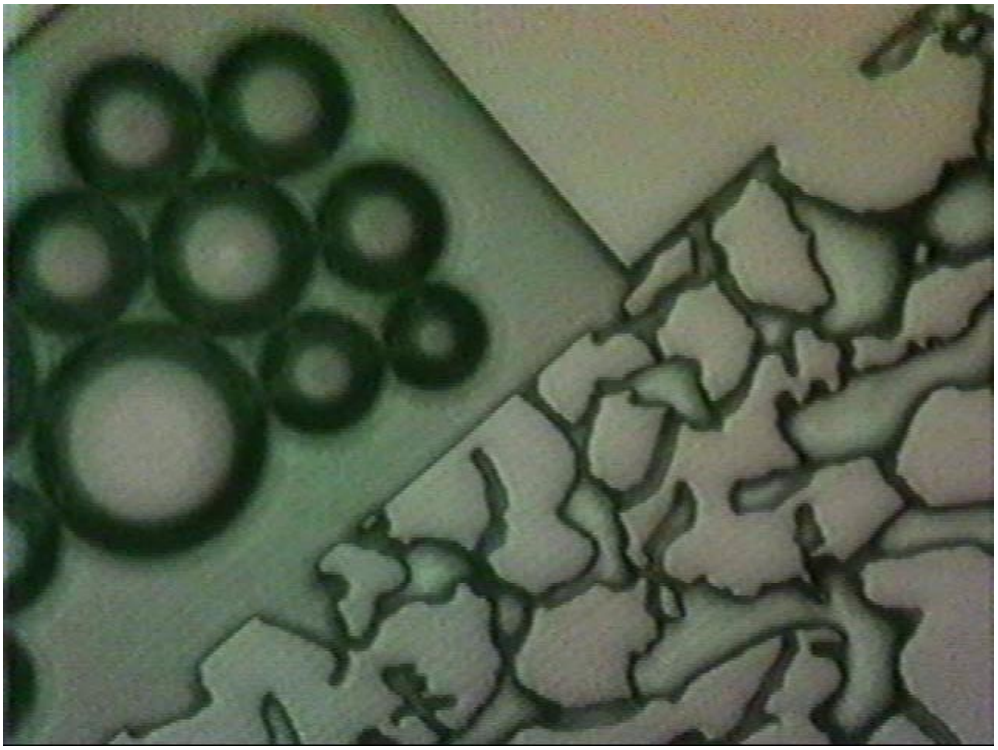

Figure 18: CO_2 bubbles have just emerged from the porous network into the outlet channel

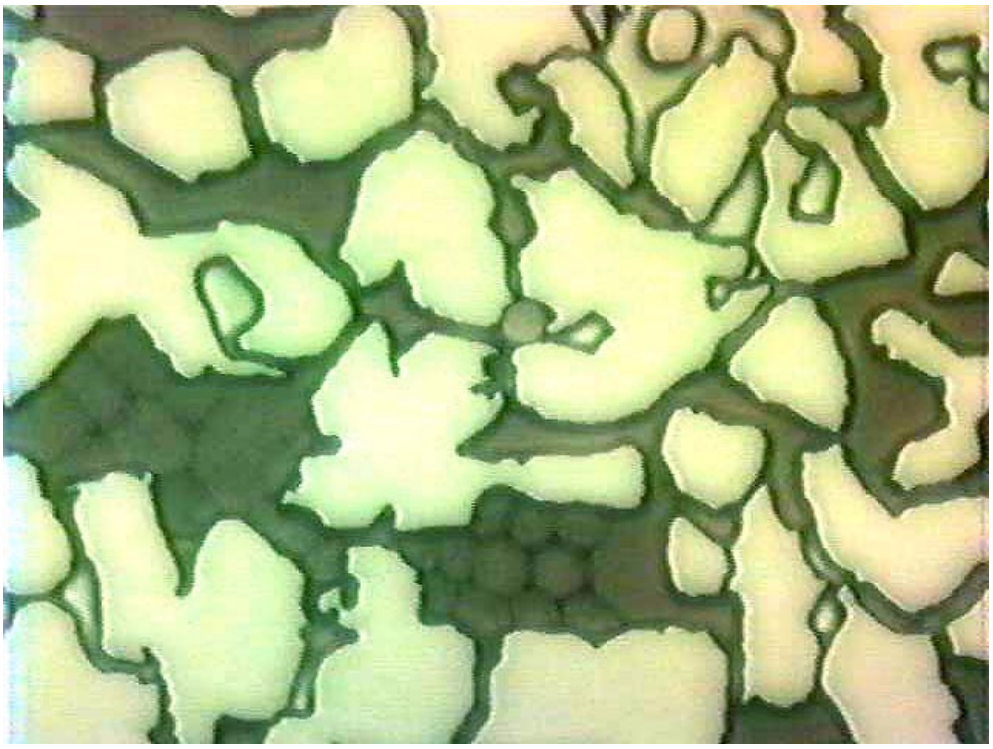

Figure 19: Crude oil emulsions seen in the large pores in the model after 0.01% surfactant flood.

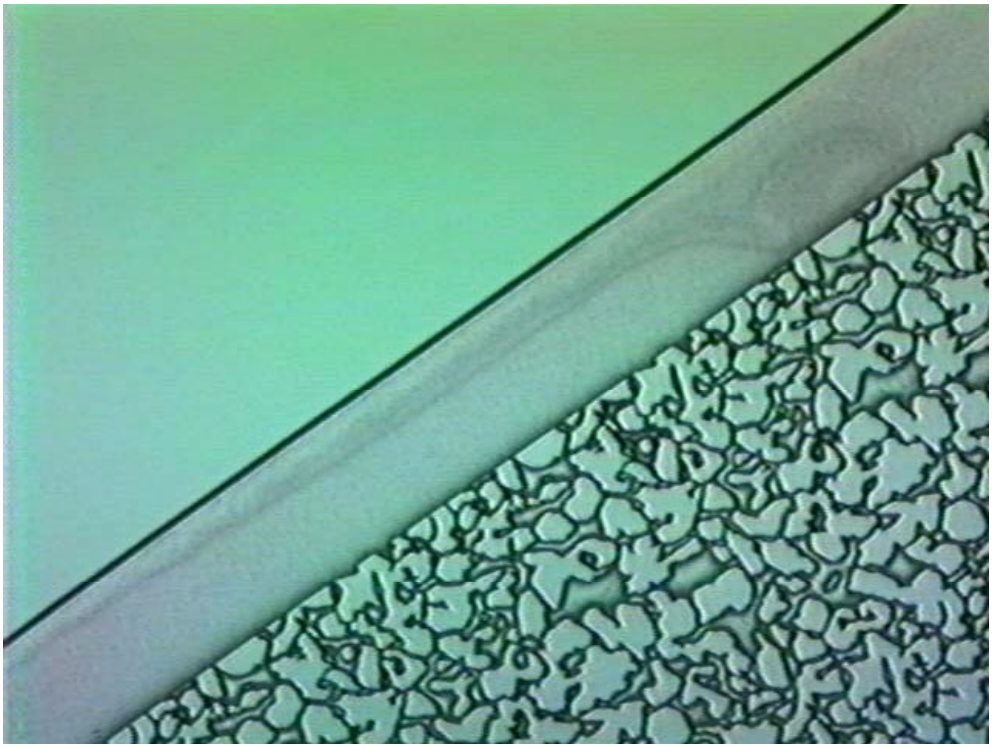

Figure 20: Water films in the outlet port during water flooding. The water contains dissolved CO_2 gas.

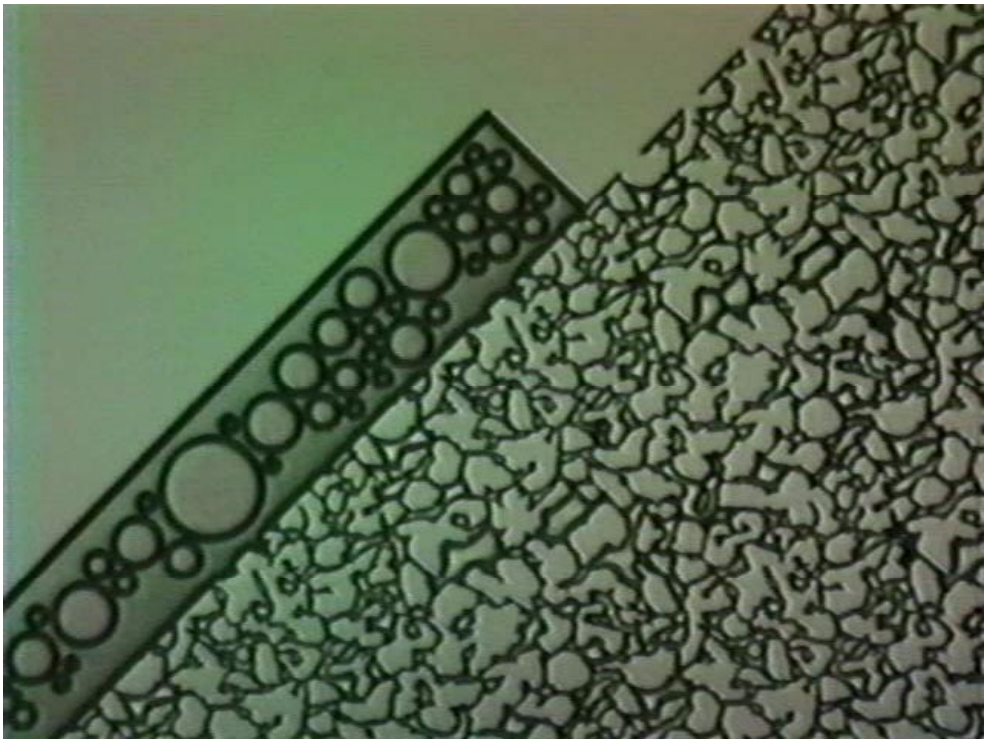

Figure 21: The CO_2 bubbles are generated near the corner. Flow is from top to bottom diagonally. The bubbles coalesce to form bigger bubbles almost instantly.

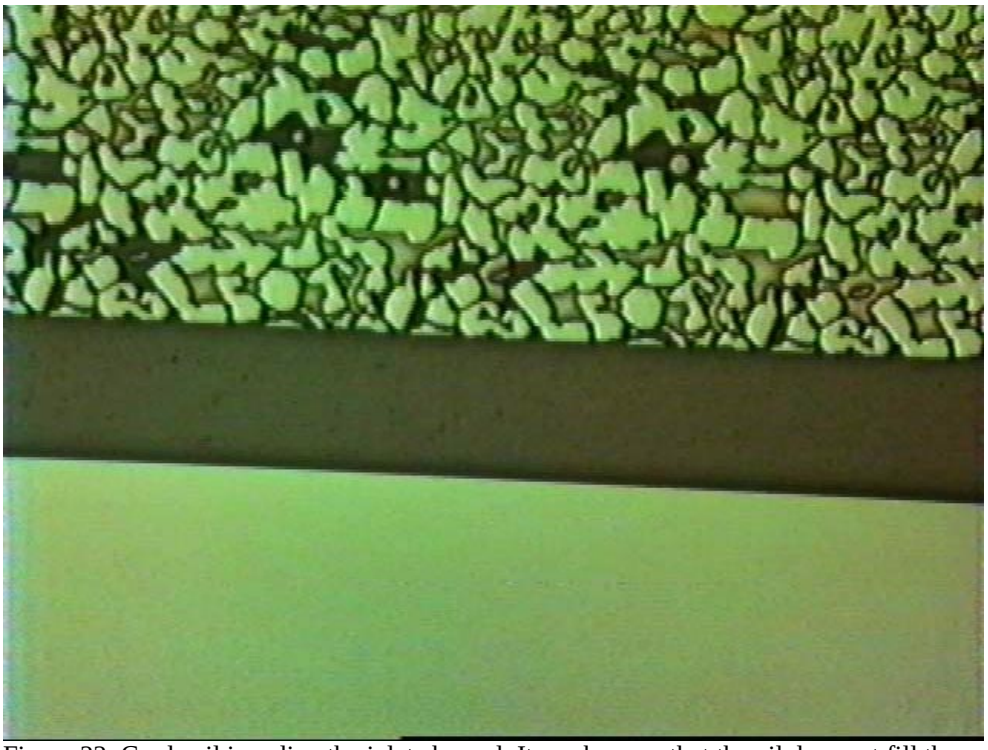

Figure 22: Crude oil invading the inlet channel. It can be seen that the oil does not fill the model uniformly.

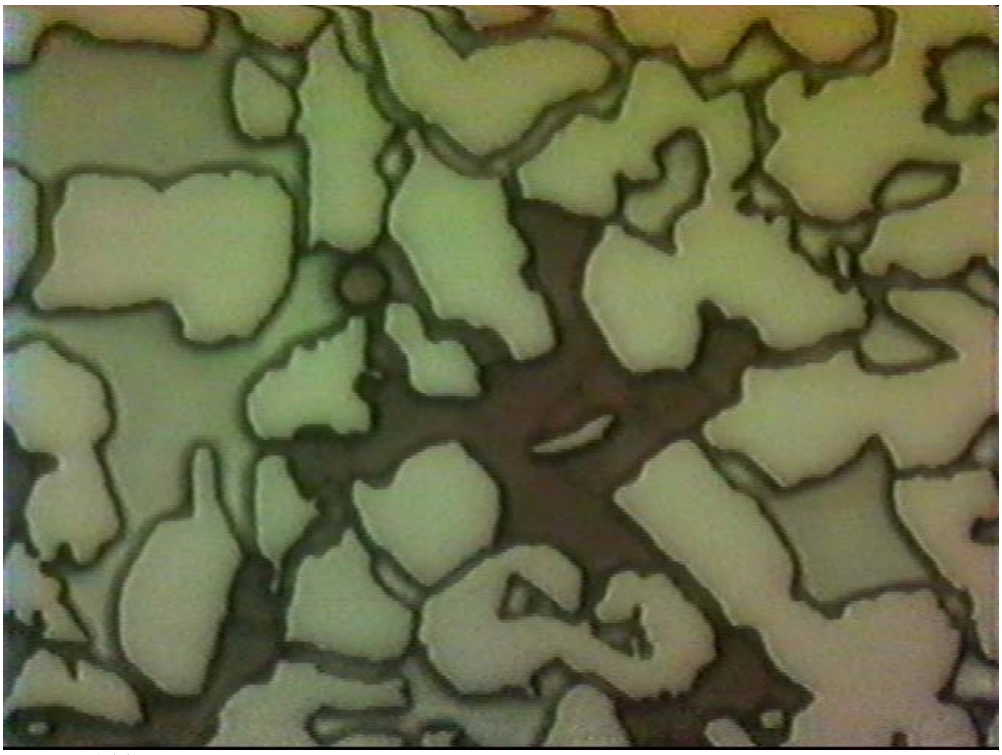
Figure 23(a)

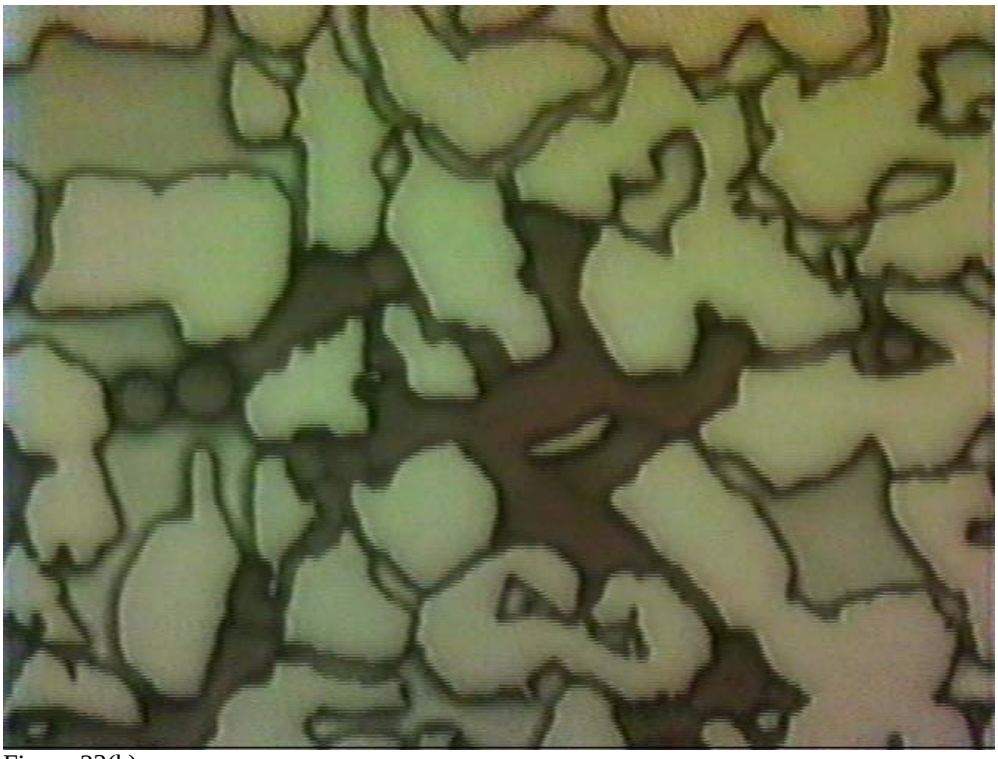
Figure 23(b)

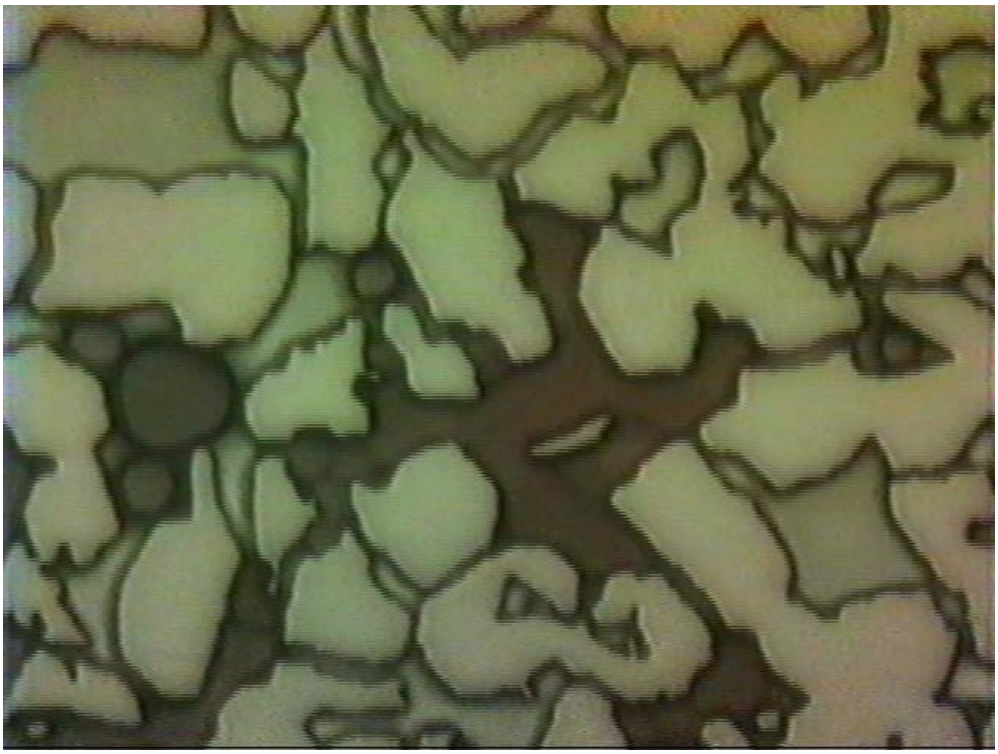
Figure 23(c)

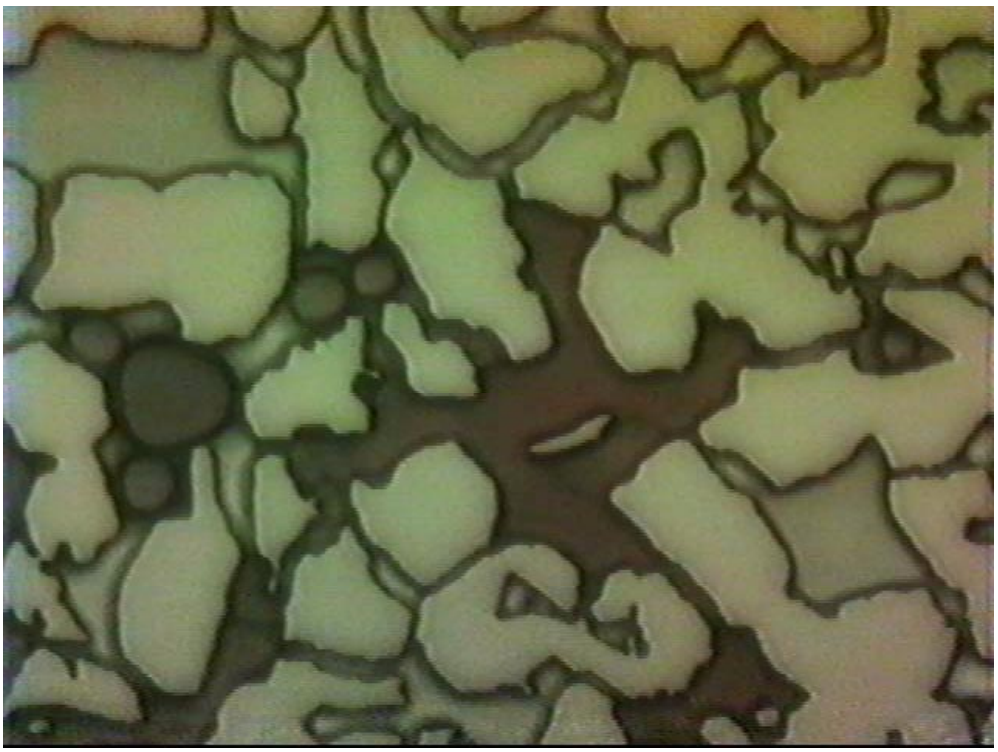
Figure 23(d)

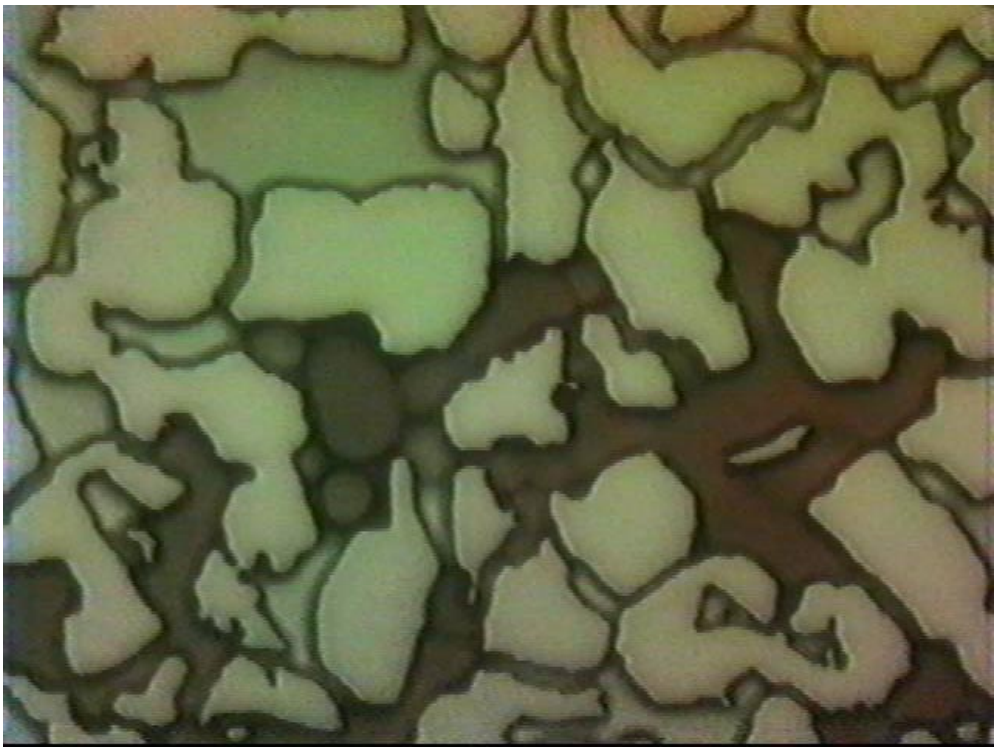
Figure 23(e)

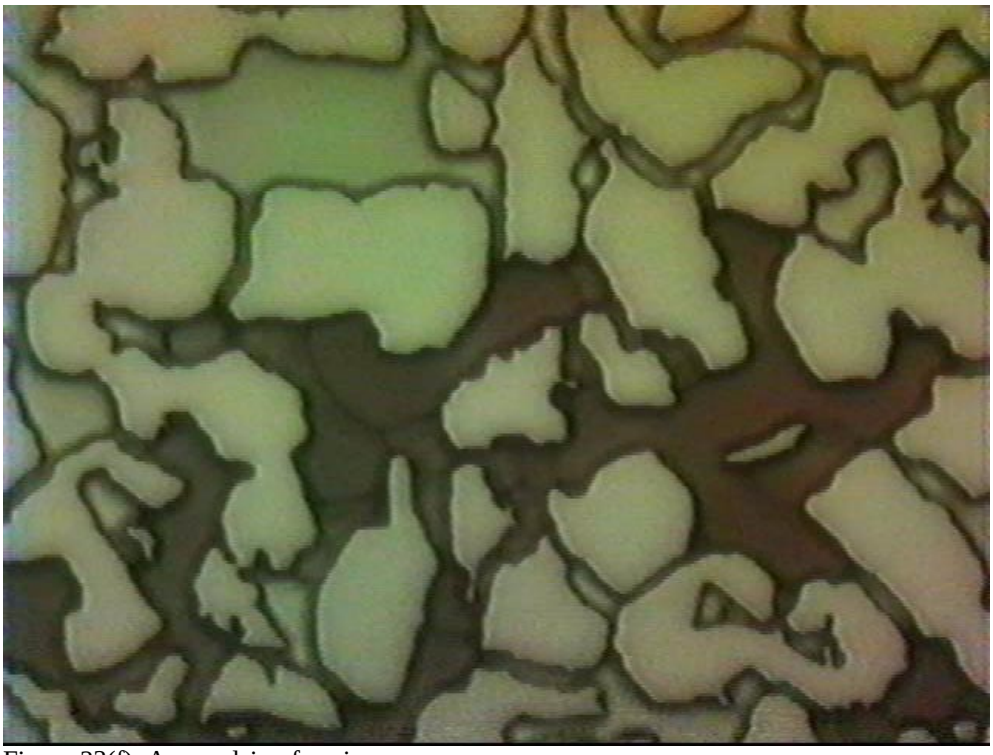
Figure 23(f): An emulsion forming sequence

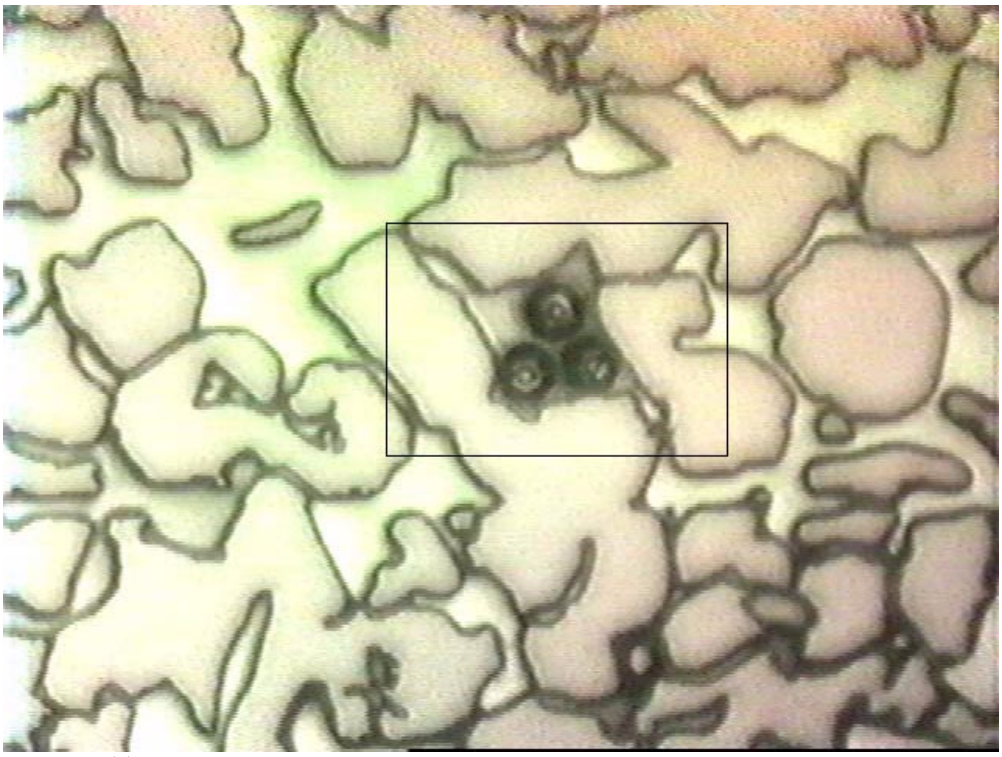

Figure 24(a)

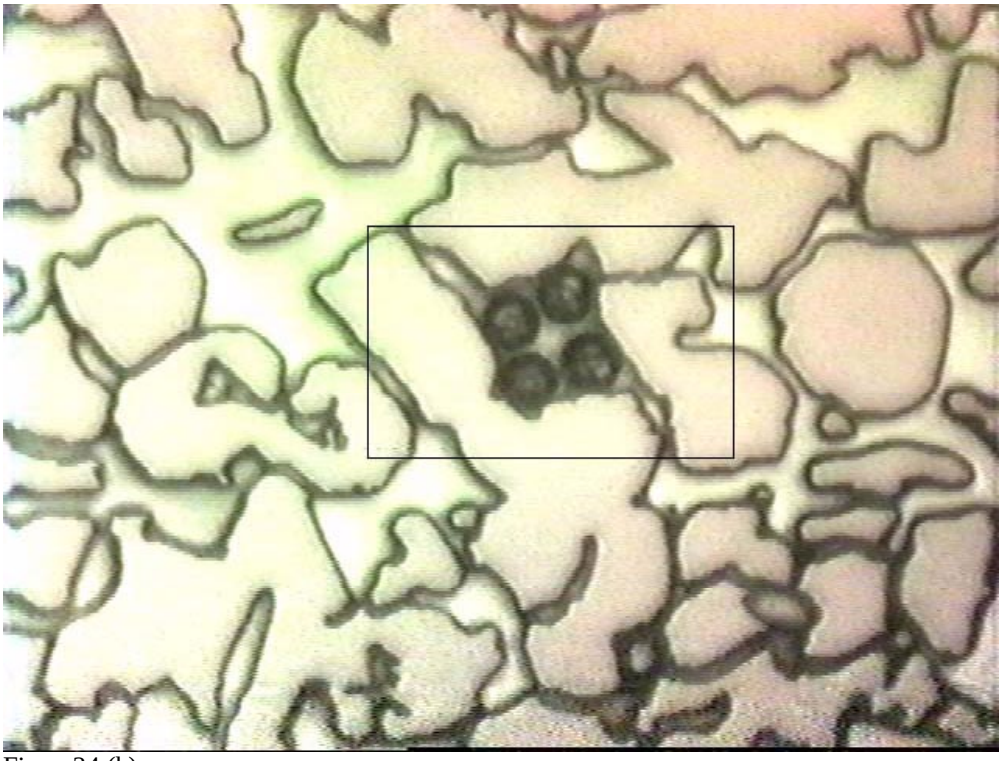

Figure24 (b)

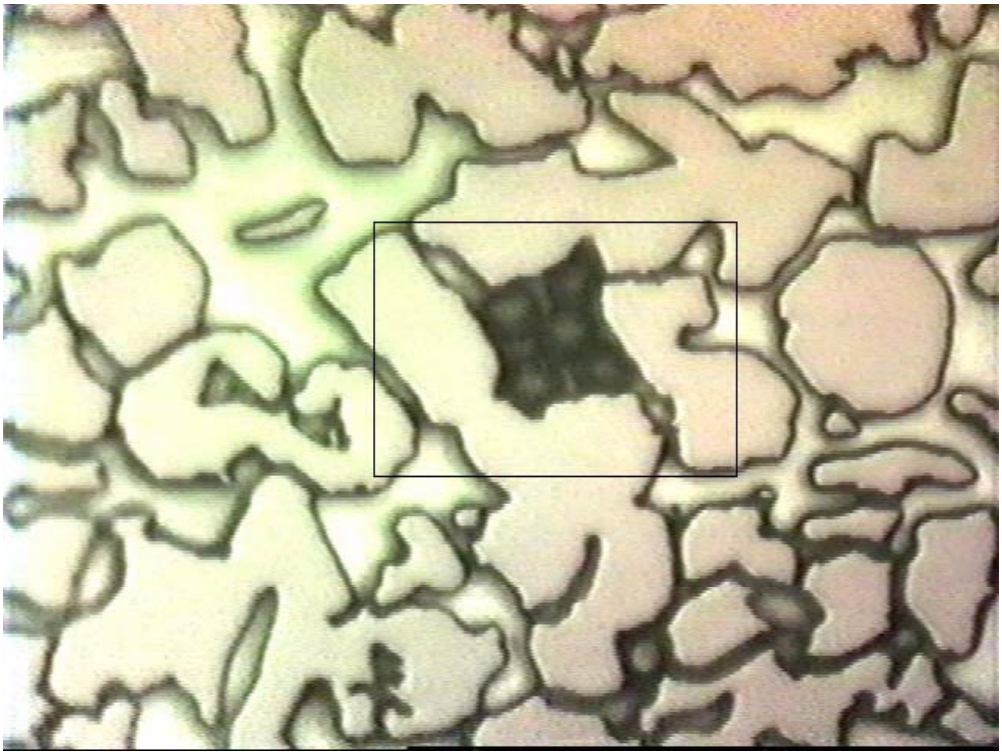
Figure 24(c)

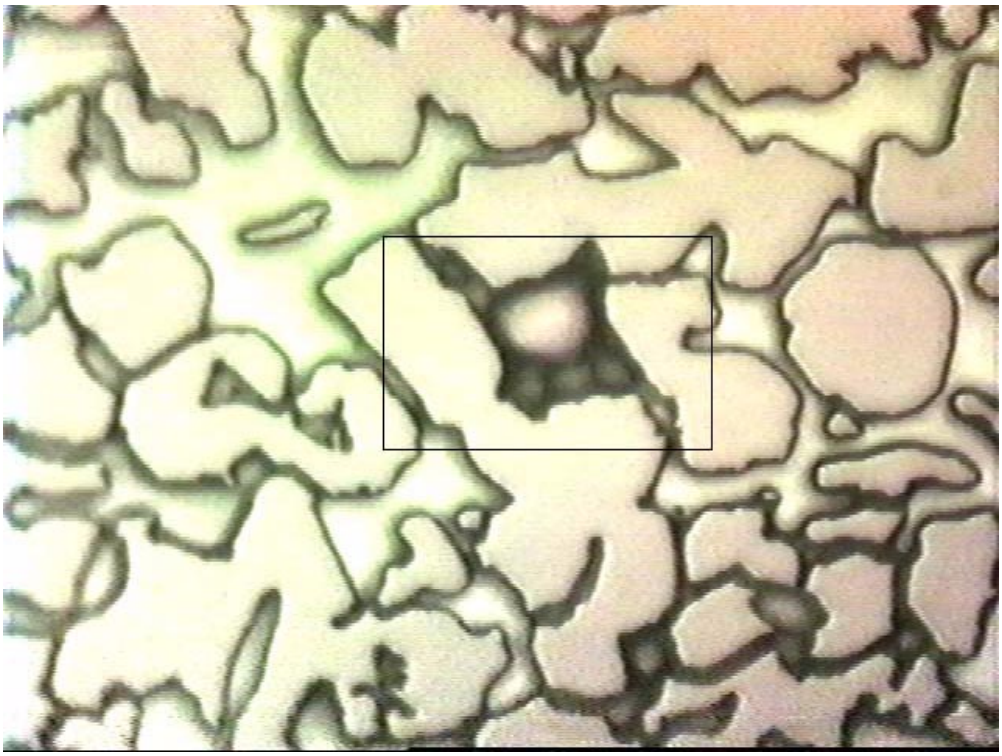
Figure 24 (d)

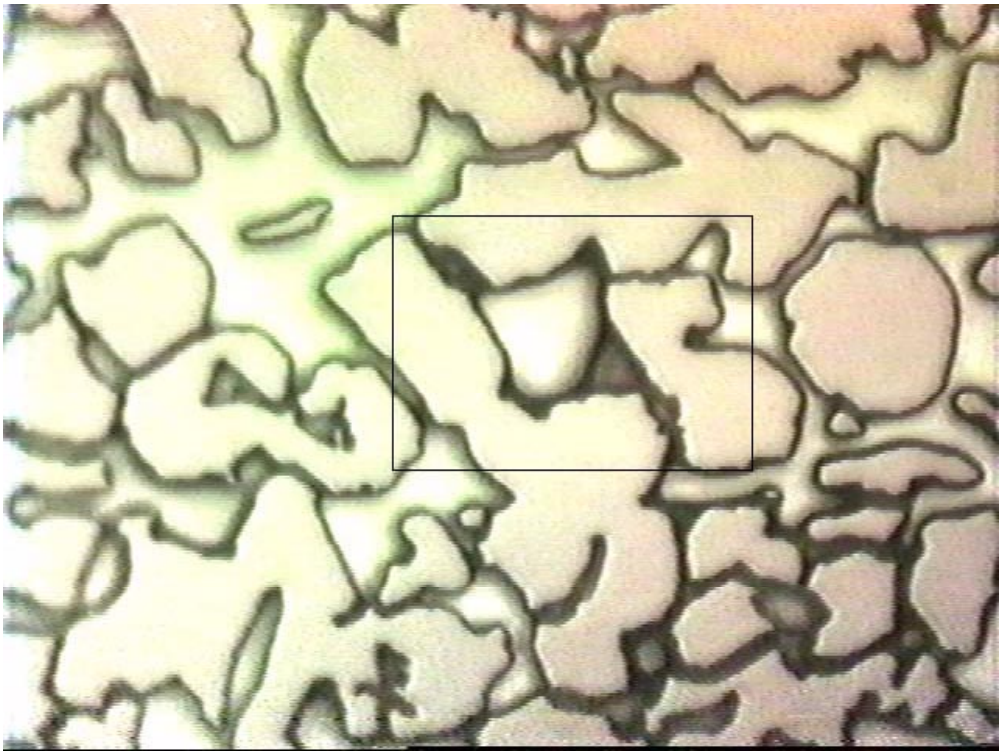
Figure 24(e): A bubble coalescence sequence.

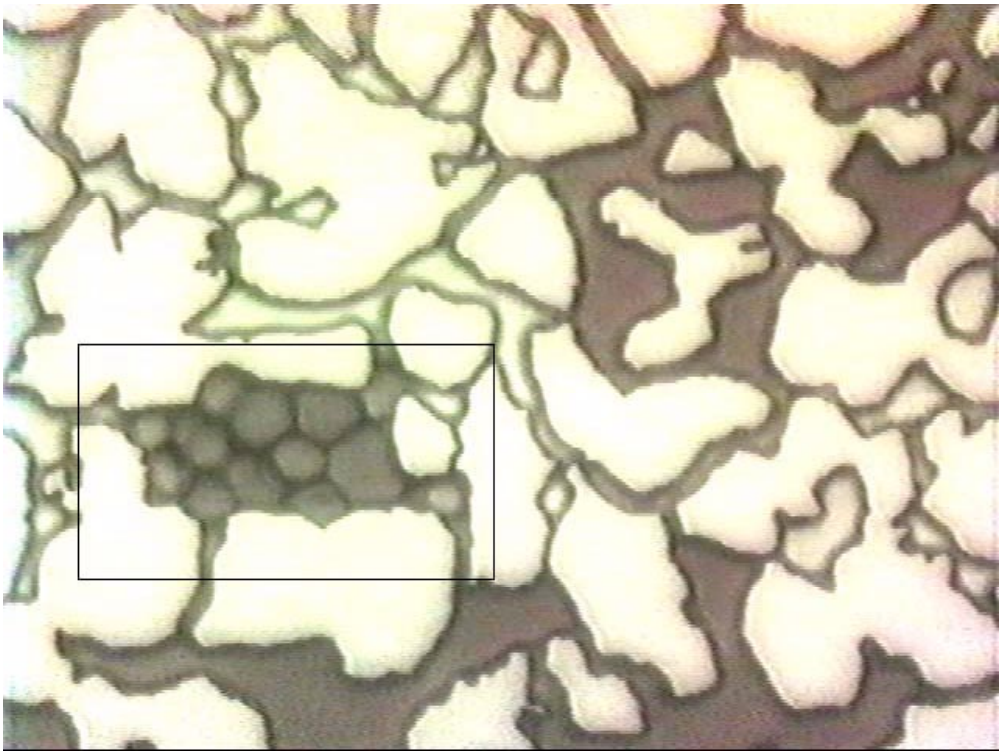

Figure 25(a)

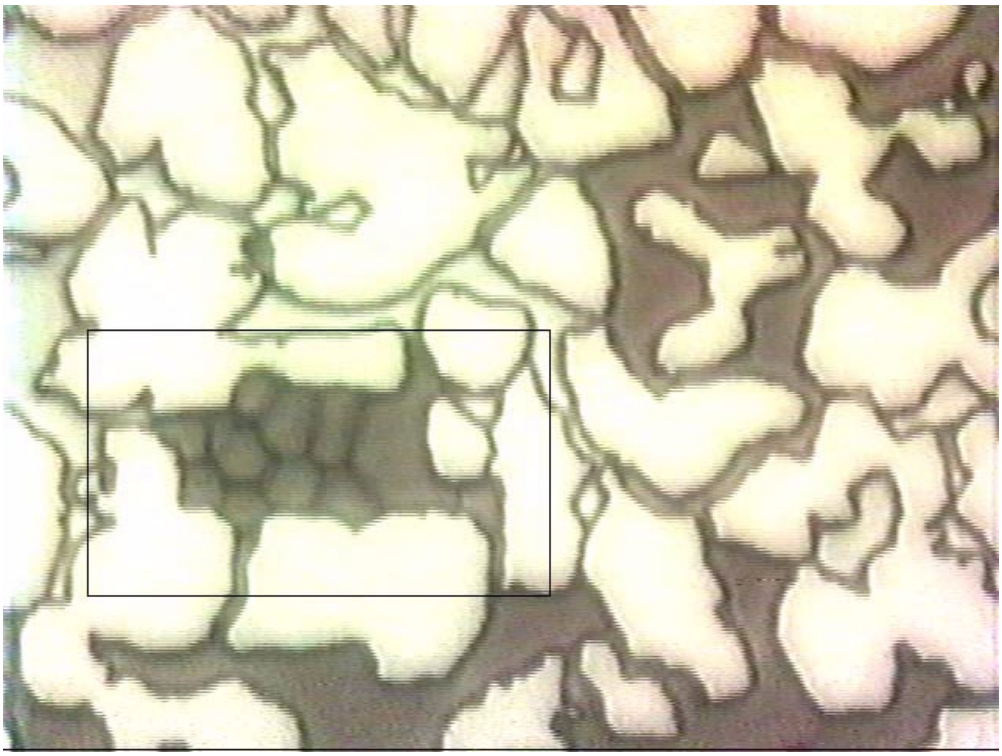

Figure 25 (b)

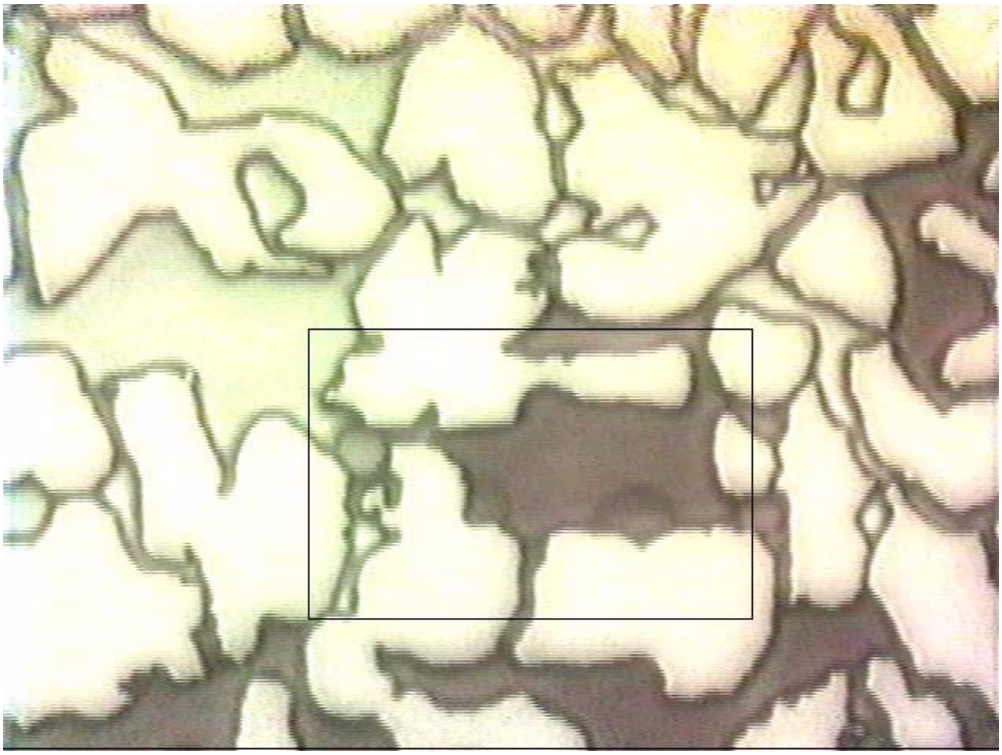
Figure 25(c): Emulsion breakdown sequence

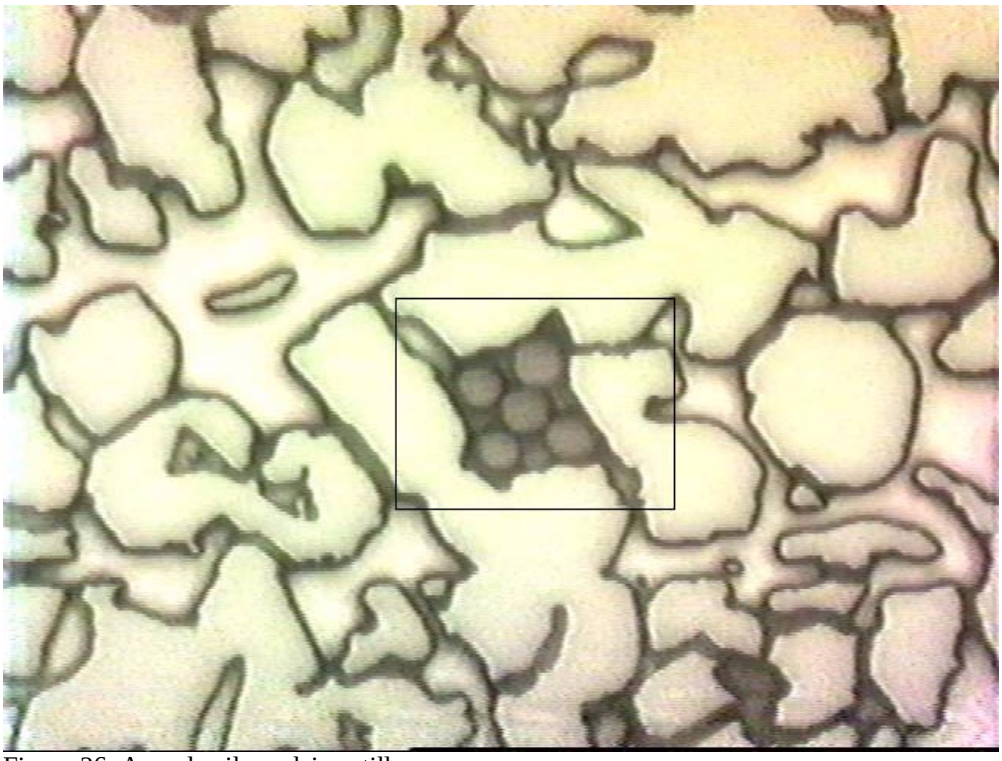

Figure 26: A crude oil emulsion still

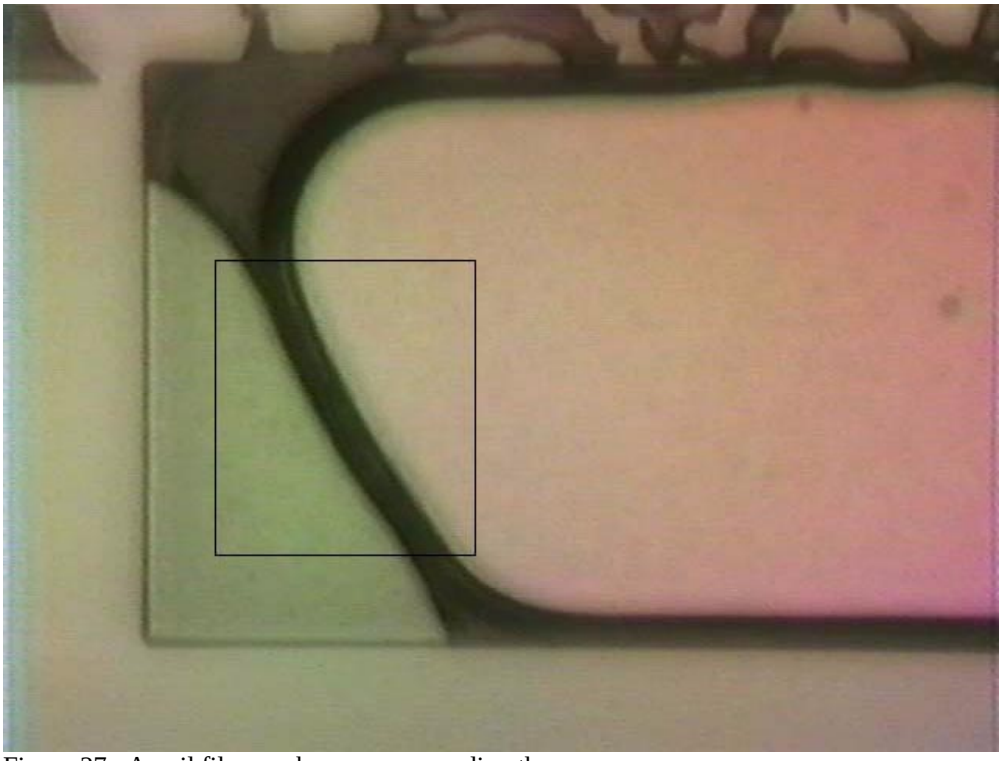

Figure 27 : An oil film can be seen surrounding the gas.

EXPERIMENT 2: FIGURES

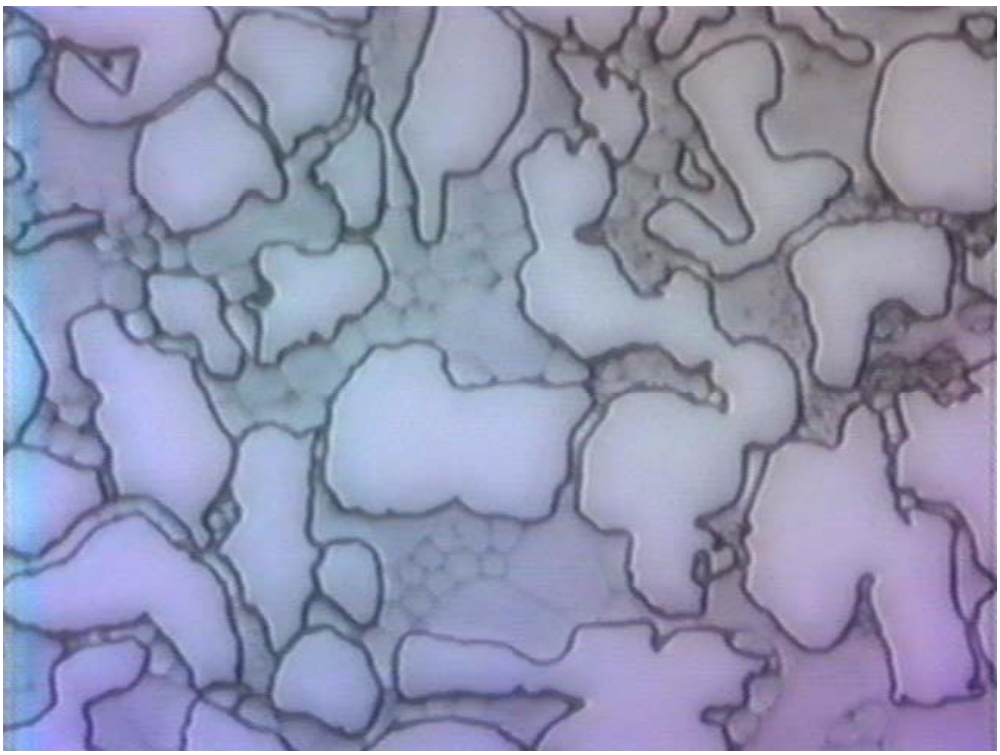
Figure 28: Emulsions as seen after 1% surfactant flood.

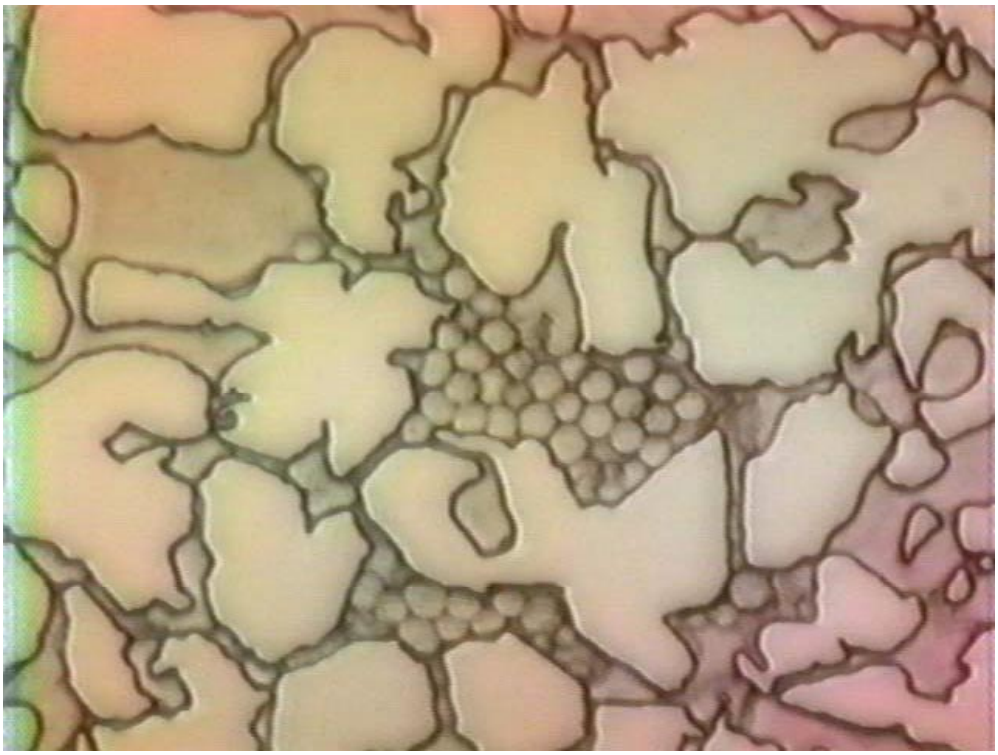
Figure 29: Very stable emulsions seen at the end of the experiment (after 1% surfactant flood).

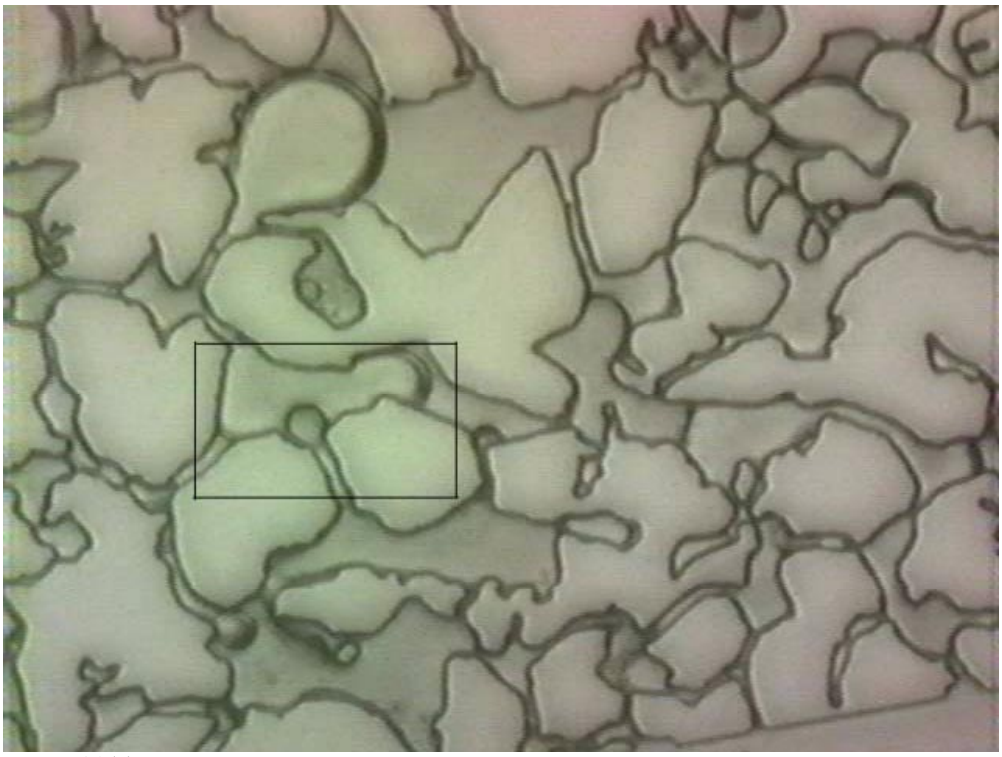

Figure 30(a)

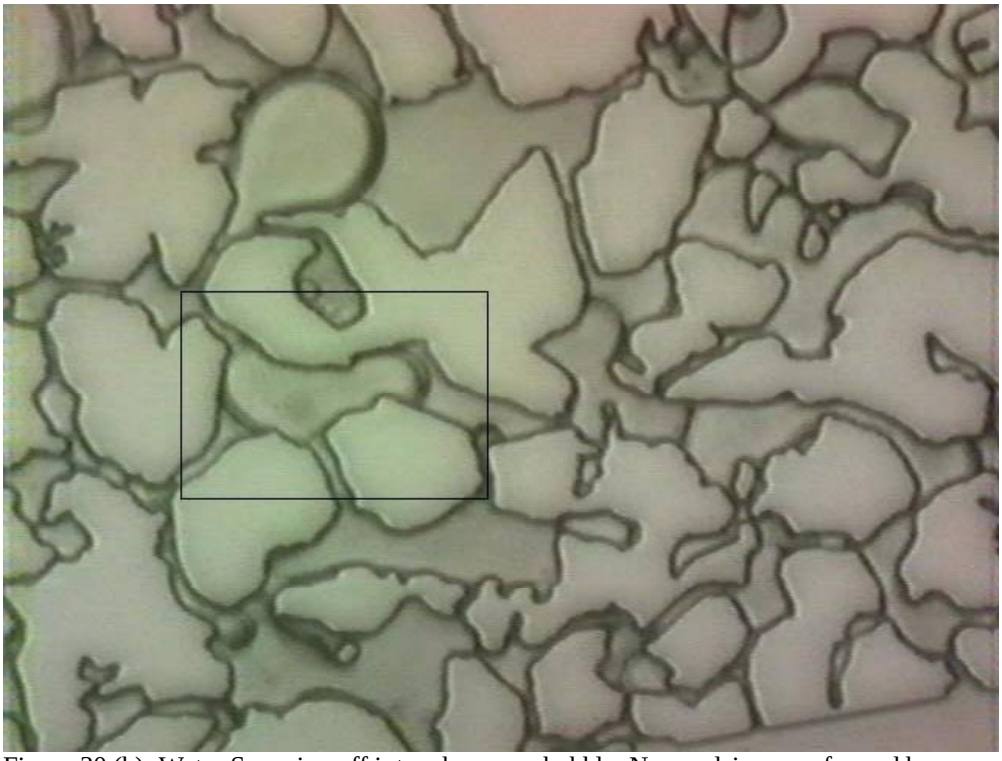

Figure 30 (b): Water Snapping off into a kerosene bubble. No emulsions are formed here as there is no surfactant present.

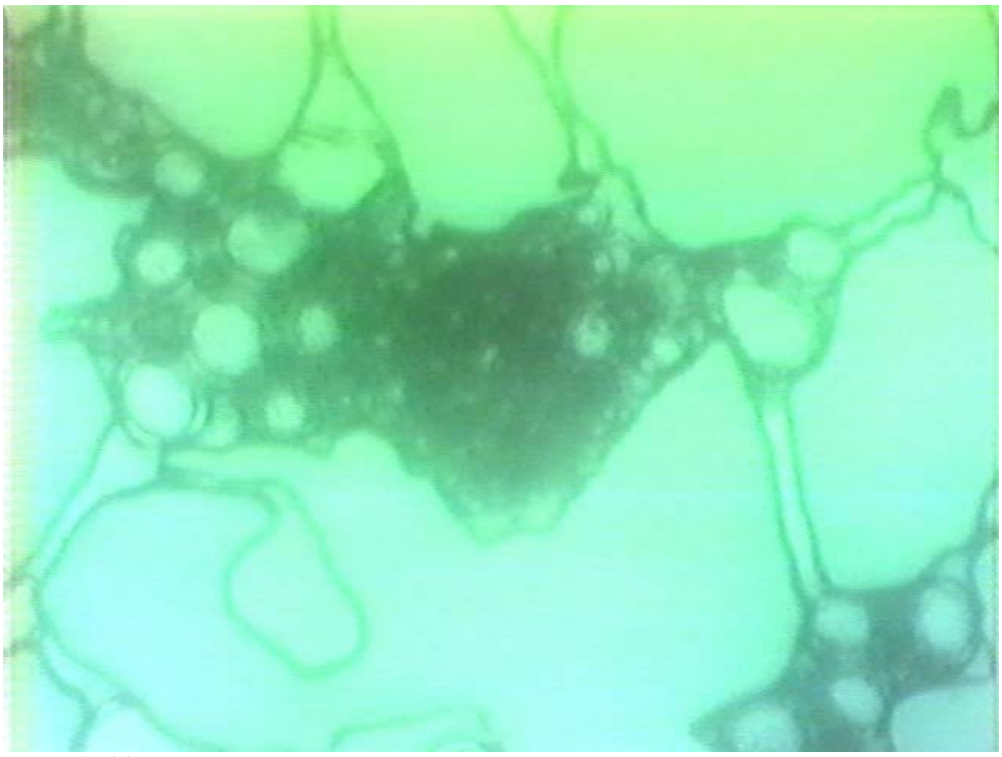

Figure 31(a)

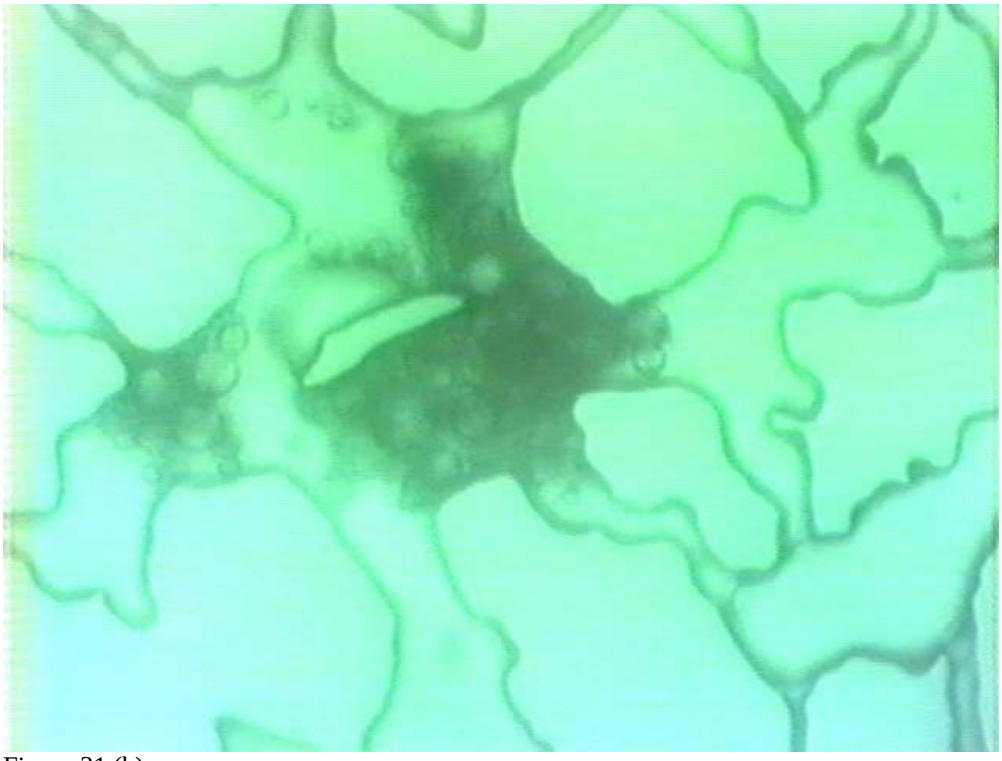

Figure 31 (b)

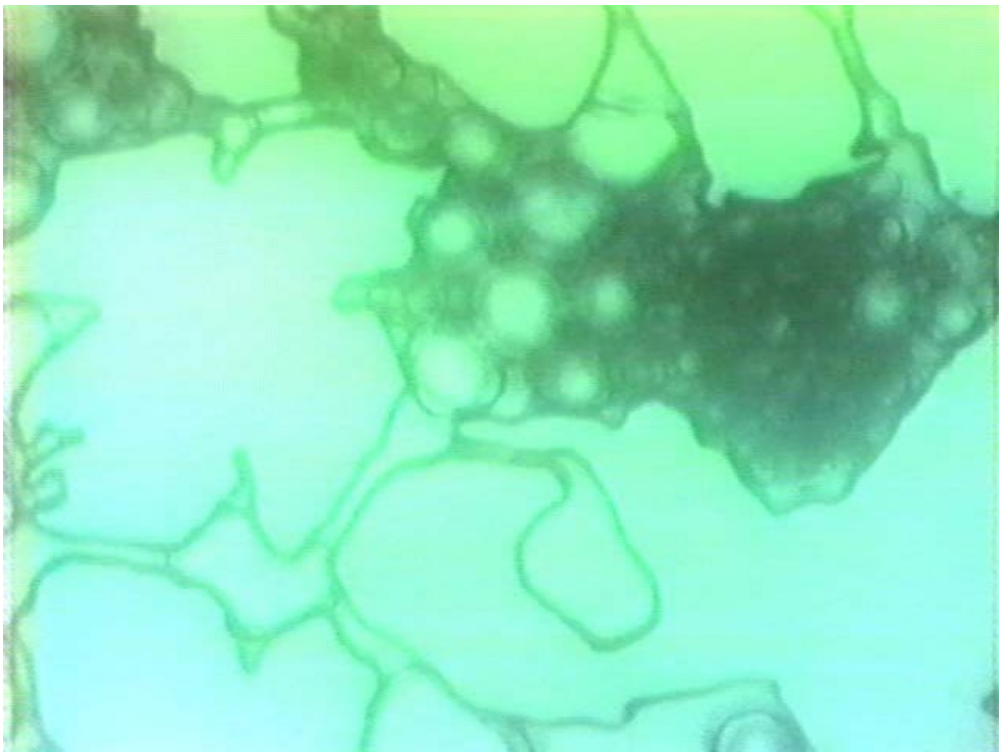

Figure 31(c)

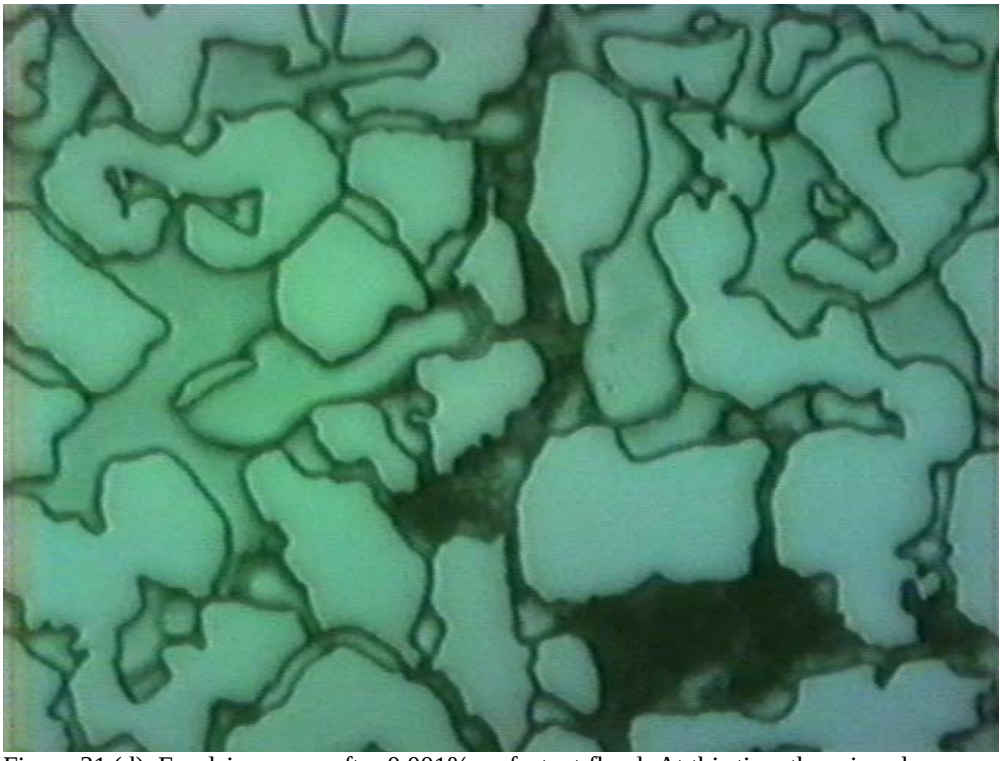

Figure 31 (d): Emulsions seen after 0.001% surfactant flood. At this time there is only kerosene and surfactant in the system and no gas is present.

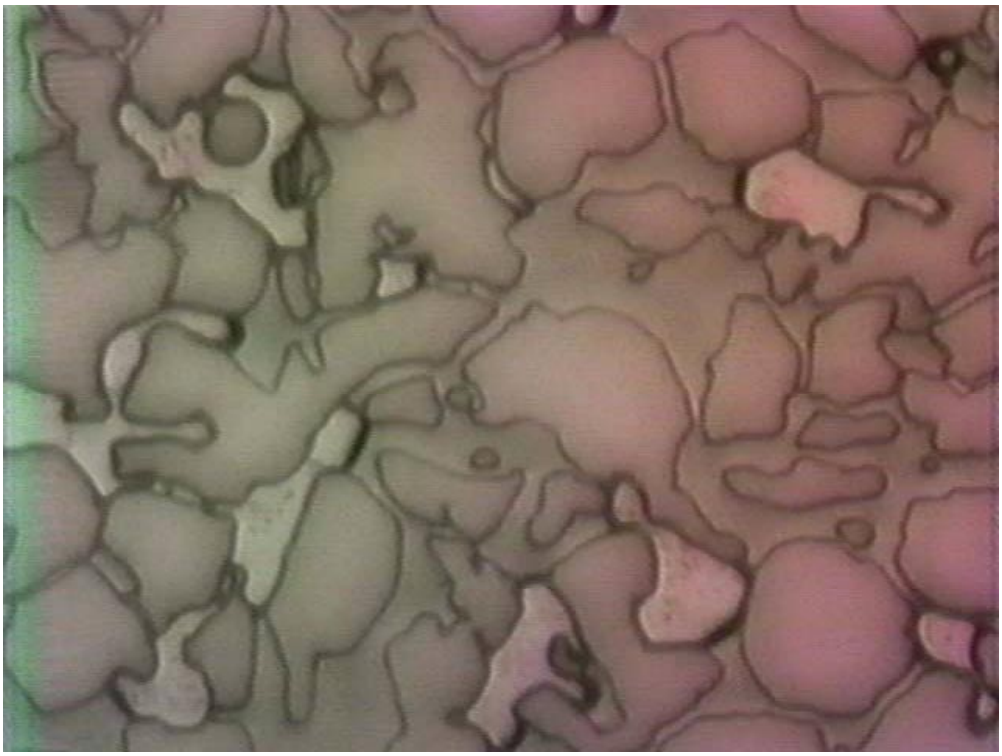

Figure 32 : CO_2 is discontinuous and does not flood the entire model. This is done after 0.001% Nansa surfactant flood.

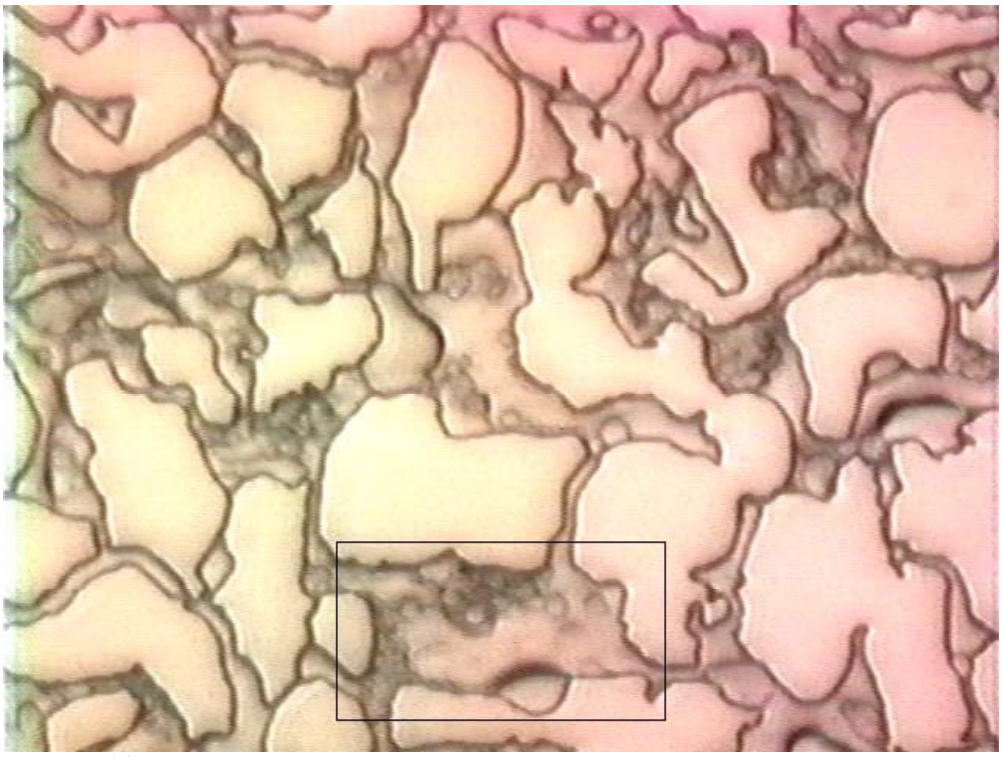

Figure 33(a)

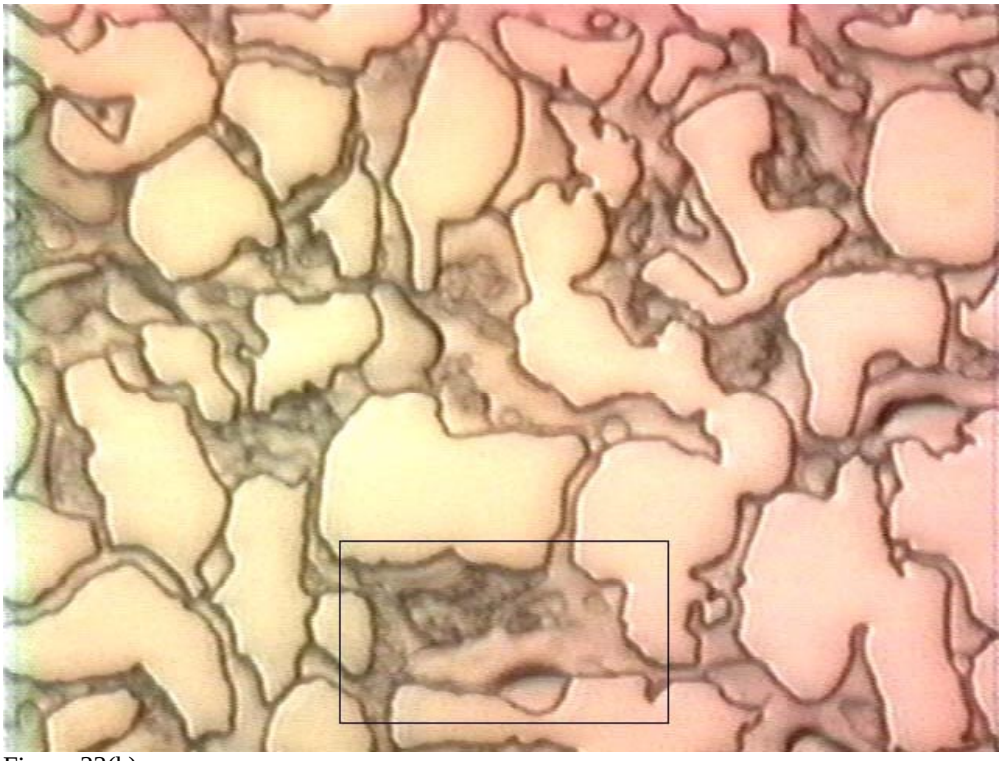

Figure 33(b)

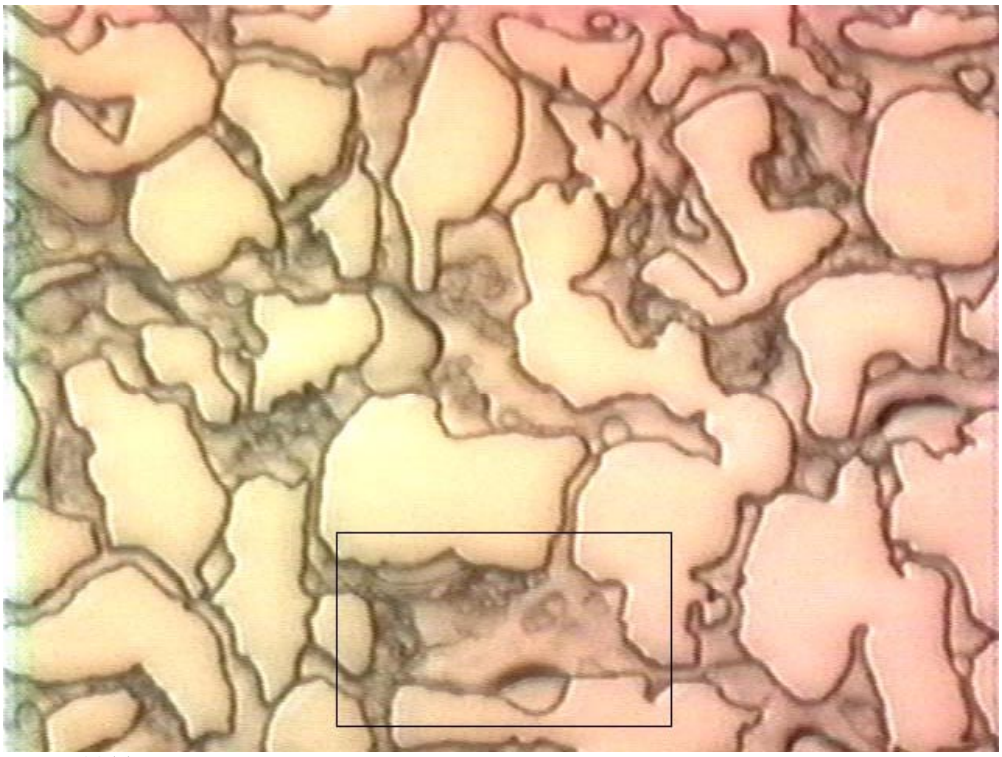

Figure 33(c)

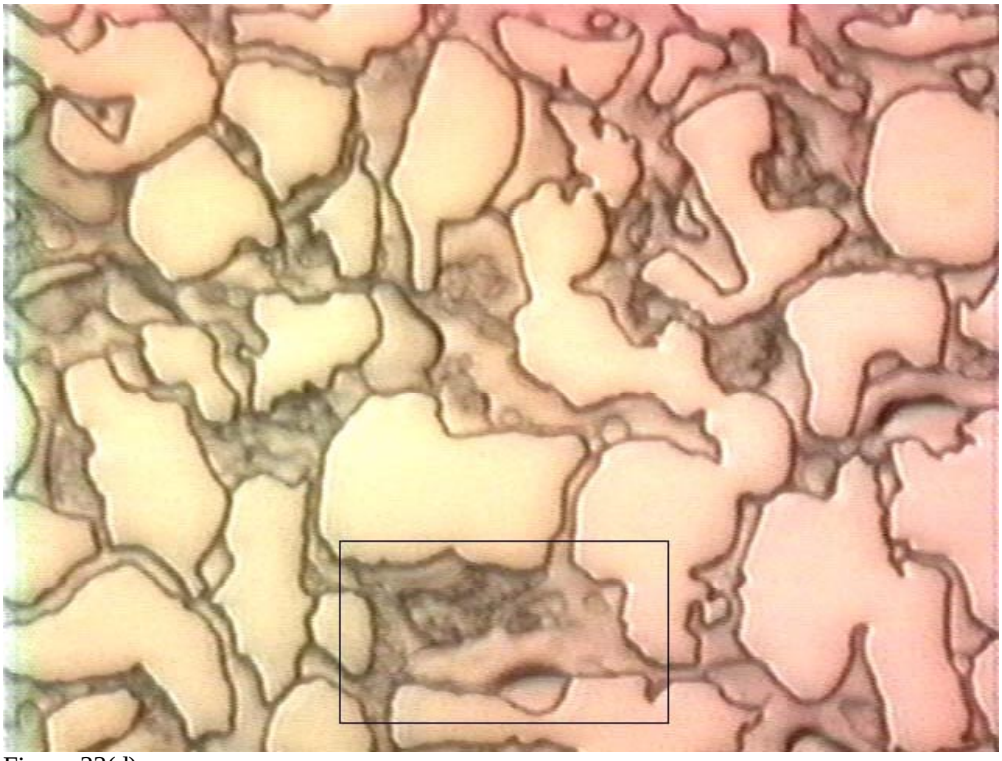

Figure 33(d)

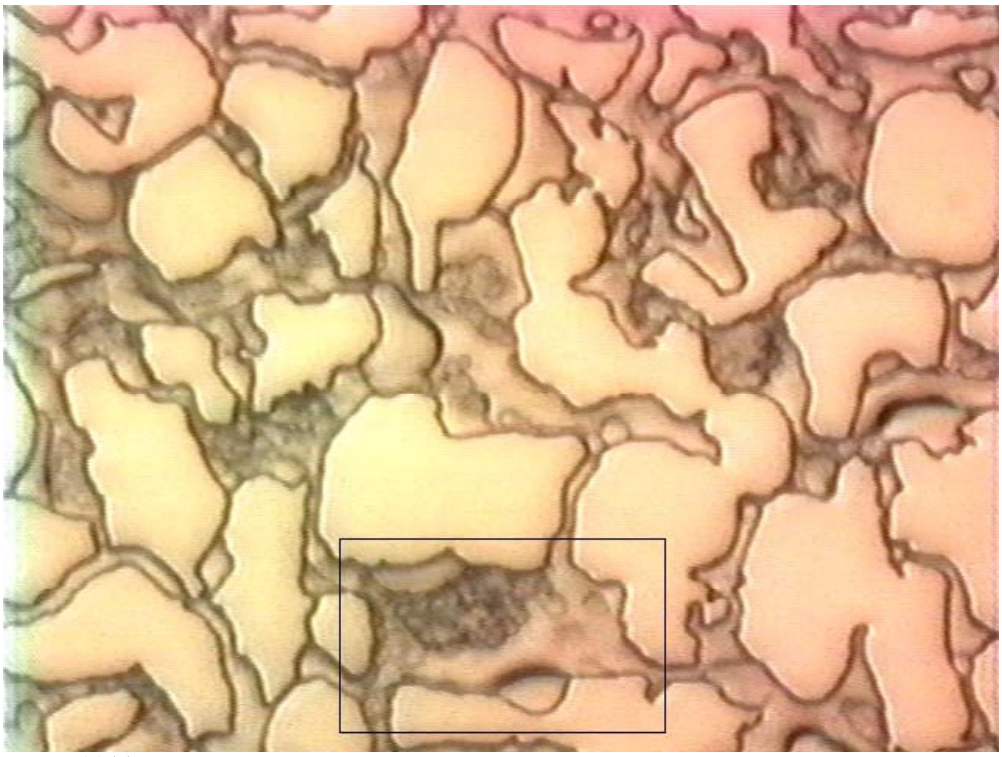

Figure 33(e)

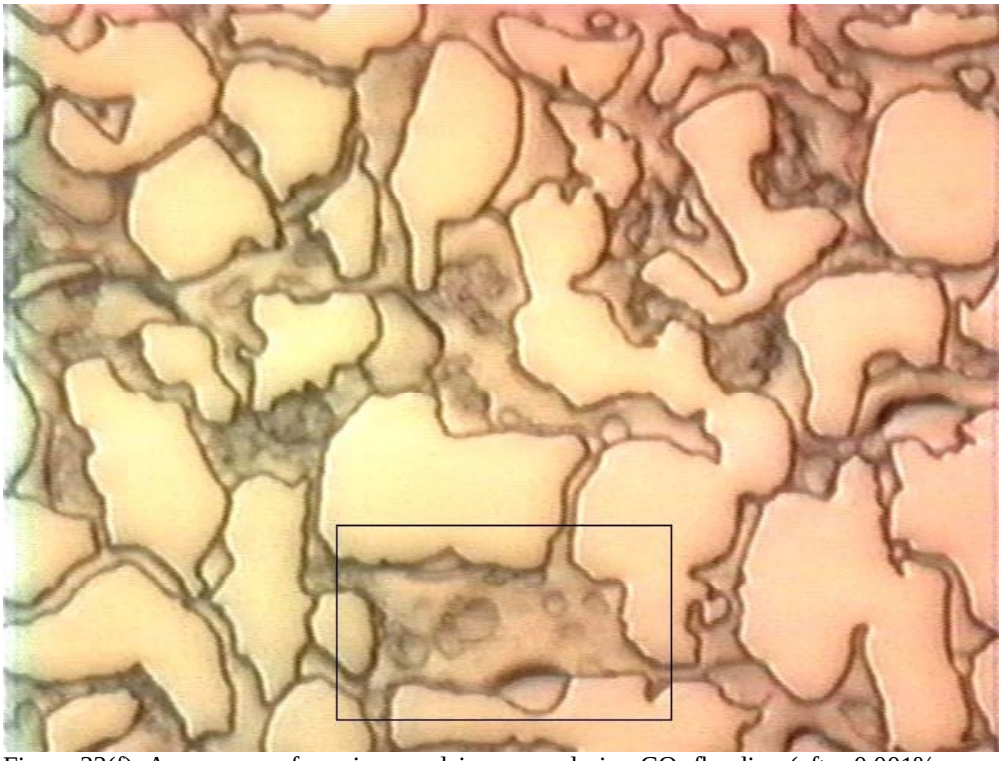

Figure 33(f): A sequence of moving emulsions seen during CO_2 flooding (after 0.001% Nansa surfactant flood). There is however not much CO_2 present in this part of the model.

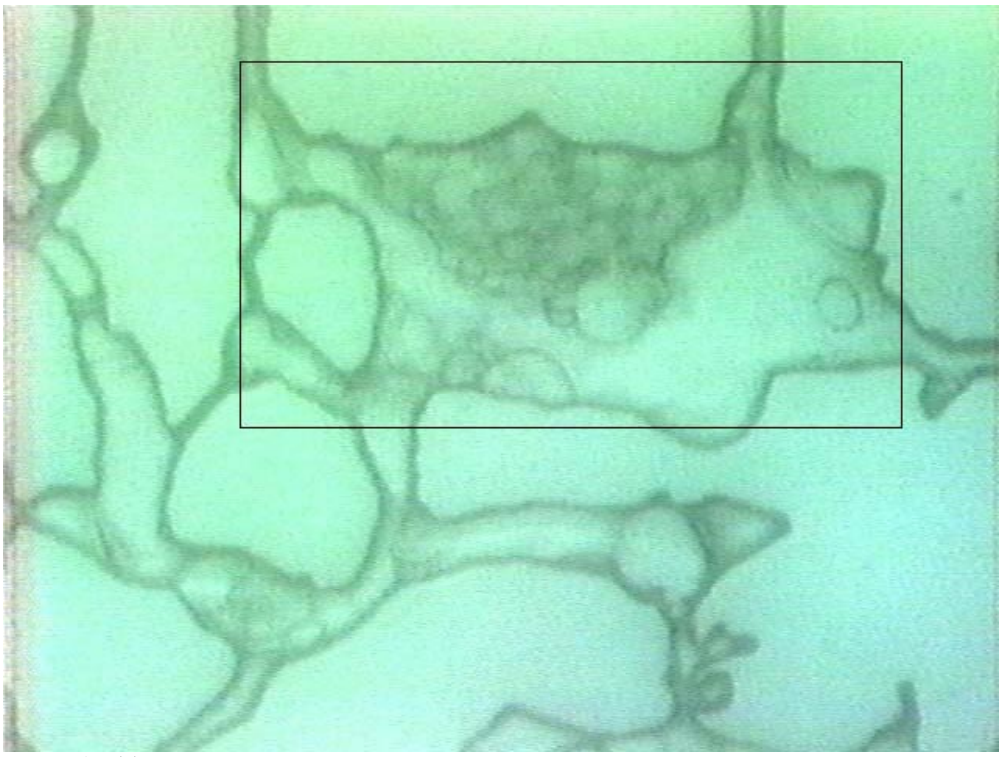
Figure 34 (a)

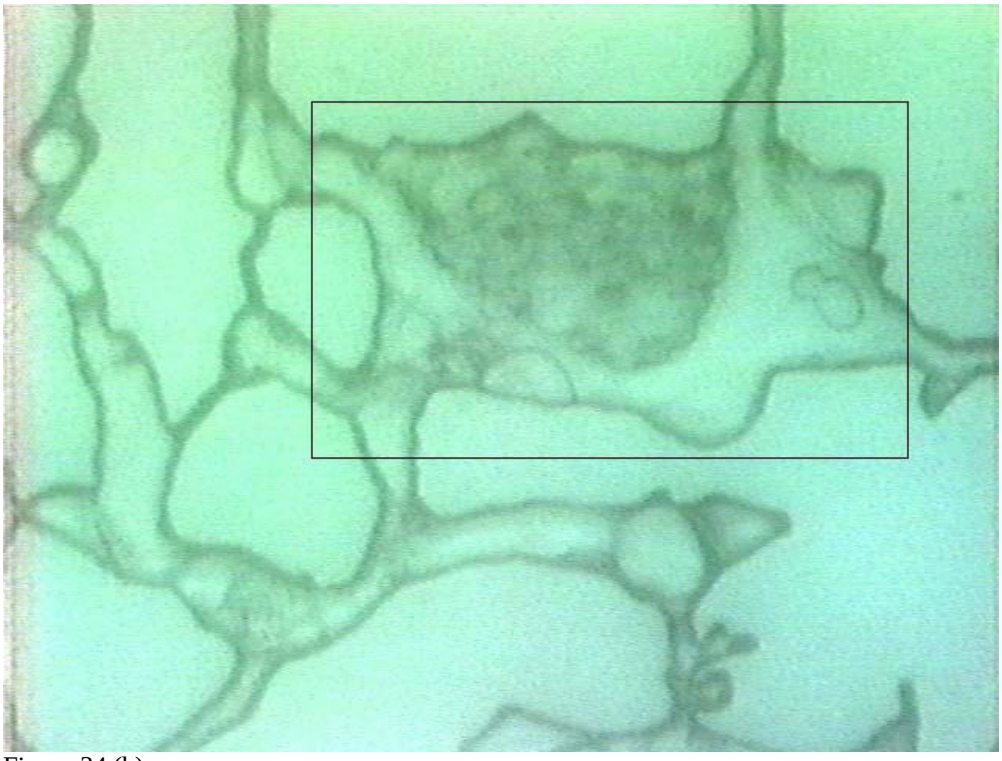
Figure 34 (b)

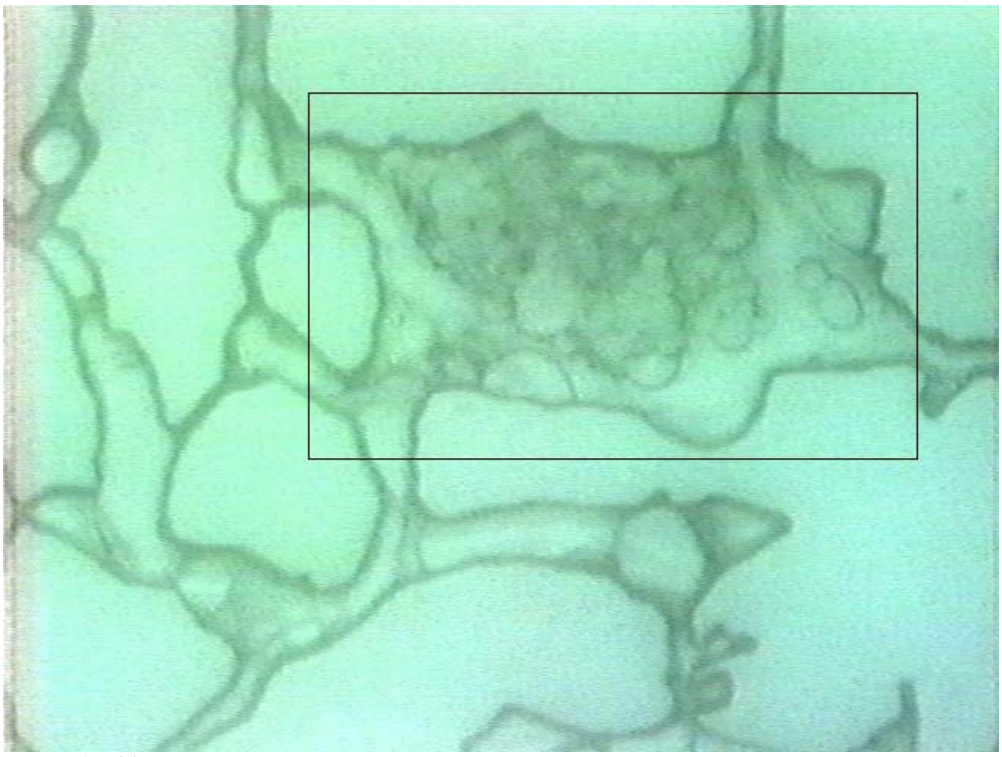

Figure 34 (c)

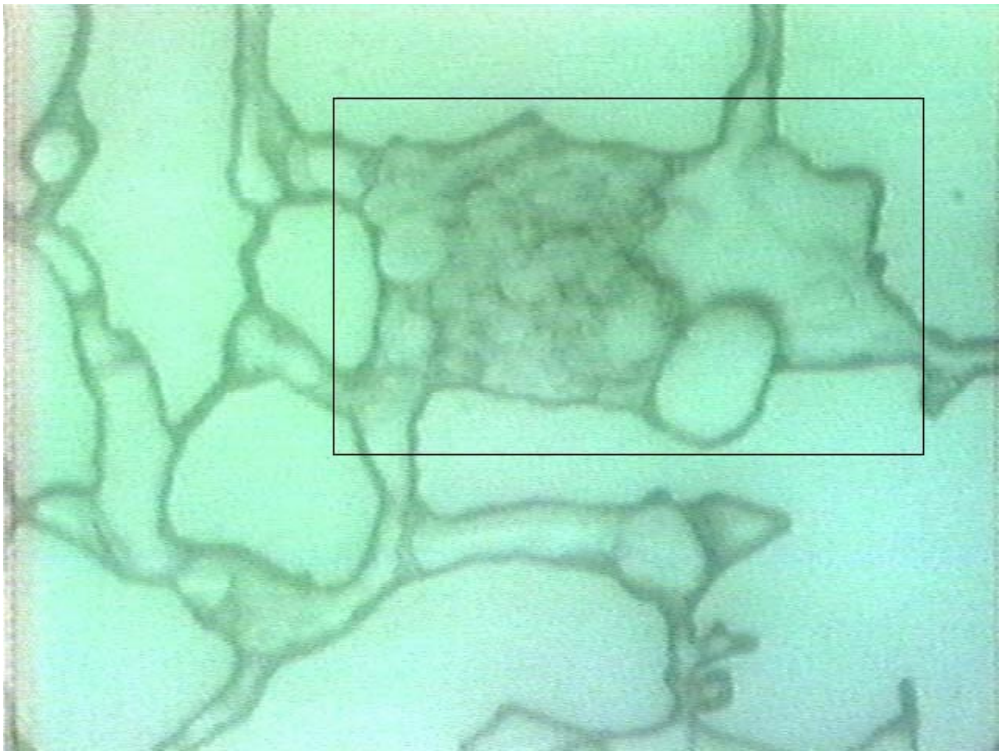

Figure 34(d): An emulsion moving sequence observed with the 40X magnification lens. As can be seen there is no CO2 present in this part of the micromodel. (after 0.001% Surfactant flood)

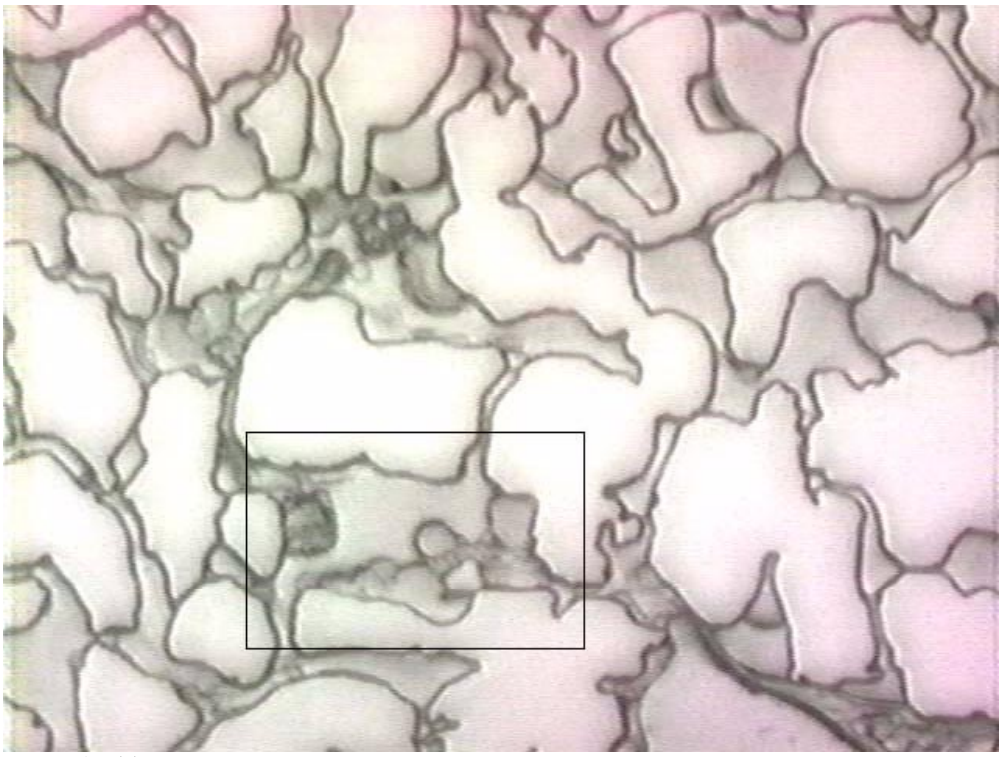

Figure 35 (a)

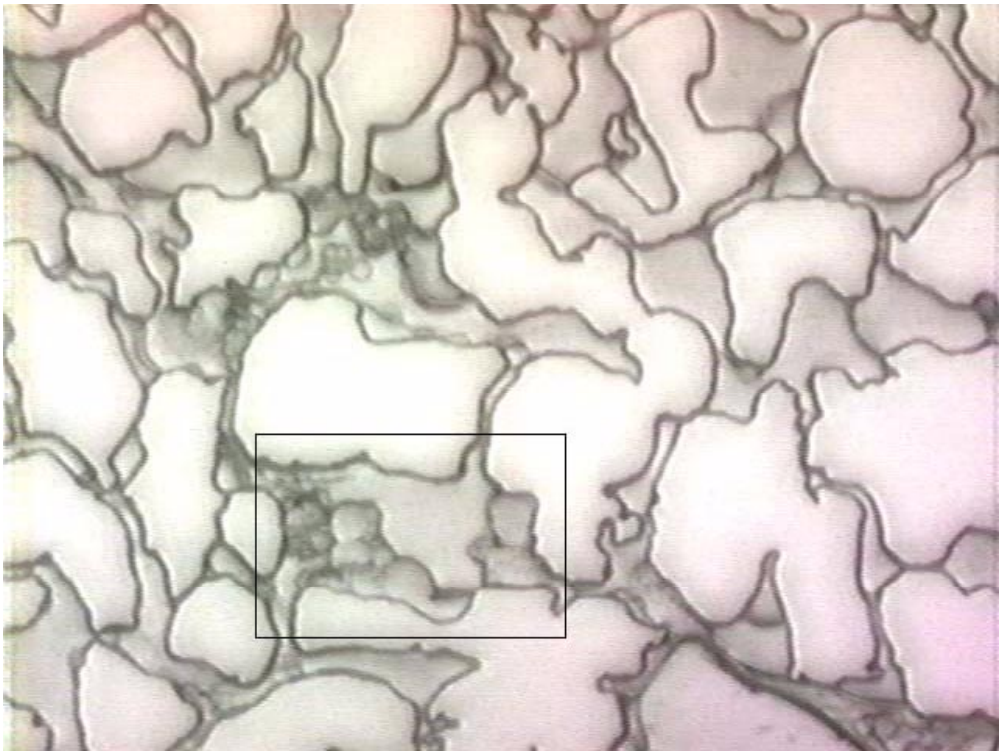

Figure 35 (b)

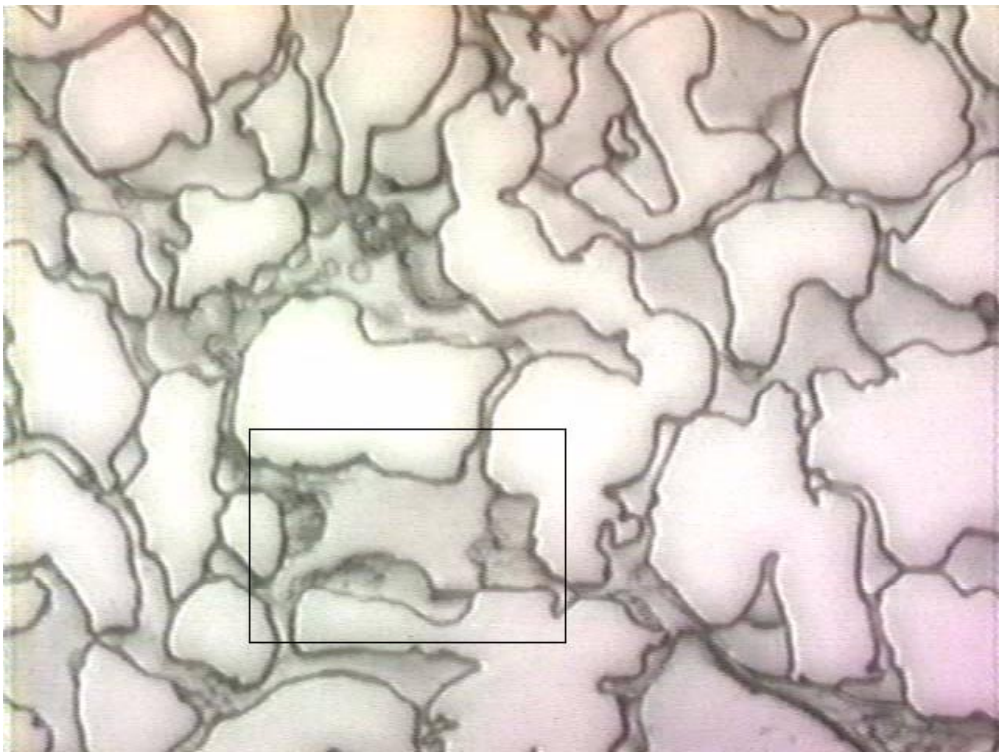

Figure 35 (c): An emulsion moving sequence observed after 0.01 % Nansa surfactant flood, just before starting CO_2 flood.

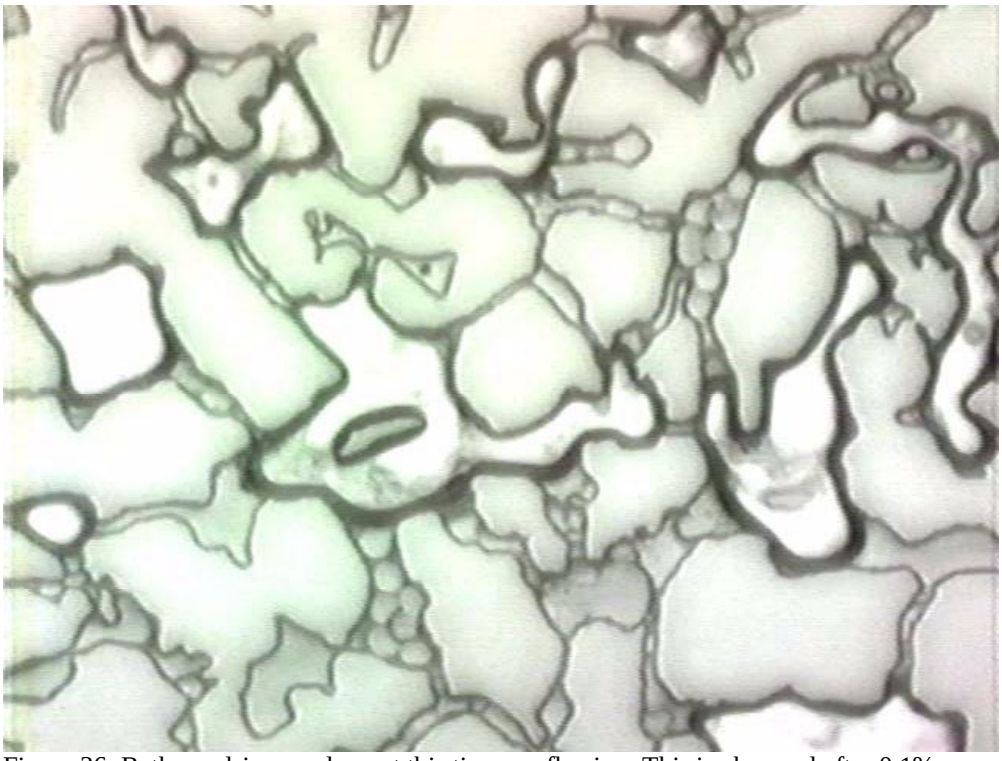

Figure 36: Both emulsions and gas at this time are flowing. This is observed after 0.1% Nansa surfactant flood.

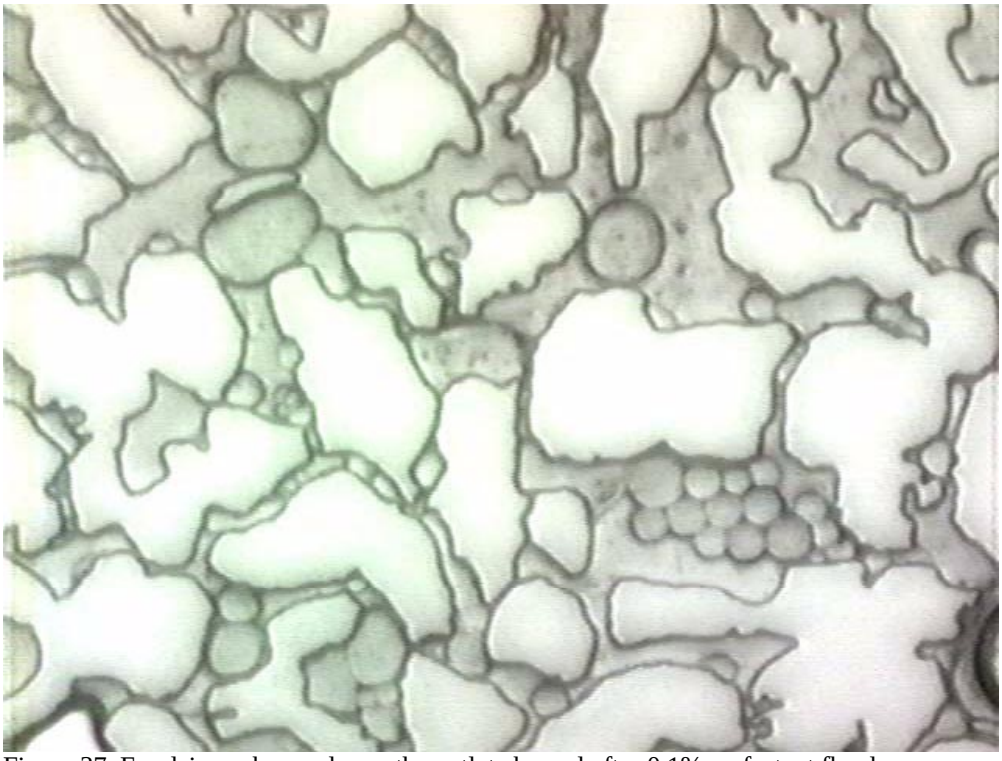

Figure 37: Emulsions observed near the outlet channel after 0.1% surfactant flood.

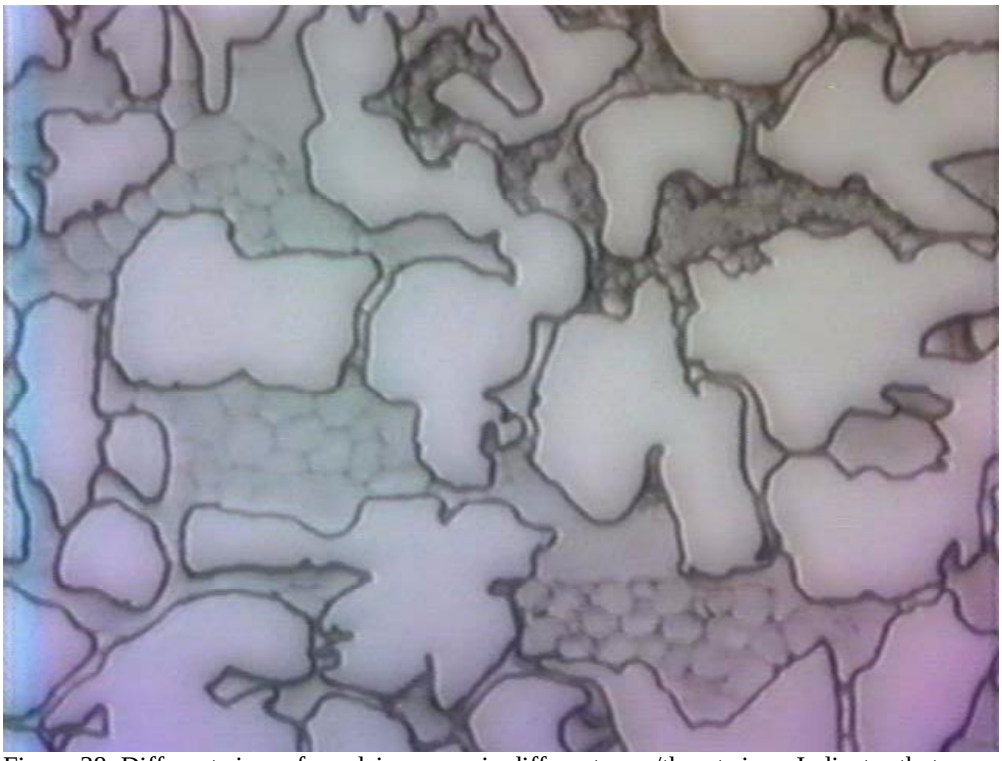

Figure 38: Different sizes of emulsions seen in different pore/throat sizes. Indicates that emulsions depend on pore/throat size.

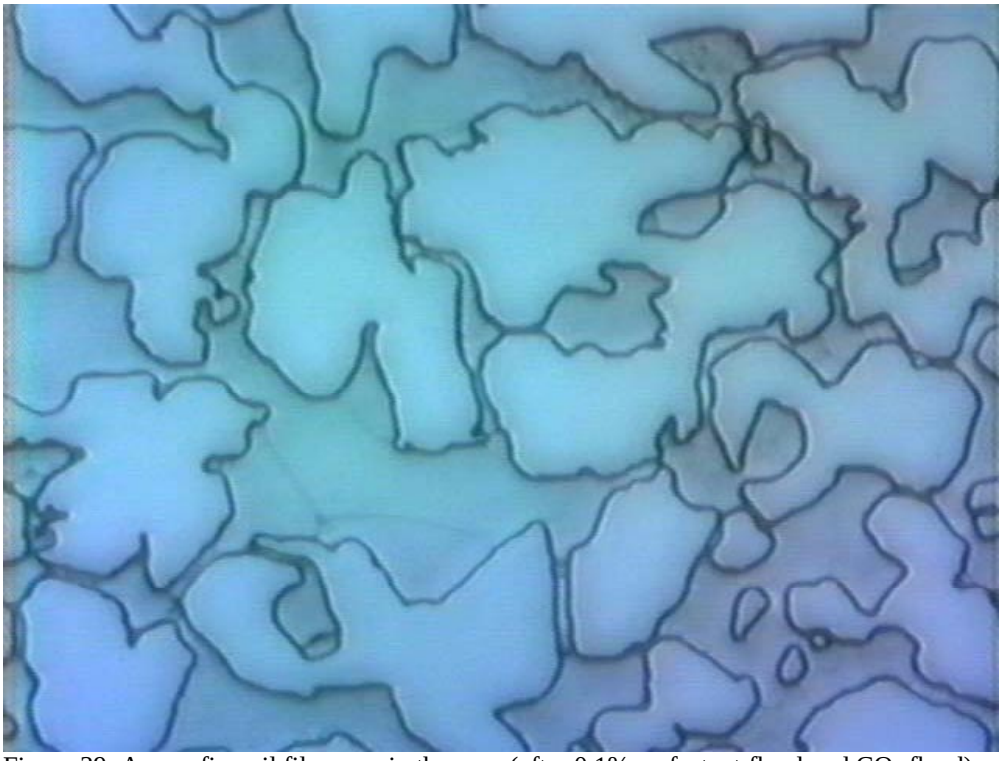

Figure 39: A very fine oil film seen in the pore (after 0.1% surfactant flood and CO_2 flood).

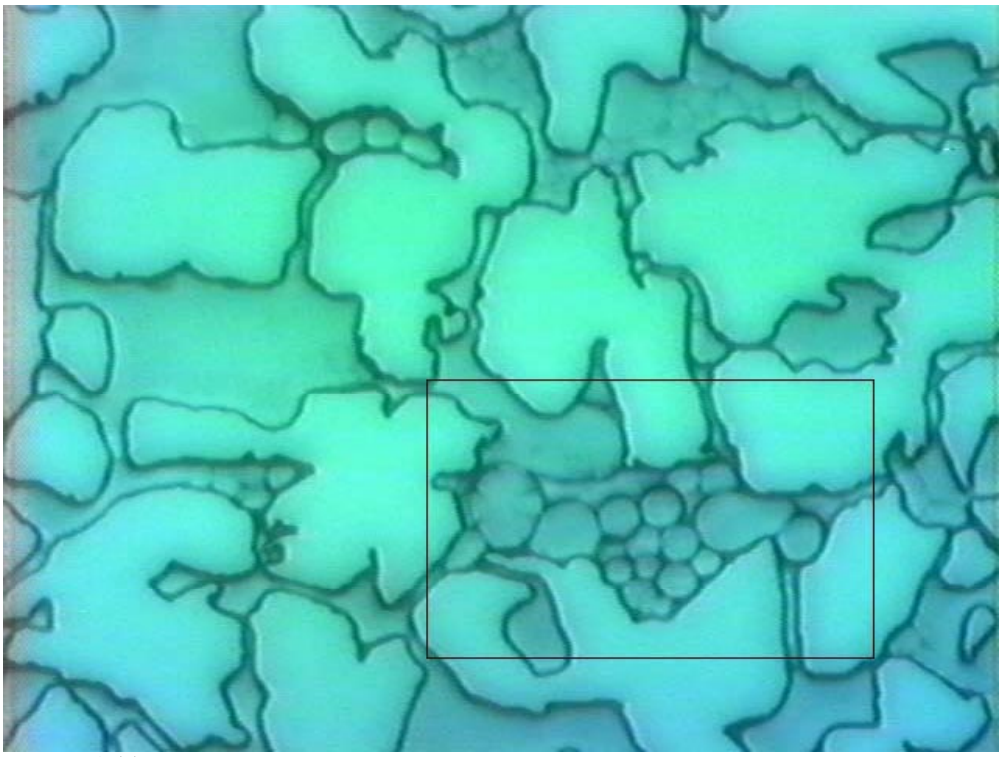

Figure 40 (a)

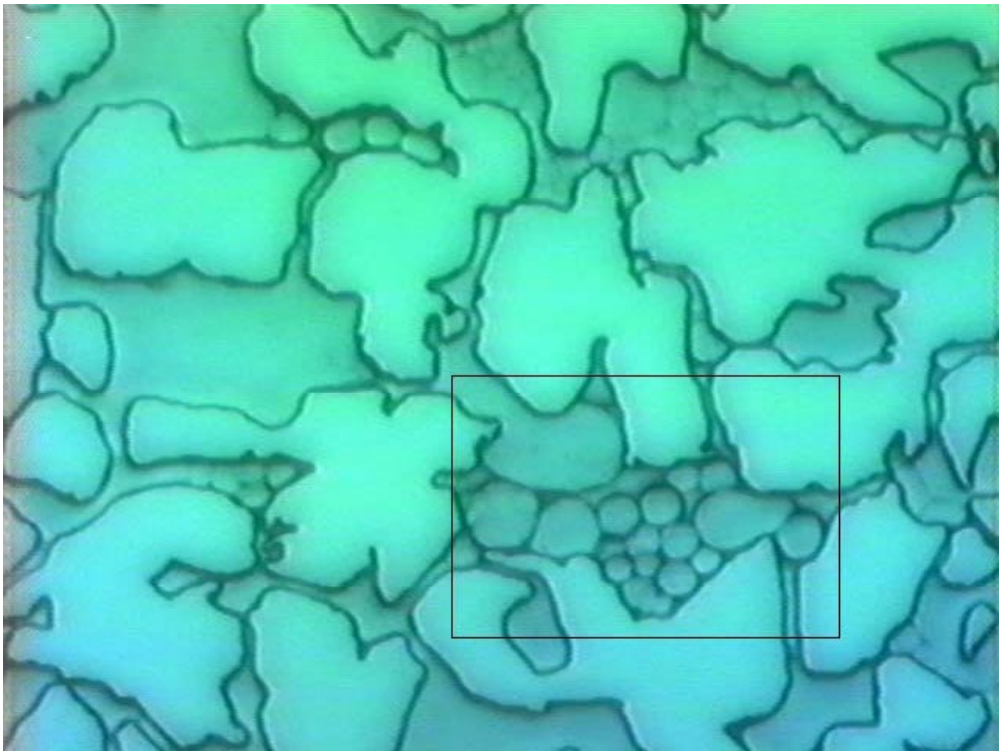

Figure 40 (b)

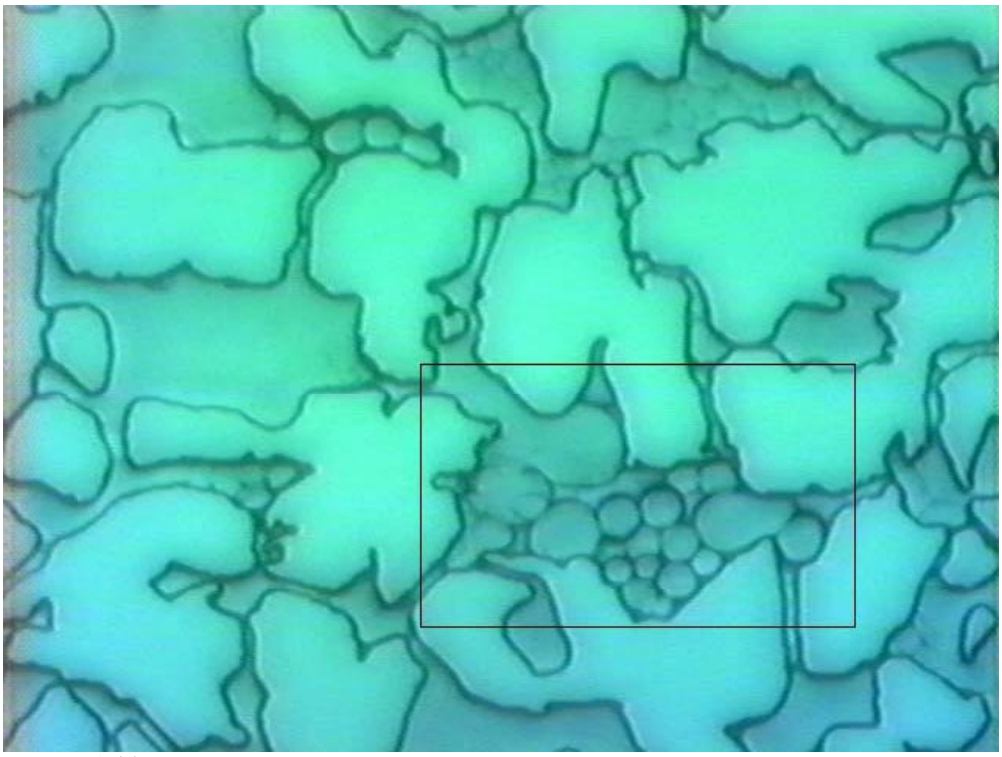

Figure 40 (c)

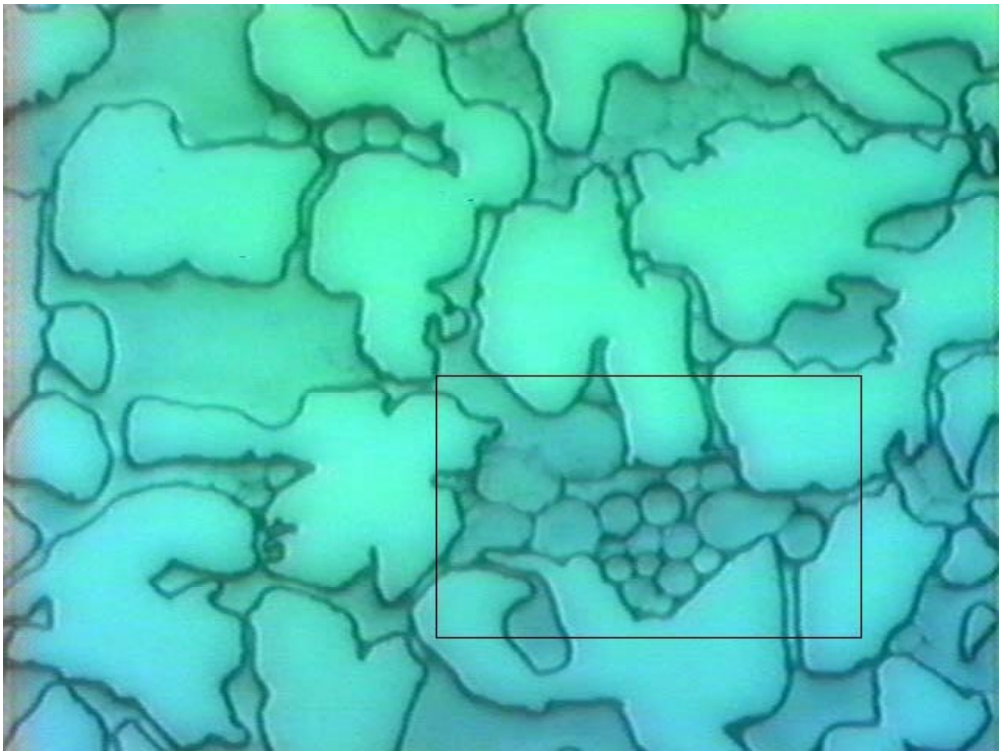

Figure 40 (d)

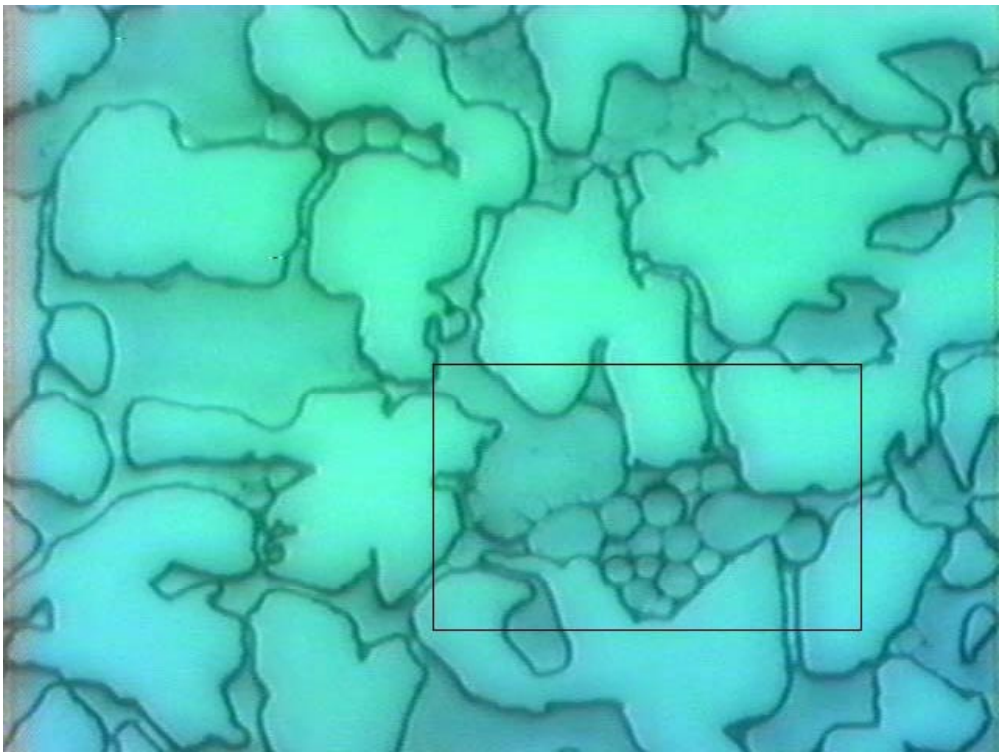

Figure 40 (e): An emulsion forming and breaking sequence observed after 0.1% surfactant flood and during CO_2 Flood. (just before beginning 1% surfactant flood)

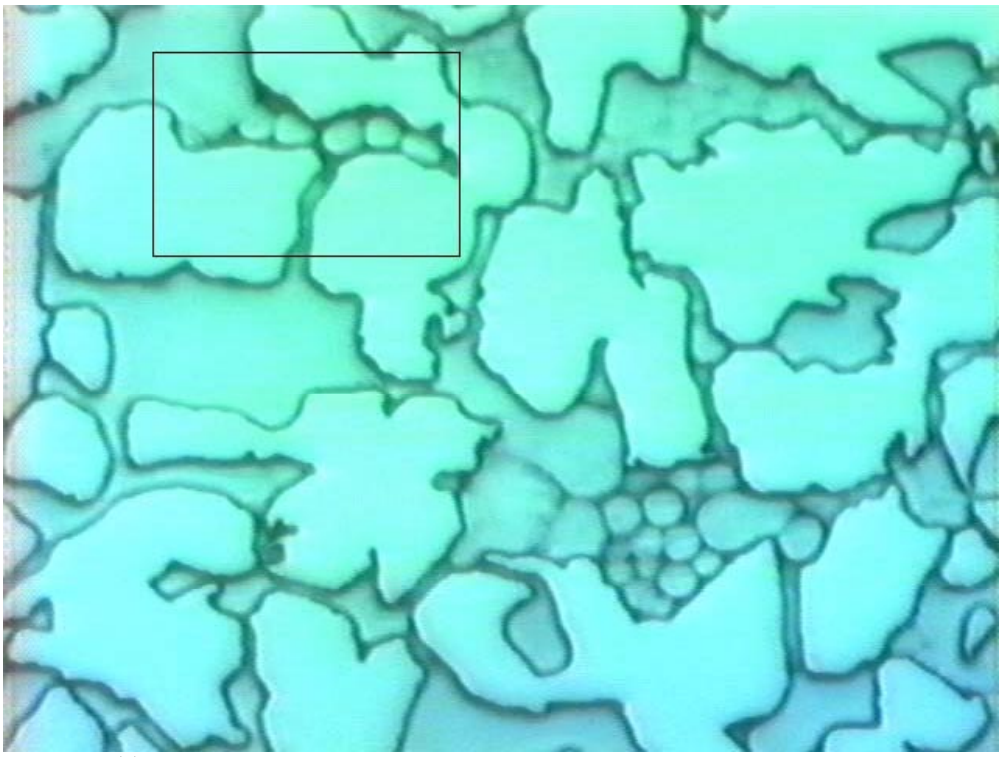

Figure 41 (a)

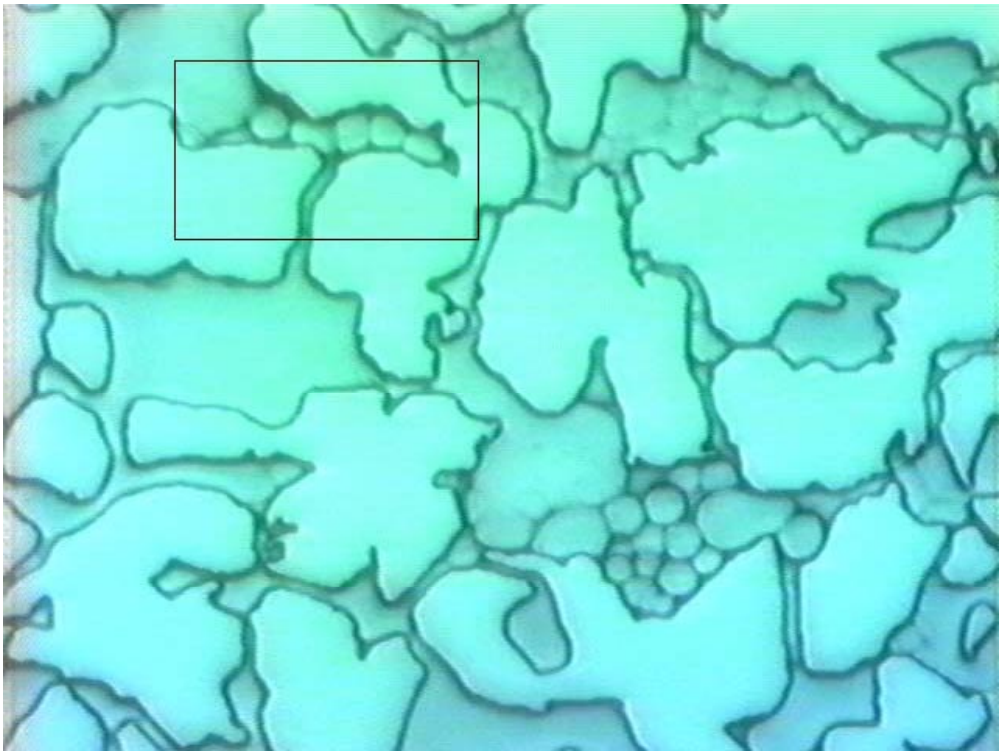

Figure 41 (b)

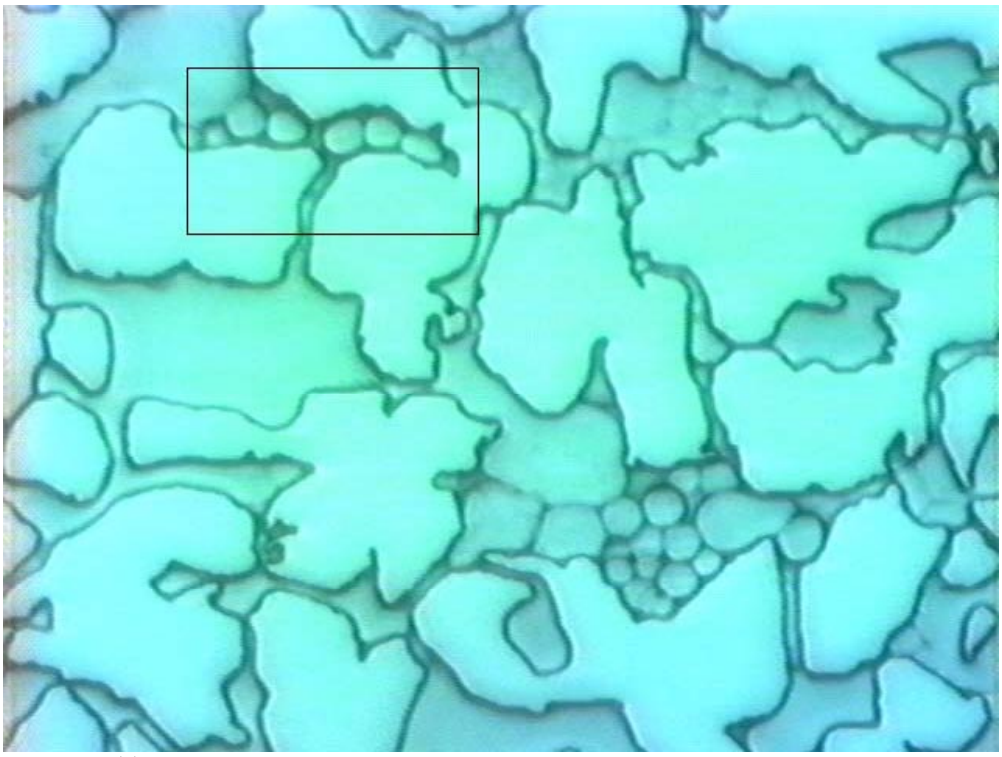

Figure 41 (c)

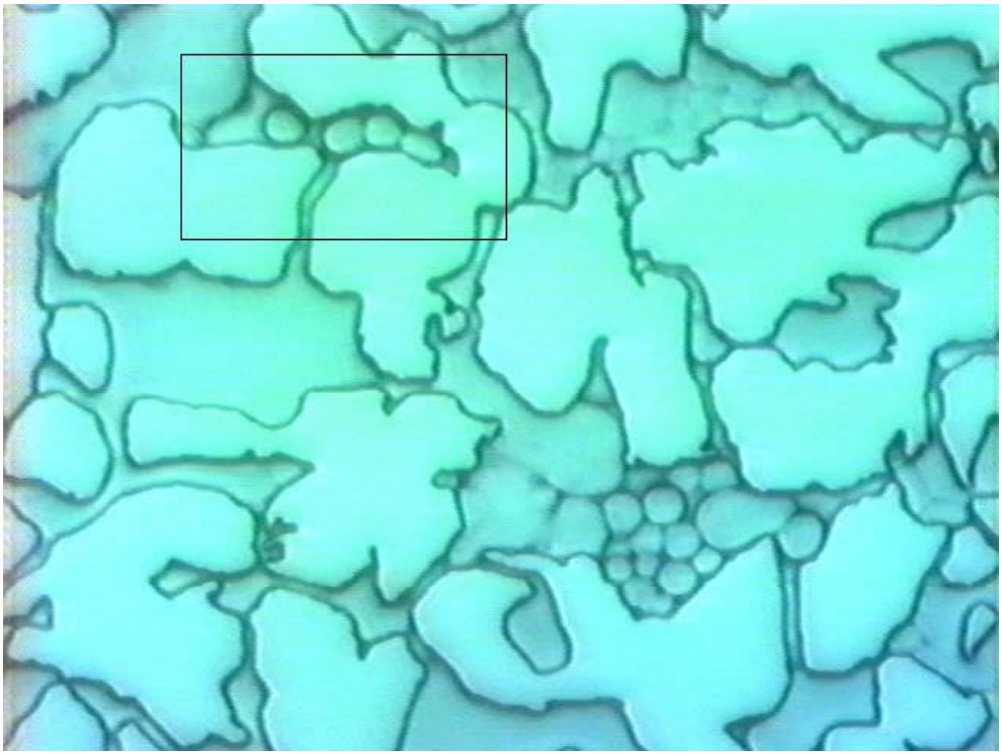

Figure 41 (d)

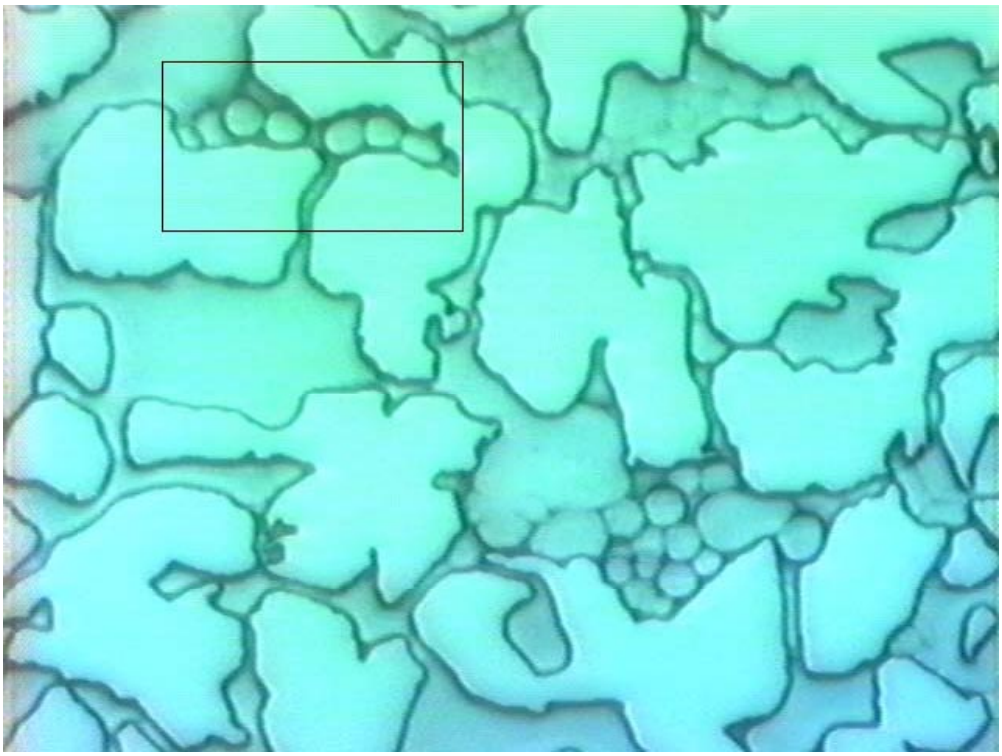

Figure 41 (e): Another emulsion forming and breaking sequence observed after 0.1% surfactant flood and during CO_2 Flood. (just before beginning 1% surfactant flood)

EXPERIMENT 3: FIGURES

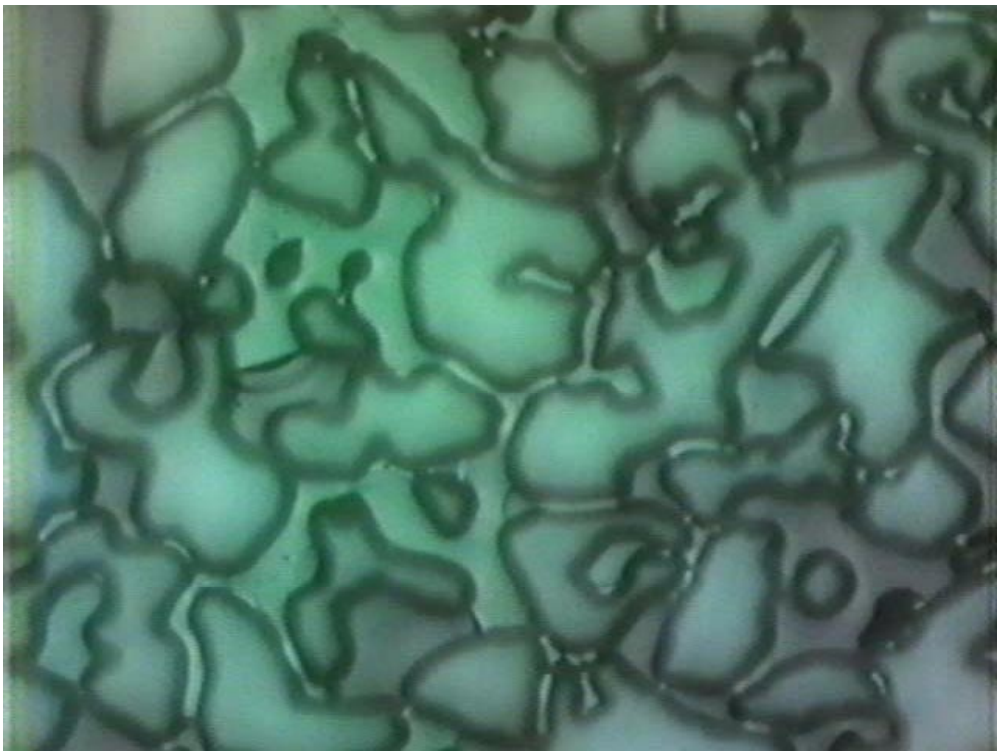

Figure 42: Water can be seen residing in the narrow throats.

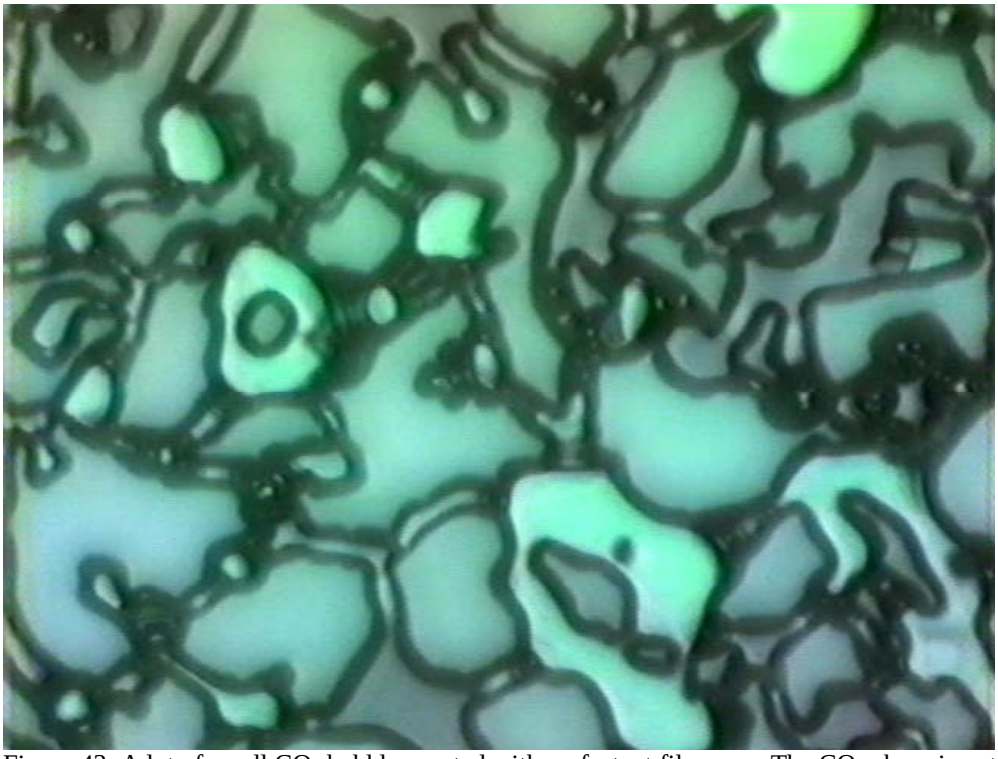

Figure 43: A lot of small CO_2 bubbles coated with surfactant film seen. The CO_2 phase is not continuous any more. Seen after 0.1% FC740 surfactant flood.

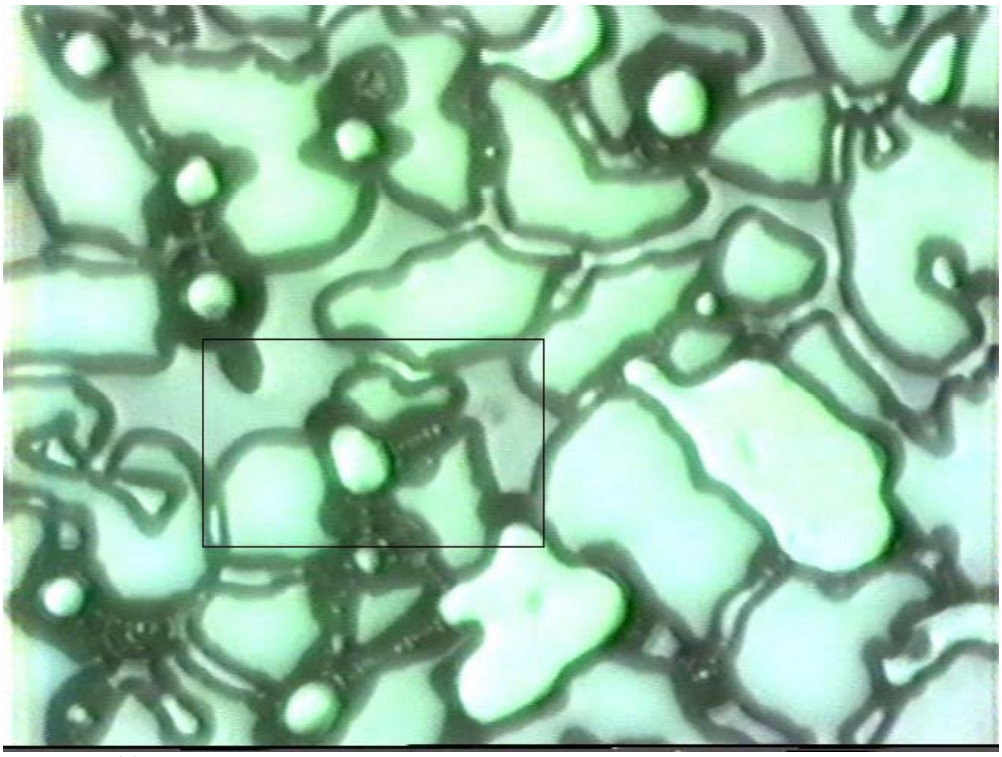

Figure 44 (a)

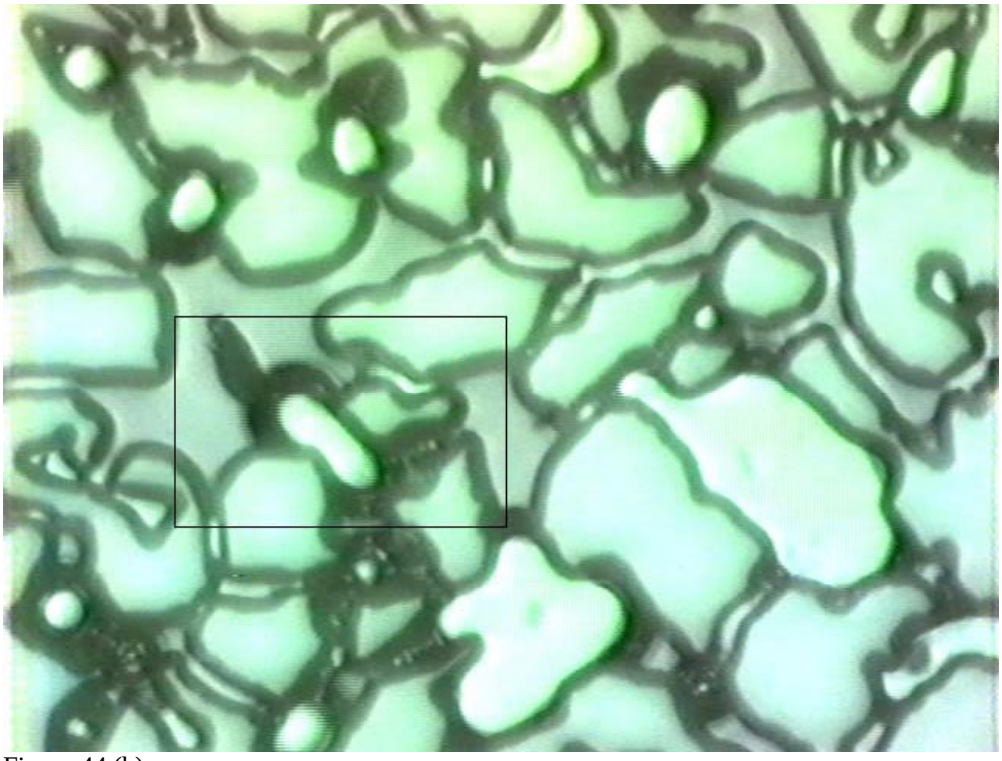

Figure 44 (b)

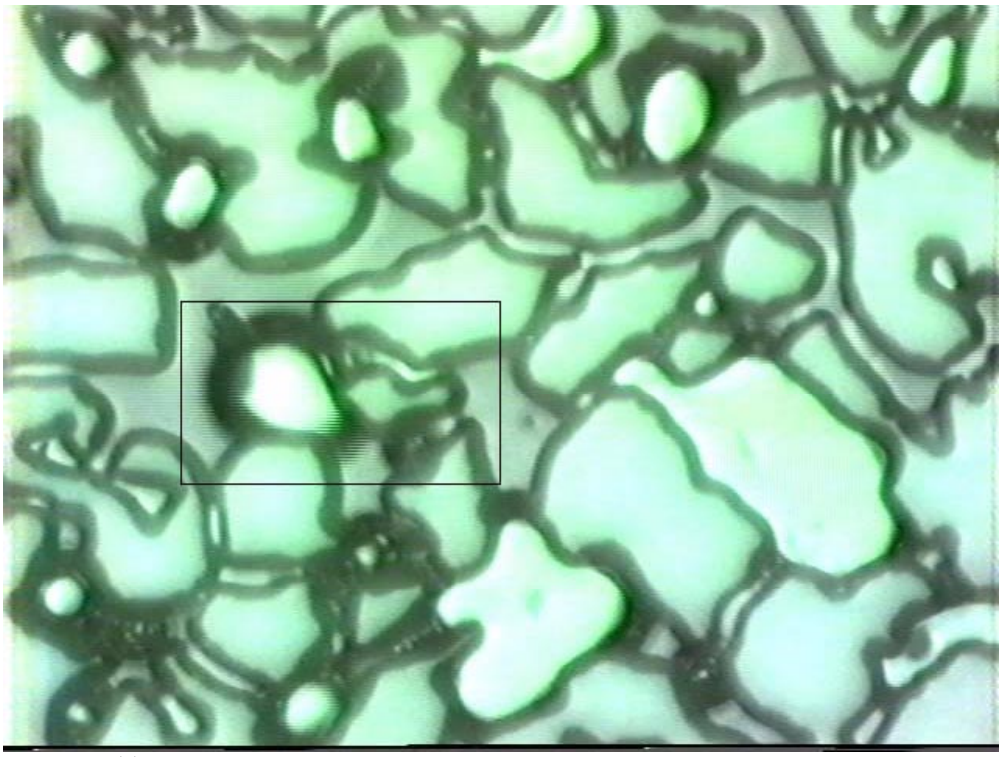

Figure 44 (c)

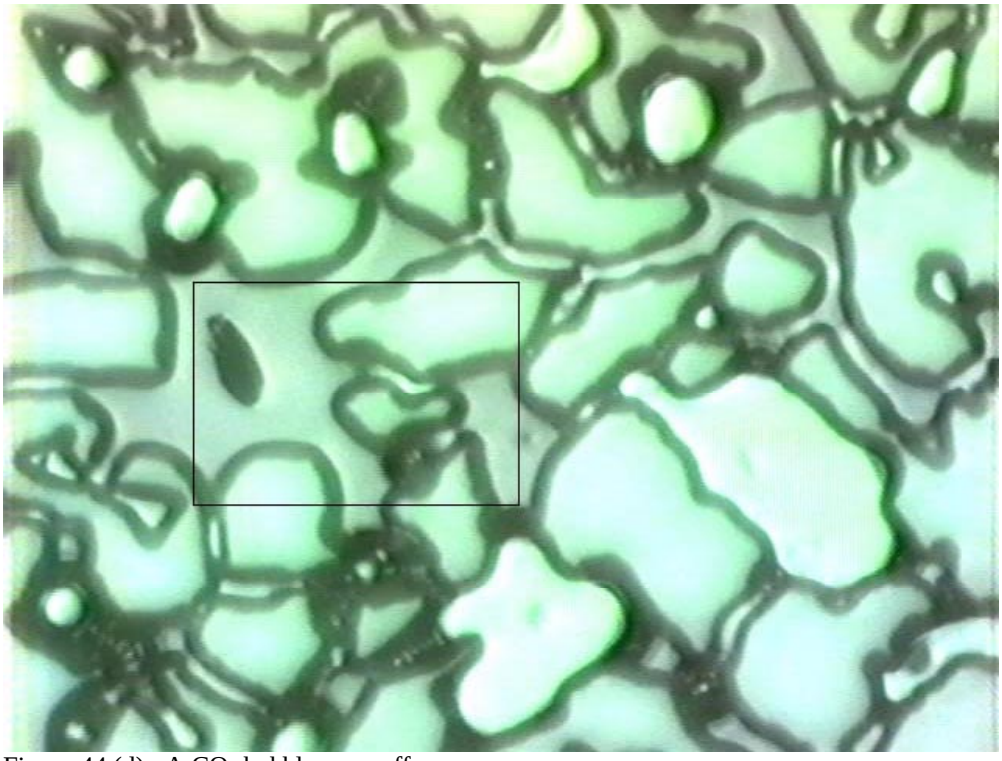

Figure 44 (d) : A CO_2 bubble snap-off sequence.

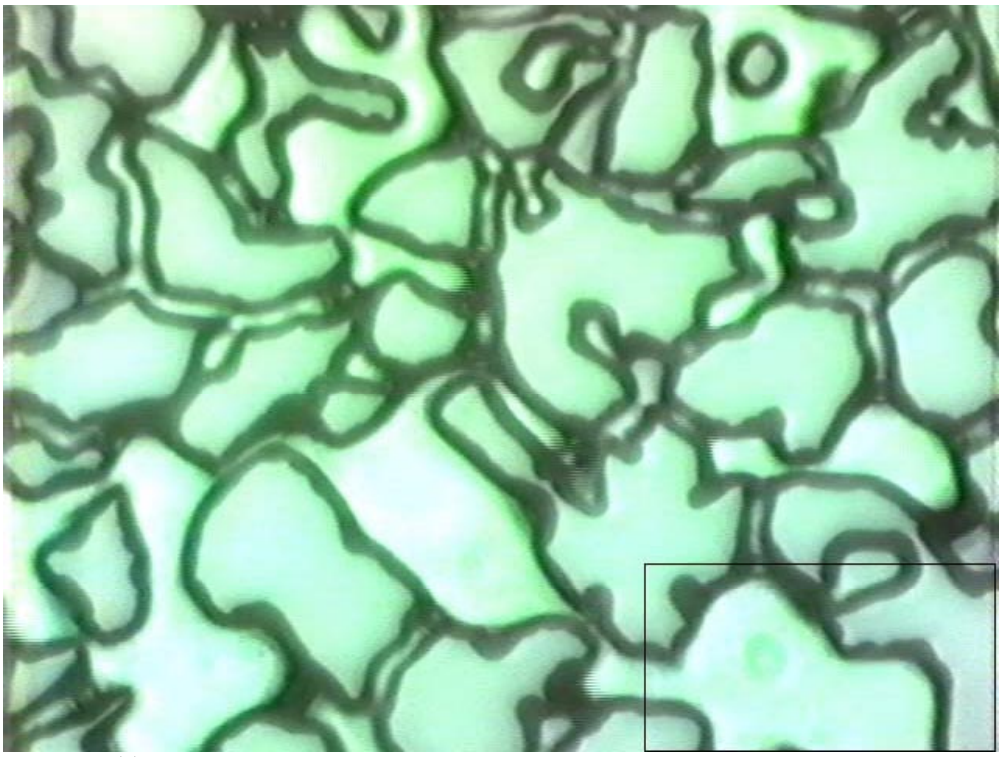

Figure 45 (a)

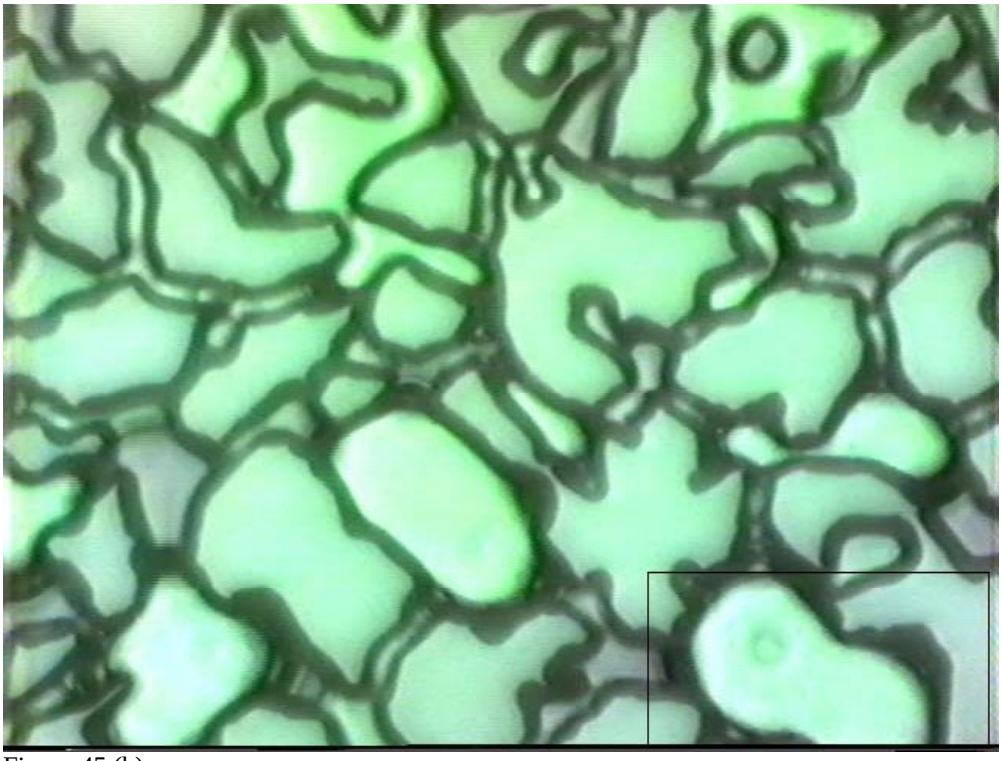

Figure 45 (b)

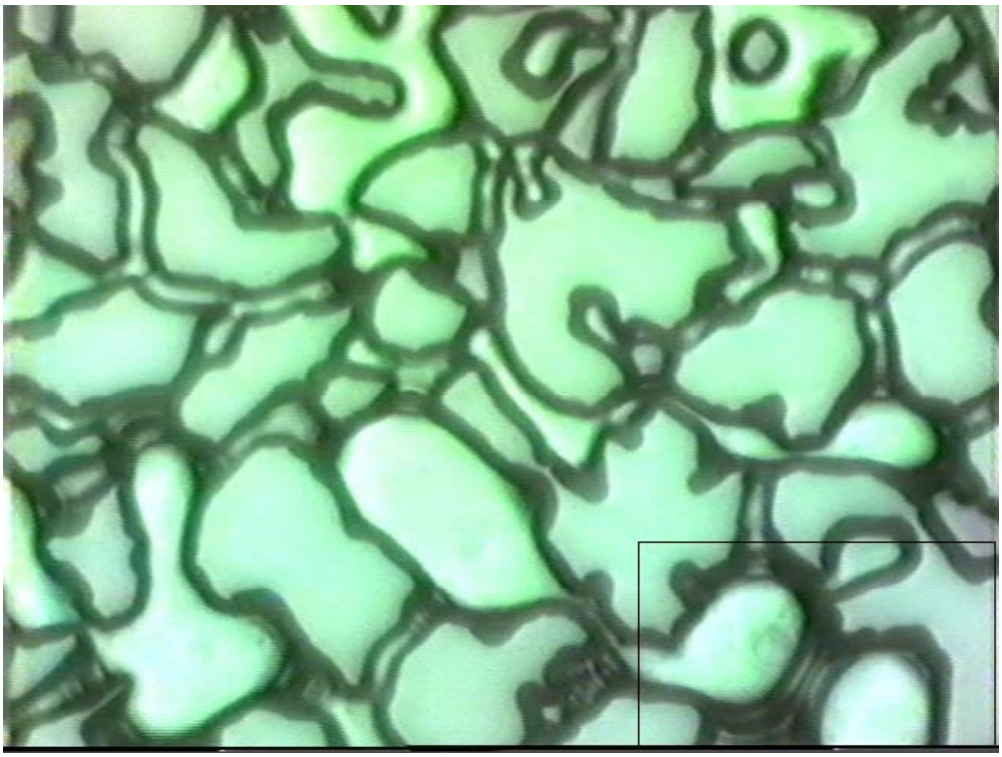

Figure 45 (c)

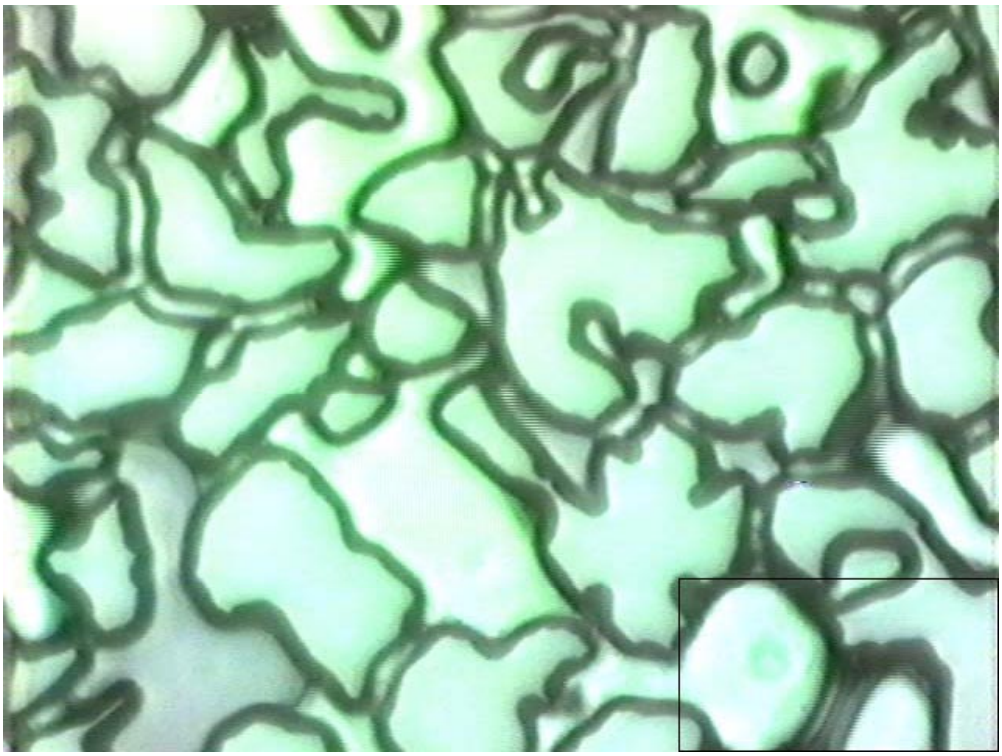

Figure 45 (d)

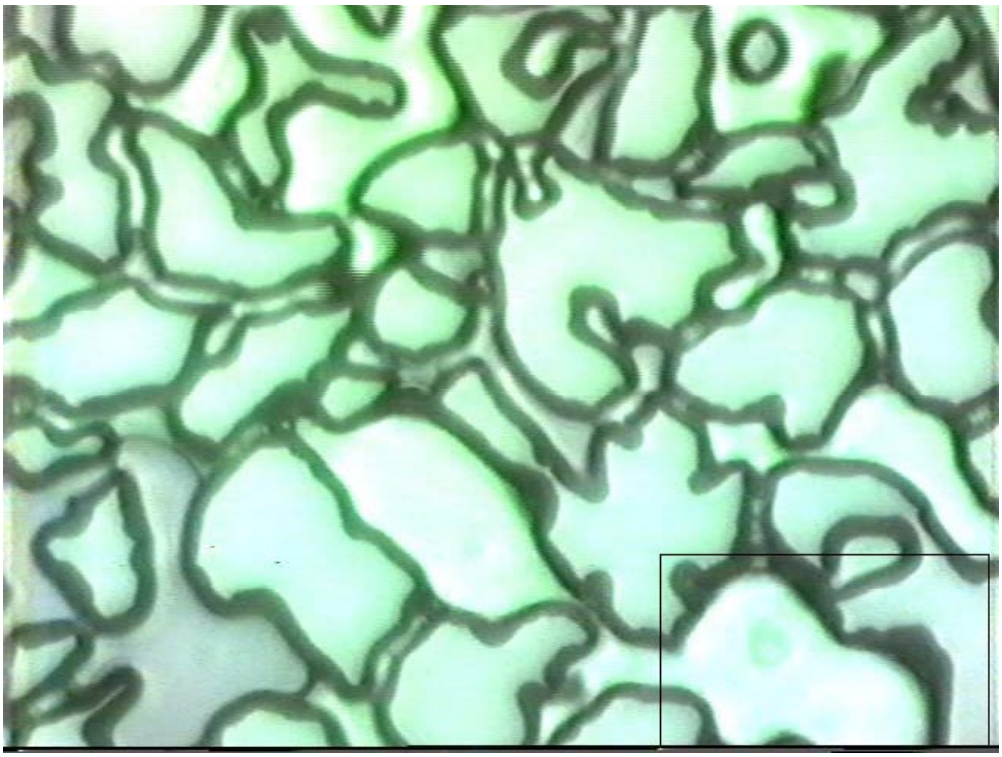

Figure 45 (e) : A lamella forming and breaking sequence observed after 0.1% FC740 surfactant flood.

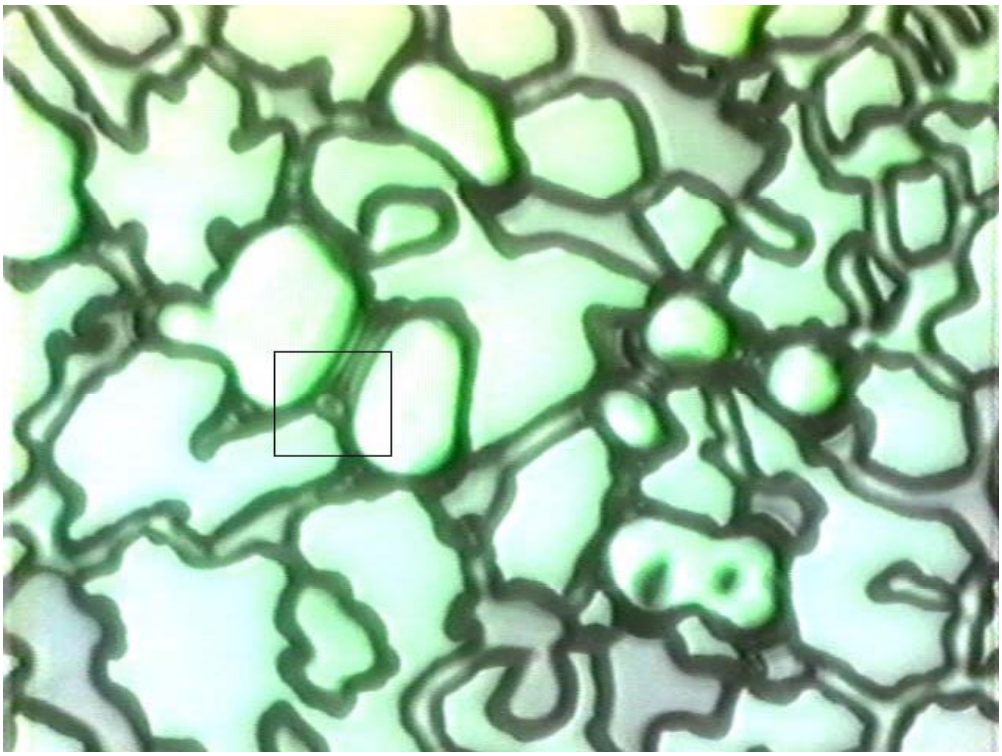
Figure 46 : A drop of water in a lamella. It doesn’t seem to affect the lamella stability.

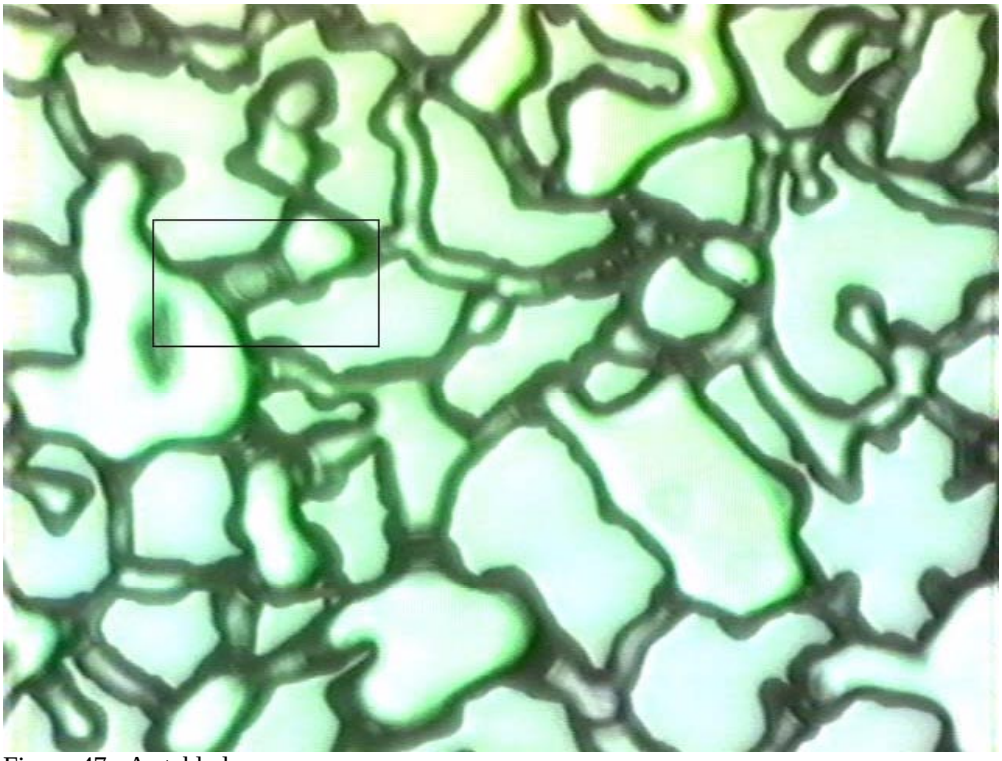
Figure 47 : A stable lens.

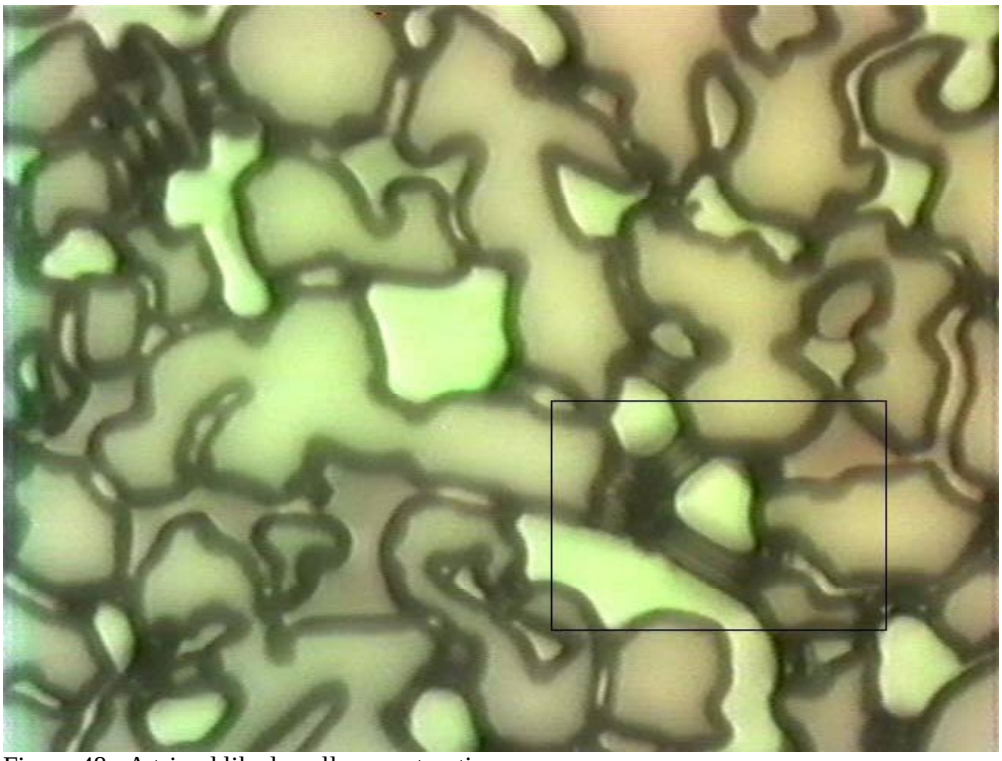

Figure 48 : A tripod like lamellae construction.

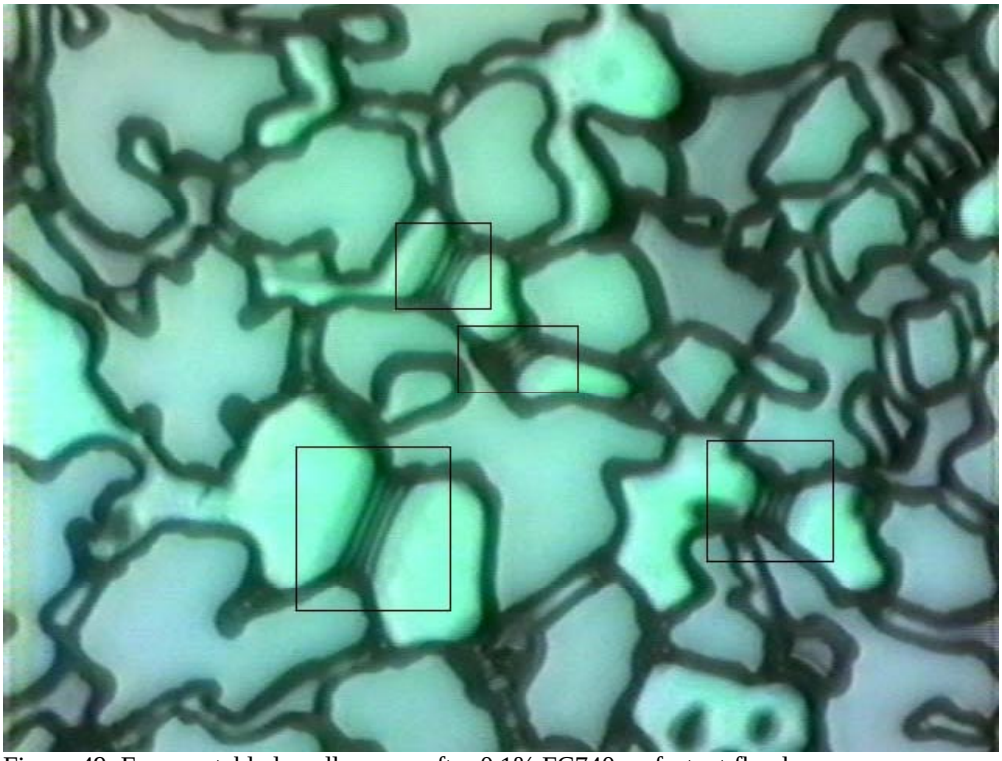

Figure 49: Four unstable lamellae seen after 0.1% FC740 surfactant flood.

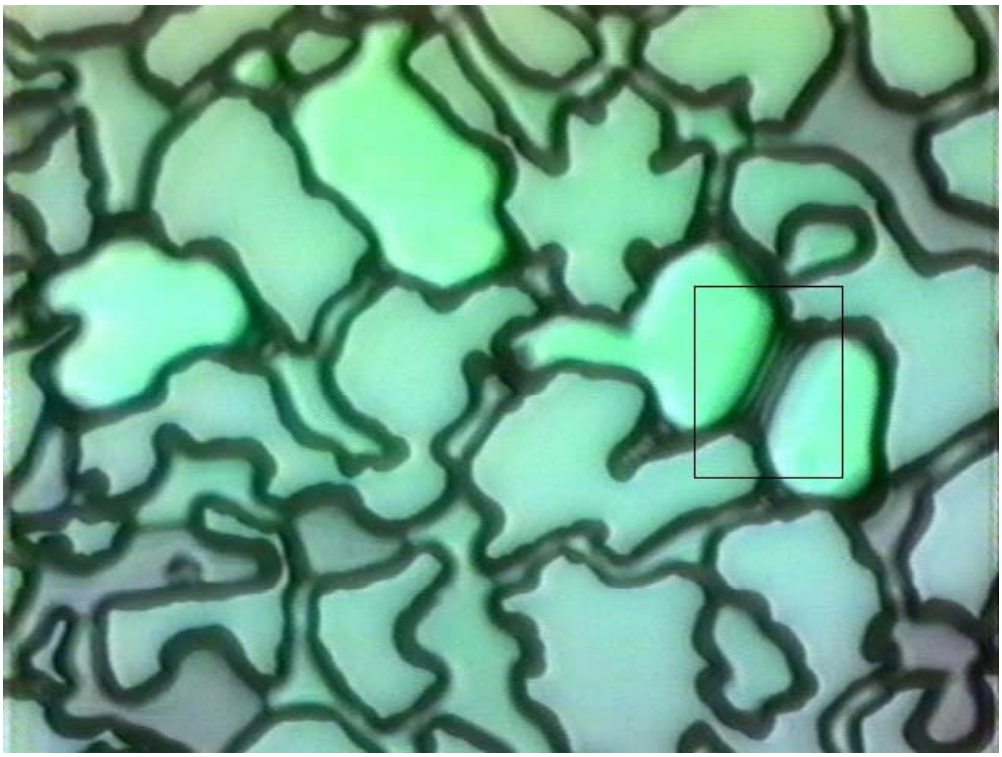
Figure 50 : Stable lamella seen in the big pore after 0.1% surfactant flood.

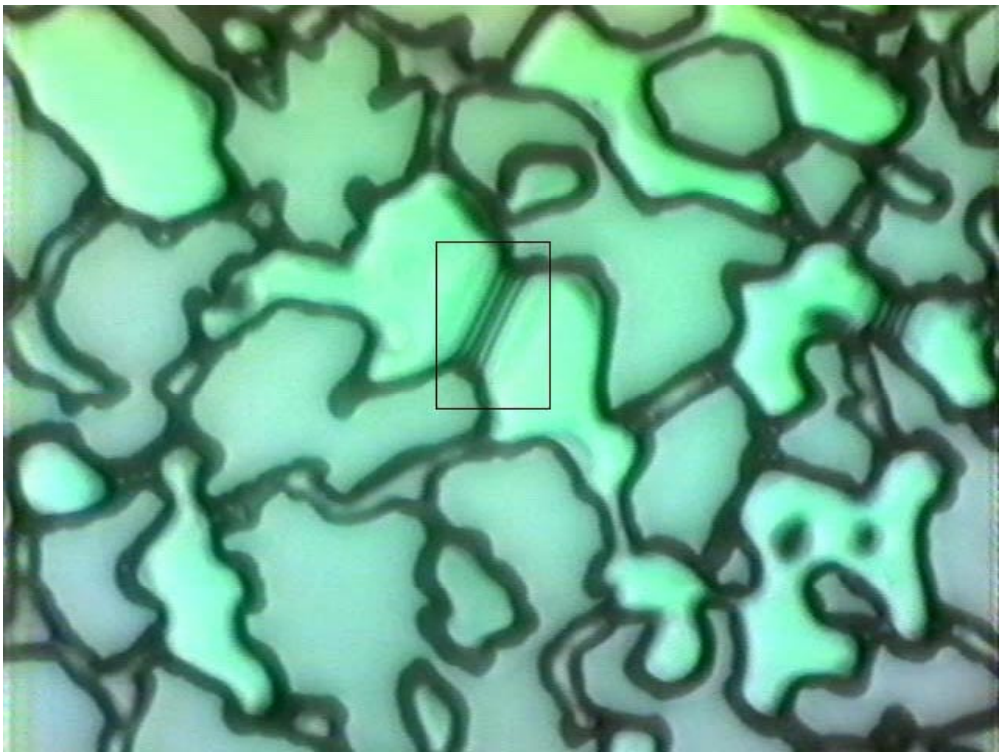
Figure 51: The foam lamella seen here seems to be thinner than usually seen in this pore geometry and is still stable.

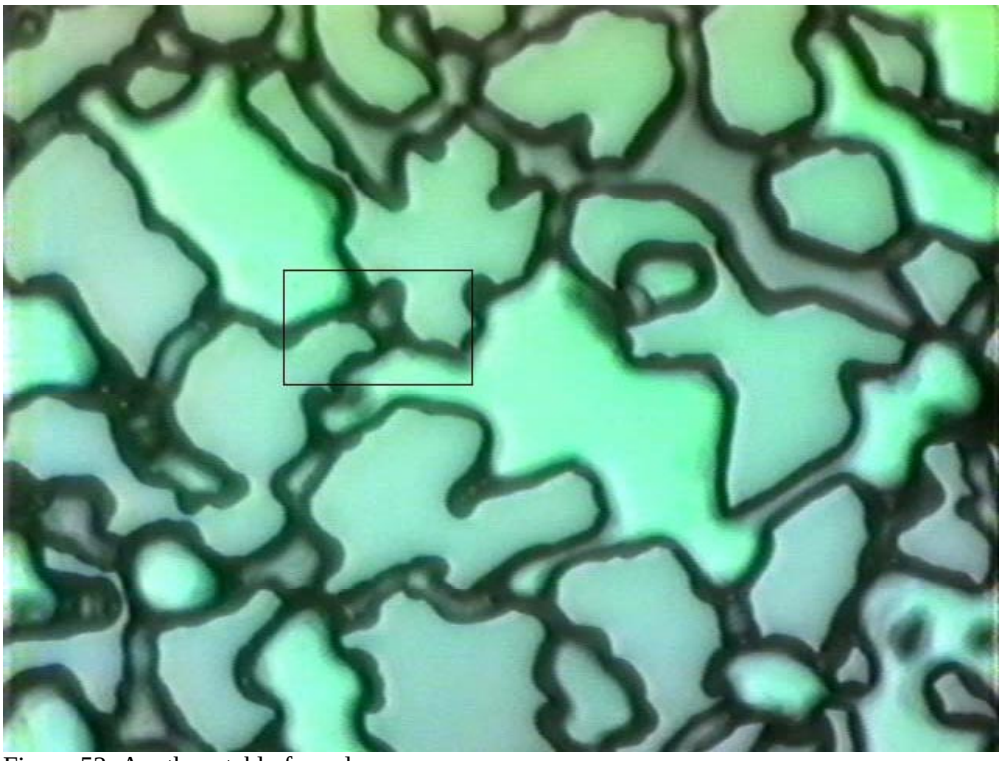

Figure 52: Another stable foam lens.

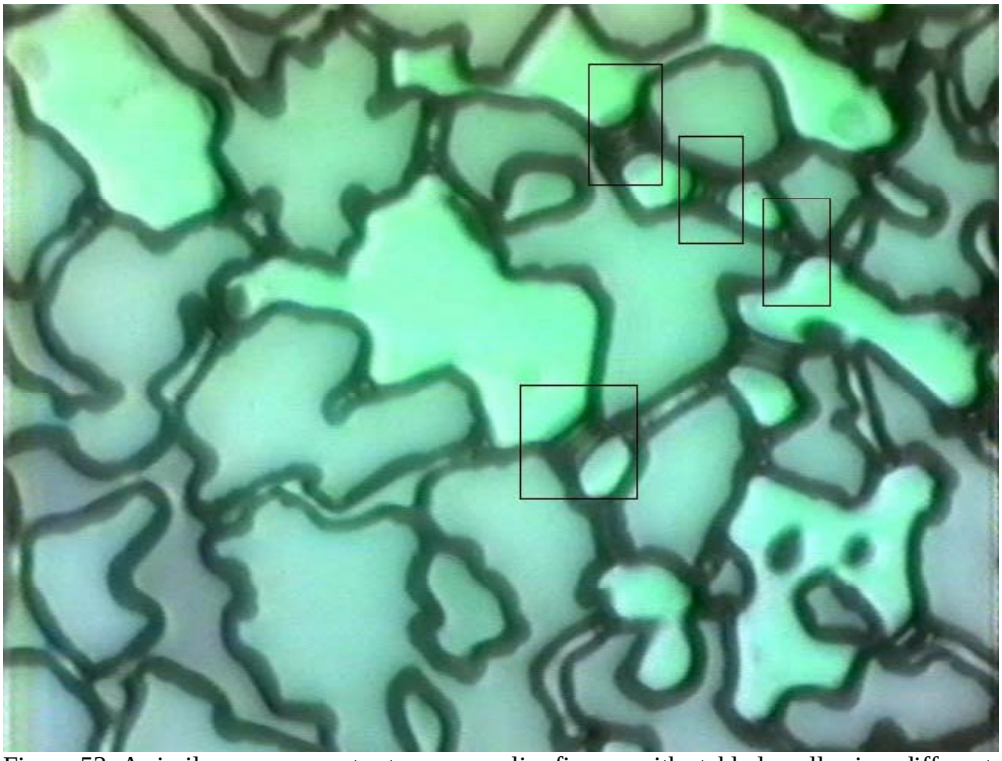

Figure 53: A similar pore geometry to some earlier figures with stable lamellae in a different configuration.

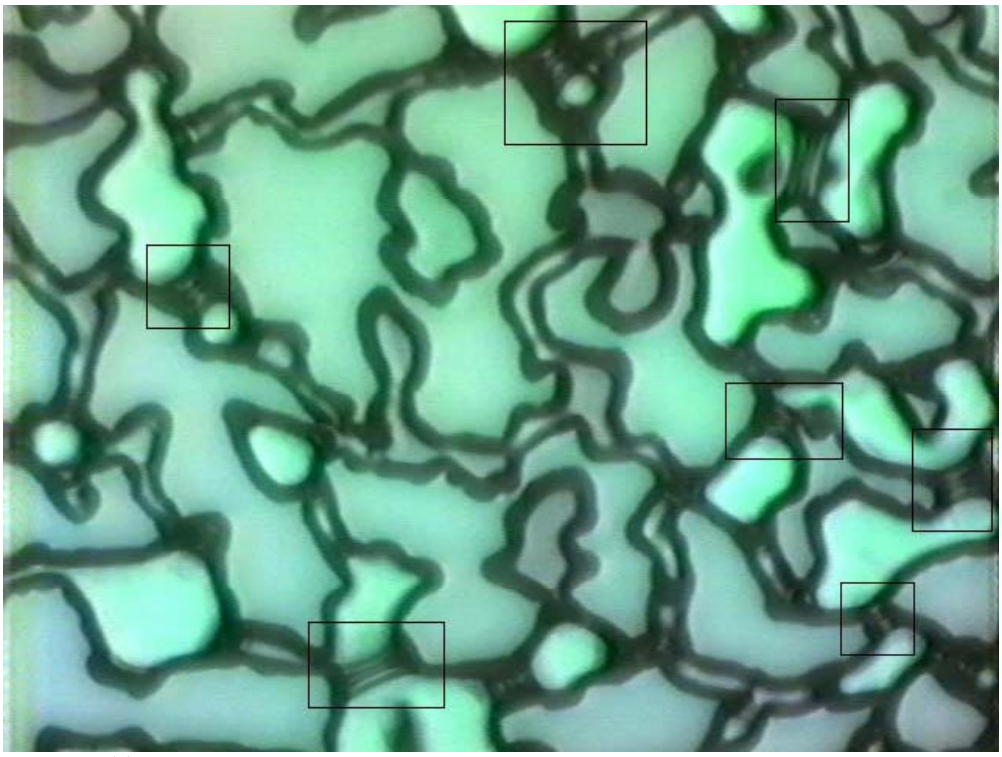

Figure 54(a)

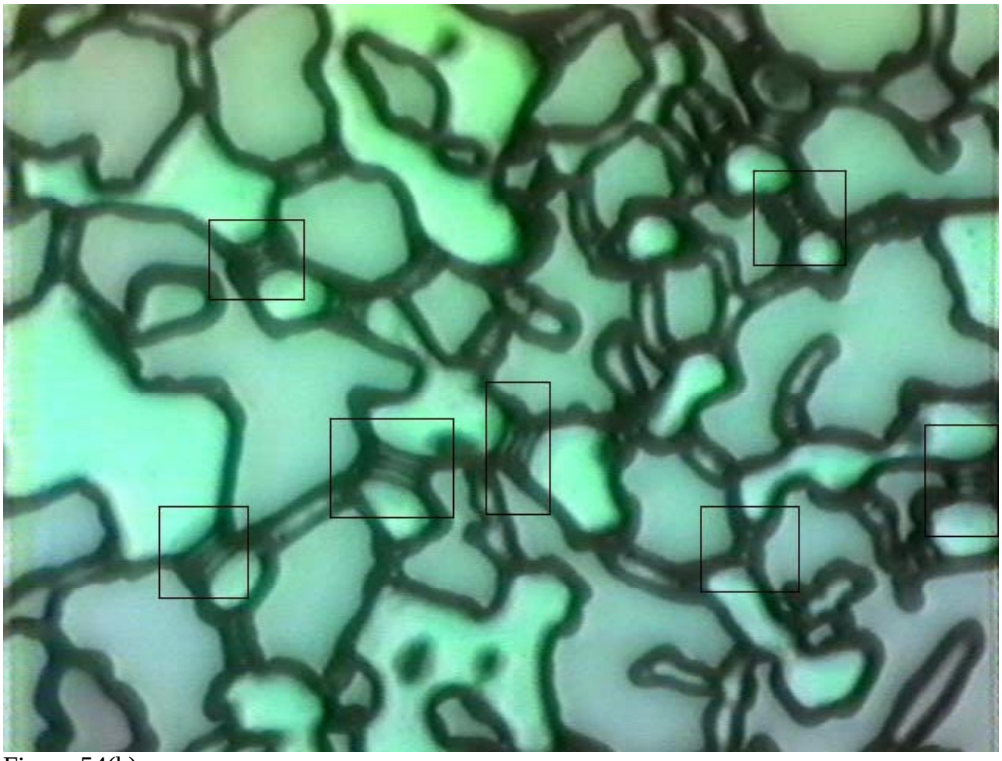

Figure 54(b)

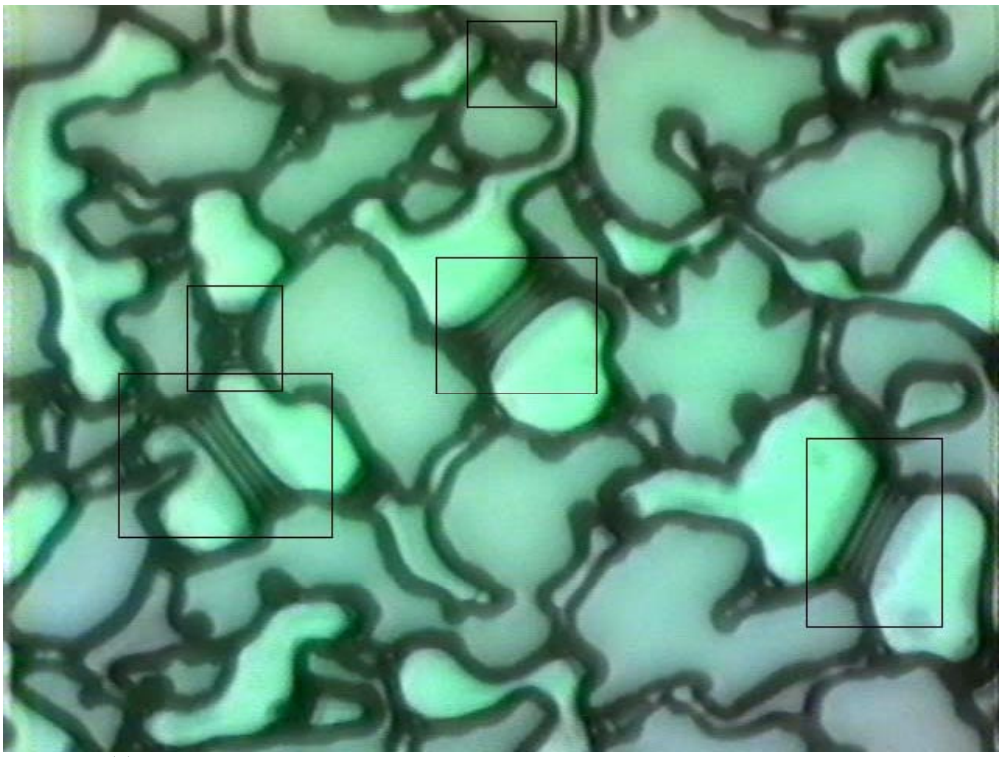

Figure 54(c)

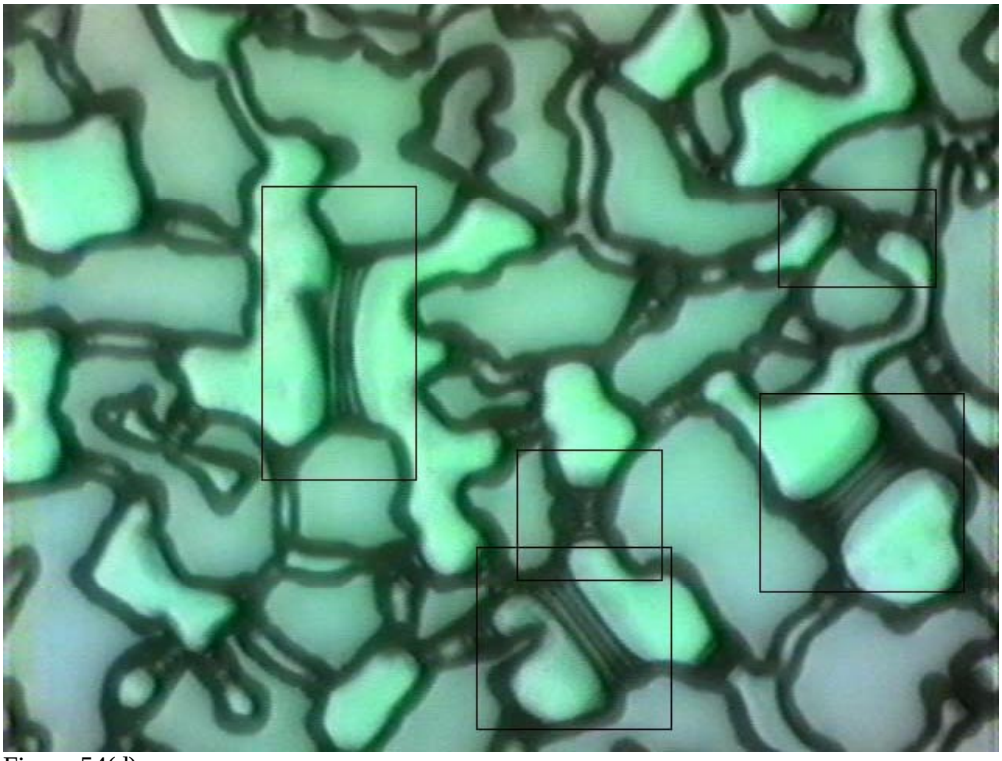

Figure 54(d)

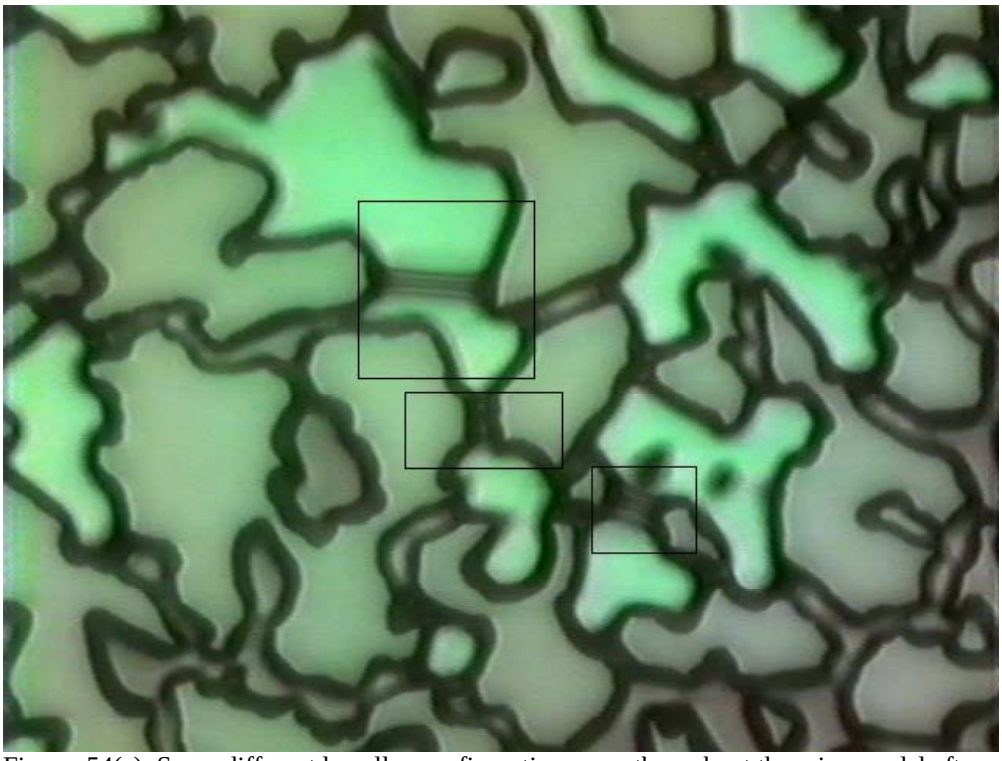

Figure 54(e): Some different lamellae configurations seen throughout the micromodel after 1% surfactant (FC740 in kerosene) flood.

Section 7
Conclusions

The silicon micromodels used in these experiments give us a realistic feel of the pore level mechanisms which would occur in reality. The three sets of experiments conducted in this study which included different oils and foamers lead us to some interesting conclusions which are outlined below.

7.1 The AOS Surfactant

With the AOS surfactant in the presence of different oils, no foam formation was seen at the pore level. However emulsions were observed which varied in size and stability with increased concentration of surfactant. The pore and throat sizes also seemed to influence the emulsion size. Most of the emulsions seen were composed of water covered with oil films. With the crude oil the water became discolored to brown. Very little oil was required to form these emulsions as could be seen at higher concentrations of surfactant after the model had been flooded with surfactant a few times.

It can be concluded that the emulsion formation with the AOS surfactant could be the reason for the delayed foam forming observed by Kristiansen *et al.* (1992). These have in the past often been ascribed to so-called “aging” or “incubation” effects. According to a mechanism suggested by Lau (1988), the emulsion scavenges all surfactant and makes it impossible to generate foam initially. Only when excess surfactant solution becomes available -through reinjection or rearrangement - foam generation can take place. This, however does not apply to our case where excess surfactant is always present.

The ability to form water-in-oil emulsions is governed by the balance of forces between those tending to keep the oil in large drops (or continuous oil areas) and those favoring formation of small emulsified oil droplets. It is well known from antifoam theory that small emulsion droplets make better antifoam agents. An attempt to develop a theory for foam destabilization by emulsified oil droplets has been published by Schramm (1990). However the lamella number fails to correlate oil tolerance data for fluorosurfactant foams; likewise it is not understood how it can explain the lack of emulsions formed with the fluorosurfactant.

The presence of oil in the system resulted in emulsions and no foam was observed. However the emulsions seen were seen to be somewhat effective in blocking the gas flow path in the system. Whether foam would actually form on continuous surfactant and gas flooding is yet to be seen in the micromodel and would be an interesting area for further research. Currently no theory explains this phenomenon which seems different from the conventional “aging” of cores, which is essentially a liquid/solid adsorption process.

7.2 The Fluoro-Surfactant

For the oil-foam with the fluoro-surfactant, a strong foam was generated both in the oil-saturated and the oil-free zones. Lamellae were observed both in oil-saturated and oil-free areas, indicating oil-tolerant behavior as expected from the negative entering coefficient and the bulk behavior. Generation sites for the foam lamellae were seen to be

controlled by pore geometry and local saturation. The foam lamellae were stabilized by the surfactant and therefore an increase in foamer concentration increased the lifetime of the lamellae and thereby the strength of the foam. However, no obvious link could be found with the number of films observed and strength of gas blockage. Although lenses were observed to be present in the system, no lens-lamella transition was observed. We can conclude from these observations that this oil-foam can be used for achieving a very favorable barrier geometry for gas-coning problems.

7.3 SEM Study

From the SEM study we can draw a conclusion on the fabrication technique used for the new micromodels (Type B). As discussed in the previous section, the extreme conditions used in the bonding process of the Corning, type 7740 pyrex wafer to the etched silicon wafer was the cause of the reduced permeability in the new models. Extreme care should therefore be taken while specifying the bonding conditions for the micromodels.

7.4 Further Research

Further research suggestions include studying the behavior of emulsions and how they effect foam properties in porous media with an emphasis on foam destabilization by emulsified foam droplets. Using different thin sections (other than Berea) to compose a mask and etching it onto the silicon wafer would help in studying flow behavior in other types of rocks. The effect of “aging” as the reason for the delayed foam forming (if any?) with the AOS surfactant also deserves more investigation. As mentioned in section 7.1, whether foam would form on continuous surfactant and gas injection would be an interesting area to be looked into to supplement the work done in this project.

The new micromodels which are currently under construction are being etched at the 'Center for Integrated Systems' at Stanford. The anodic bonding apparatus will be set up in the laboratory which would enable us to complete the micromodels in house. Different etch depths varying form 15µm to 35µm would be available. Effect of varying etch depth on the flow behavior and foam formation and stability would further enhance the understanding of oil-foam interaction.

References

1. Bikerman, J.J.: Foams ; Springer-Verlag : New York, 1973

2. Coombe, D. A.; Mohammadi, S. S.: " Characteristics of steam-foam drive process in massive multi-zone and single-zone reservoirs.' Paper SPE 24030 presented at SPE California Regional Meeting, Bakersfield, 1992

3. Castanier, L. M.; Hornbrook, J.W.: Observation of foam/oil interactions in a new, high resolution micromodel" paper SPE 22631 resented at the 66th Annual Technical Conference and Exhibition, Dallas, 1991

4. Dalland, M.; Hanssen, J.E.: Oil Interaction with foams at static and flowing conditions in porous media. Paper at the 13th EOR workshop and symposium, Banff 1992

5. Falls, A. H.; Hirasaki, G. J.; Patzek, P. W.: "Development of a mechanistic foam simulator: The population balance and generation by snap-off." SPE Reservoir Engineering, 3: 884-892, August 1988

6. Fried, A.N.: "The Foam-Drive Process for increasing the recovery of Oil", Report of Investigations 5866; U.S. Department of the Interior, Bureau of Mines, Washington, D.C. 1961

7. Hanssen, J.E.; Dalland, M.: Proceedings of the SPE/DOE 7th Enhanced Oil Recovery Symposium; Society Of Petroleum Engineers : Richardson, TX ; paper CIM 86-37-01, 1990

8. Hanssen, J. E.: " Foam as a gas-blocking agent in petroleum reservoirs II: Mechanisms of gas blockage." Journal of Petroleum Science and Engineering, 135-156. 10: 2, 1993

9. Hanssen, J. E.: " Foam as a gas-blocking agent in petroleum reservoirs I: Empirica Observations and parametric study." Journal of Petroleum Science and Engineering, 117-134. 10: 2, 1993

10. Harkins, W. D.: Journal of Chem. Phys. 9, 552-568, 1941

11. Holm, L.W.; " The Mechanisms of Gas and Liquid Flow Through Porous Media in the Presence of Foam" , SPEJ, 359-369, December 1968

12. Hornbrook, J. W.; Castanier L. M.; Pettit, P: " Visualizaition of foam/oil in a new high resolution sandstone replica micromodel." Report SUPRI TR-86, Stanford University, 1992

13. Huh, D. G.; Cochrane, T. S.; Kovarik, F. S.: " The Effect of Microscopic Heterogeneity on CO_2/ Foam Mobility: Part 1- A mechanistic study" SPE 17359 paper presented at the SPE/ DOE EOR Symposium, Tulsa, April 1988

14. Huh, D. G.; Cochrane, T. D.; Kovarik, F.S.: " The effect of microscopic heterogeneity on CO_2 foam mobility: Part 1- mechanistic study." Journal of Petroleum Technology, 872-879, 41: August 1989

15. Jensen, J.A. ; Friedmann, F. : Proceedings of the California Regional Meeting of SPE; Society Of Petroleum Engineers : Richardson, TX ; SPE/DOE 16375, 1987

16. Kovscek, A.R.; and Radke C.J.: " Simulation of foam transport in porous media." Paper SPE 26402 presented at 68th SPE Annual Technical Conference and Exhibition, Houston, 1993

17. Kovscek A. R.; Radke C. J.: " Fundamentals of foam transport in porous media" in Foams: Fundamentals and Applications in the Petroleum Industry. L. L. Schramm, Editor. Advances in Chemistry Seies, 242. American Chemical Society, Washington, DC, 1994

18. Kovscek, A. R.; Patzek, T. W.; Radke, C.J.: " Mechanistic Prediction of Foam Displacement in Multidimensions: A Population Balance Approach" SPE/DOE 27789, presented at the 9th Symposium on Improved OIl Recovery, Tulsa, April 1994

19. Kristiansen, T. S.; Holt, T.: "Proceedings of the 12th International Workshop and Symposium of the IEA Collaborative Project on Enhanced Oil Recovery"; AEA Technology: Winfrith, United Kingdom, 1991

20. Kristiansen, T. S.; Holt, T.: " Properties of flowing foam in porous media containing oil" Paper SPE 24182 presented at the 8th SPE Symposium on Enhanced Oil Recovery, Tulsa 1992

21. Kuhlman, M.I.: Proceedings of the SPE/DOE Enhanced Oil Recovery Symposium; Society Of Petroleum Engineers : Richardson, TX ; SPE/DOE 17356, 1988

22. Lau, H. C.; O'Brien, S. M.: " Effects of spreading and non-spreading oils on foam propagation through porus media." SPE Reservoir Engineering, 893-896, 3: August 1988

23. Lolomari, T.O.; " Micromodel Studies of Three Phase Flow in Porous Media", MS Thesis, Stanford University, 1996

24. Manlowe, J.D.; Radke, C. J.: " A Pore-Level Investigation of Foam/Oil Interactions in Porous Media." SPE Reservoir Engineering, November 1990.

25. Marsden, S. S.: "Foams in Porous Media", SUPRI TR-37, Stanford University, 1986

26. Mast, R. F.: : Microscoppic behavior of foam in porous media." Paper SPE 3997 presented at the 47th SPE Annual meeting, San Antonio, 1972

27. Nikolov, A. D.; Wasan, D. T.; Huang, D.W.; Edwards, D.A.: "The Effect of OIl on Foam Stability, Mechanisms and Implications for Oil Displacement by Foam in Porous Media" SPE paper 15443 presented at the 61st Annual Technical Conference and Exhibition, New Orleans, 1986

28. Novosad, J. J.; Ionescu, E. F.: "Proceedings of the 38th Annual Technical Meeting of CIM"; Canadian Institute of Mining, Mettalurgy, and Petroleum: Calgary, Canada; Paper CIM 87-38-80, 1987

29. Owete O. S.; Castanier, L.M; Brigham, W.E.: : Folow of foam through porous media" Report SUPRI TR-37, Stanford University, 1984

30. Owete, O. S.; Castanier, L.M; Brigham, W.E.: "Flow Behaior of foam: A Porous Micromodel Study." SPE Reservoir Engineering. 315-323, 2: August 1987

31. Radke, C.J. ; Ransohoff, T. C.: "Mechanisms of Foam Generation in Glass Bead Packs" SPE 15441, paper presented at the 61st Annual Technical Conference and Exhibition, New Orleans, 1986

32. Radke, C. J.; Chambers, K. T.: "Capillary phenomenon in foam flow through porous media." in Interfacial Phenomenon in Petroleum Recovery, N.R. Morrow, Editor. Surfactant Science Series. Marcel Dekker, Inc. New York, pp 191-255, 1991

33. Robinson, J.W.: Woods, W. W. ; J. Soc. Che. Ind. 67, 361-365, 1948

34. Roof, J. G.: " Snap-off of oil droplets in Water-Wet pores." Society of Petroleum Engineers Journal, 85-90. 10: March 1970

35. Ross, S.; McBain, J. W.: Ind. Eng. Chem. 36(6), 570-573, 1944

36. Sanchez, J.M.; Schechter, R.S.: " The effect of Trace Quantities of Surfactant on Nitrogen/Water Relative Permeabilitie" SPE 15446. Paper presented at the 61st Annual Technical Conference, New Orleans, 1986

37. Sanchez, J.M.; Hazlett, R.D.: " Foam Flow through Oil-Wet Porous Medium: A Laboratory Study", SPE 19687, paper presented at the SPE Annual Technical Conference and Exhibition, San Antonio, 1989

38. Sanchez, J. M.; Hazlett, R. D.: SPE Res. Eng. 7(1), 91-97, 1992

39. Schramm, L. L.; Novosad, J. J.: "Micro-visualization of foam interactions with a crude oil." Colloids and Surfaces, 21-43, 46: 1990

40. Schramm, L.L.: Emulsions: Fundamentals and Applications in the Petroleum Industry; American Chemical Society, Washington D.C. 1992

41. Schramm, L.L.: Foams: Fundamentals and Applications in the Petroleum Industry ; American Chemical Society, Washington D.C. 1994

42. Surguchev, L. M.; Coombe, D.; Hanssen, J. E.; Svorstøl, I.: "Simulation of WAG and gas Injection with potential sweep improvement by application of foam". Paper presented at 8th European Symposium on Improved Oil Recovery, Vienna, 1995

43. Terry, C. S.: " A Gas Chromatography System Fabricated on a Silicon Wafer Using Integrated Circuit Technology" Integrated Circuits Laboratories Technical Report No. SEL-75-011, Stanford University, 1975

44. Woody, F.; Blunt, M.; Castanier, L.M.: "Pore level visualization of foam flow in a silicon Micromodel" SUPRI TR-100, Stanford University, 1995

APPENDIX A

```
c       This program computes the Interfacial tension from the spinning
c       drop apparatus output.

        write(*,10)
10      format('Input speed in msec/round')
        read(*,20)speed
20      format(f7.3)

        write(*,30)
30      format('Input top level of drop in mm')
         read(*,40)top
40      format(f8.5)

        write(*,50)
50      format('Input bottom level of drop in mm')
        read(*,60)bot
60      format(f8.5)

        write(*,70)
70      format('Input density of liquid 1 in g/cc')
        read(*,80)den1
80      format(f8.5)

        write(*,90)
90      format('Input density of liquid 2 in g/cc')
        read(*,100)den2
100     format(f8.5)

        r=abs(top-bot)*1e-3/2.

c       converting the speed to rad/s
        s=2*3.14*1000/speed

        deltad=abs(den1-den2)*1000

        ten=deltad*s*s*r*r*r/4
        ten=ten*1e3

        write(*,1)ten
1       format('The IT between the fluids in dynes/cm is ',f5.3)
        stop

        end
```

APPENDIX B

Material Information
Corning Pyrex : 7740

Description:

Glass Type - Soda Borosilicate
Color- Clear

Properties

Mechanical	**Metric**	**English**
Density	2.23 g/cm^3	139.2 lb/ft^3
Young's Modulus	6.4 x 10^3 kg/mm^2	9.1 x 10^6 psi
Poisson's Ratio	0.20	
Shear Modulus	2.67 x 10^3 kg/mm^2	3.8 x 10^6 psi
Knoop Hardness (KHN_{100})	418	
Viscosity		
Working Pt. (10^4 poises)	1252°C	2286°F
Softening Pt. (10$^{7.6}$ poises)	821°C	1510°F
Annealing Pt. (10^{13} poises)	560°C	1040°F
Strain Pt. (10^{14} poises)	510°C	950°F
Thermal		
Coefficient of Expansion (0-300°C)	32.5 x 10^{-7}/°C	18.1 x 10^{-7}/°F
(25°C to Set Point 515°C)	35.0 x 10^{-7}/°C	19.5 x 10^{-7}/°F
Specific Heat, 25°C	0.18 cal/g°C	0.18 Btu/lb°F
Thermal Conductivity, 25°C	0.0027 $\frac{cal\ cm}{sec\ cm^2 °C}$	0.63 $\frac{Btu\ ft}{h\ ft^2 °F}$
Thermal Diffusivity, 25°C	0.0069 cm^2/sec	0.00107 in^2/sec

CORNING

Optical

Refractive Index (589.3 nm)	1.474
Birefringence Constant	394 $\frac{nm/cm}{kg/mm^2}$
Transmission @ 440nm	91.0%*
560nm	91.8%*

*Through a sample thickness 1.0 mm

Electrical

Log_{10} Volume Resistivity @ 250°C	8.1 ohm-cm
@ 350°C	6.6 ohm-cm
Dielectric Constant @ 20°C; 1 MHz	4.6
Loss Tangent @ 20°C; 1 MHz	0.4%

Chemical

Weathering	* 1
Acid Durability	** 1

* Weathering is defined as corrosion by atmospheric-borne gases and vapors such as water and carbon dioxide. Glasses rated 1 will almost never show weathering effects; those rated 2 will occasionally be troublesome, particularly if weathering products cannot be removed; those glasses rated 3 require more careful consideration.

** The Acid Durability column classifies glasses according to their behavior in 5% hydrochloric acid at 95°C (203°F) for 24 hours.

Classification	Thickness Loss (in.)
1	$< 10^{-6}$
2	$10^{-6} - 10^{-5}$
3	$10^{-5} - 10^{-4}$
4	$> 10^{-4}$

Values are listed with four degrees of accuracy. Those that are underscored (e.g. 2) result from recent determination and are reliable. Values not underscored are estimates offered with confidence. When two values are listed with one underscored, this indicates the range within which the true value lies: the underscored value is the more probable one (e.g. 2-3). A question mark indicates considerable uncertainty.

VISCOSITY

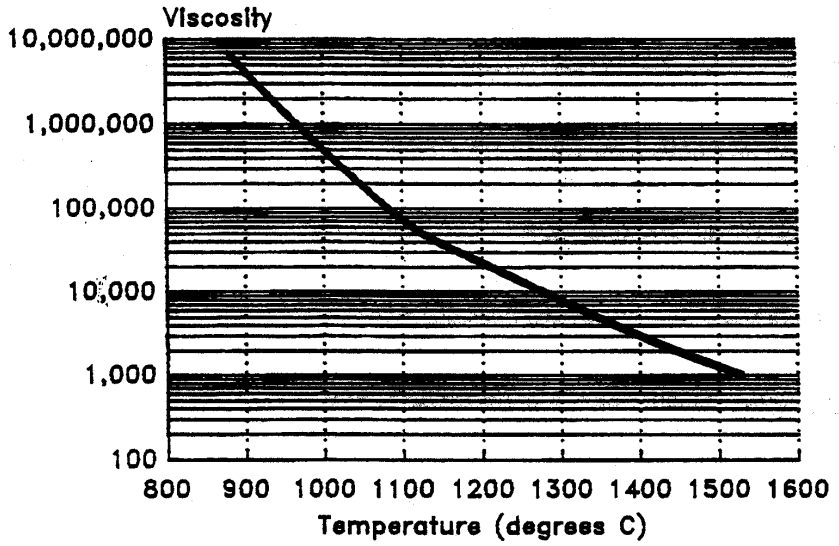

THERMAL EXPANSION

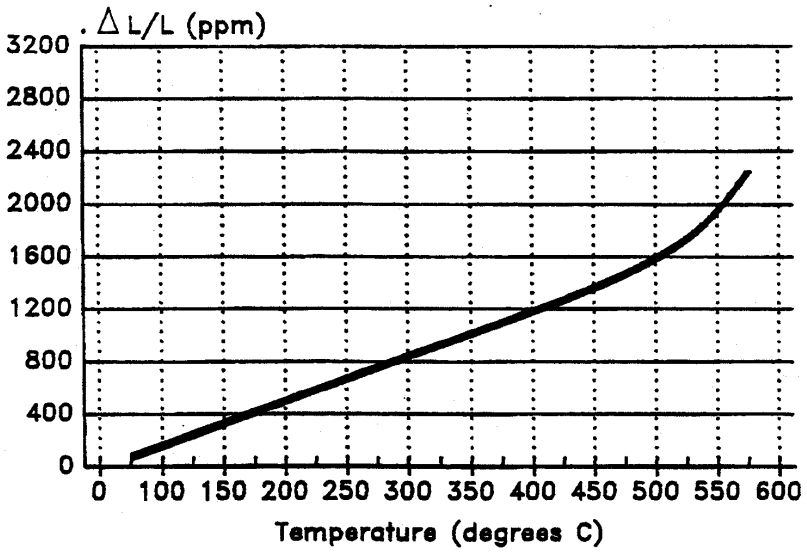

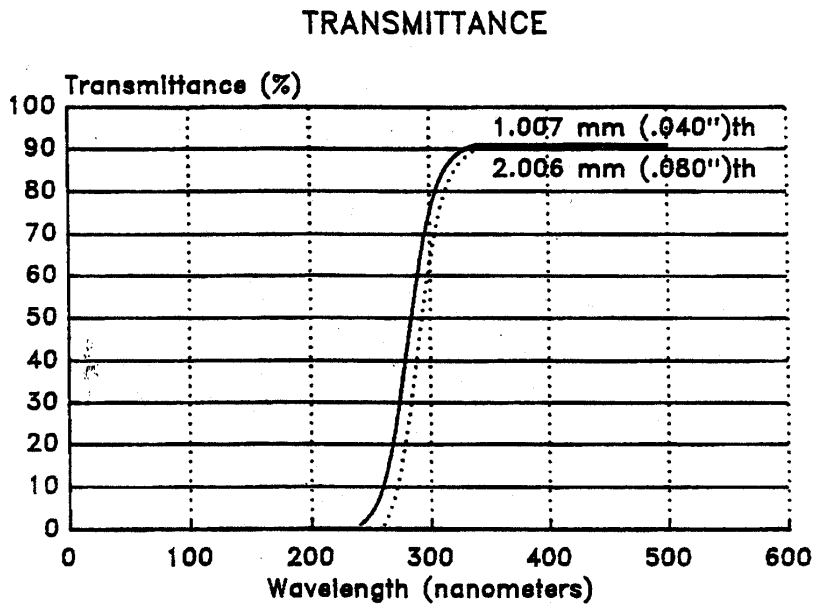

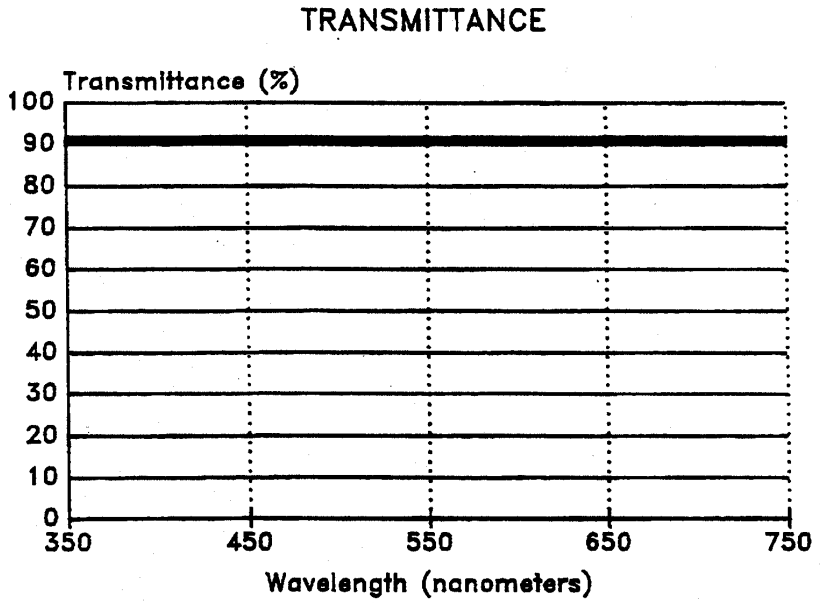

1.007 mm thickness

TRANSMITTANCE

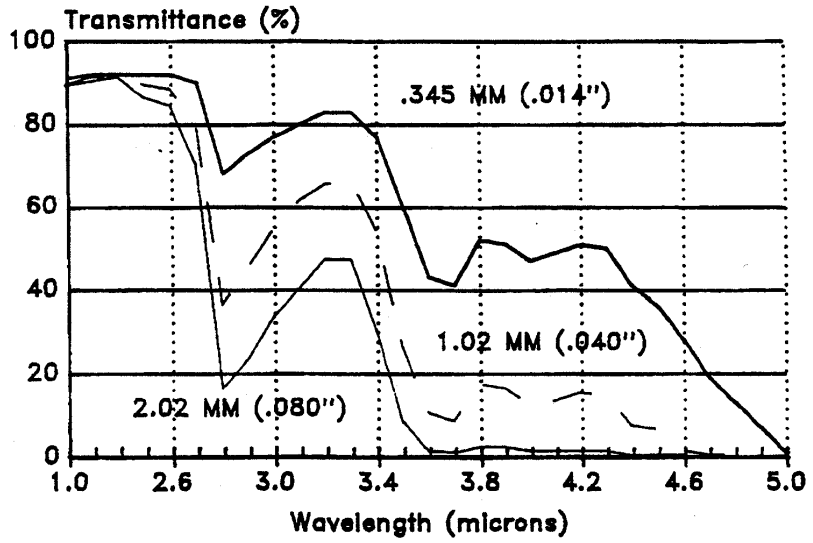

DC VOLUME RESISTIVITY

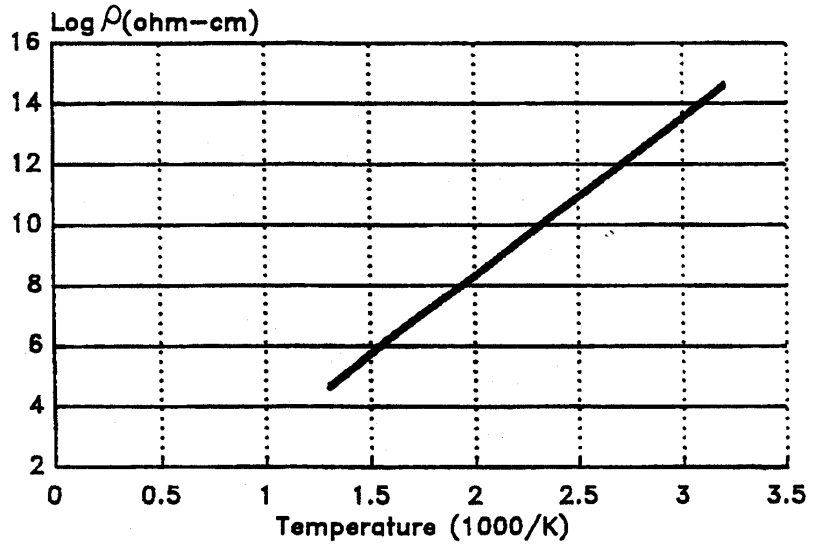

DIELECTRIC CONSTANT

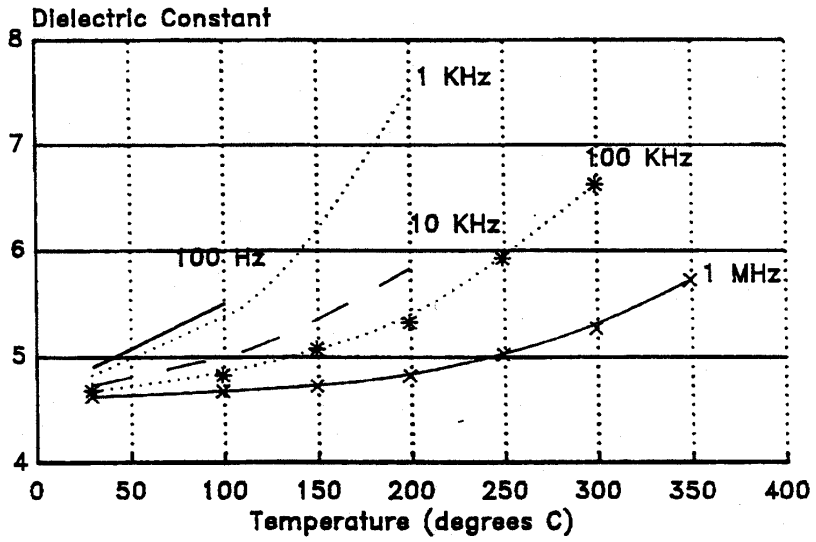

LOSS TANGENT